CZECH TECHNICAL UNIVERSITY IN PRAGUE

Faculty of Mechanical Engineering

Department of Mechanics, Biomechanics and Mechatronics

Mechanical Properties of Perivascular Adipose Tissue and its Effect on Biomechanics of Abdominal Aorta

Doctoral Thesis

Tereza Voňavková

Doctoral study program: Mechanical Engineering

Field of study: Biomechanics

Supervisor: Doc. Ing. Lukáš Horný, Ph.D.

Prague 2020

Abstract

The dissertation thesis aims to show that perivascular adipose tissue may significantly change the mechanical state of the abdominal aorta. To this end, uniaxial tensile tests with perivascular fat tissue were carried out. In the subsequent regression analysis, stress-strain data were fitted by the polynomial strain energy density. A constitutive model of adipose tissue was used in the analytical simulation of the inflation-extension behavior of the human abdominal aorta. The computational model was based on the theory of the bi-layered thick-walled tube. In addition to the effect of perivascular tissue, the effect of axial prestretch was also studied. It was found that the presence of perivascular tissue reduces the distensibility of the aorta. Axial prestretch applied to aortas embedded in adipose tissue had an effect opposite to that of adipose tissue. Axially prestrained aortas exhibited higher distensiblity than non-prestrained aortas. It was also shown that the perivascular envelope bears some portion of the pressure loading and thus reduces the mechanical stresses inside the wall of aorta. A similar effect was found for axial prestretch.

Key words

Perivascular adipose tissue, abdominal aorta, aortic pathology, uniaxial tensile tests, Yeoh model, hyperelasticity, nonlinear behavior, thick-walled bilayer tube, inflation-extension simulation, axial prestretch.

Anotace

Cílem této dizertační práce je ukázat, že perivaskulární tuková tkáň může významně měnit mechanický stav břišní aorty. Za tímto účelem byly provedeny jednoosé tahové testy s perivaskulární tukovou tkání. V následné regresní analýze byly napěťově-deformační křivky nafitovány pomocí polynomické hustoty deformační energie. Konstitutivní model perivaskulární tukové tkáně byl použit v analytické simulaci chování inflace-extenze lidské abdominální aorty. Výpočetní model byl založen na teorii dvouvrstvé silnostěnné válcové trubice. Kromě účinku perivaskulární tkáně byl také studován vliv axiálního předpětí. Bylo zjištěno, že přítomnost perivaskulární tkáně snižuje roztažnost aorty. Axiální předpětí, aplikované na břišní aortu zabudovanou v tukové tkáni, mělo opačný účinek než účinek tukové tkáně. Axiálně předepjaté aorty vykazovaly vyšší roztažnost než nepředepjaté aorty. Dále bylo ukázáno, že perivaskulární obal nese určitou část tlakového zatížení a tím snižuje mechanické napětí uvnitř stěny břišní aorty. Podobný účinek byl nalezen pro axiální předpětí.

Klíčová slova

Perivaskulární tuková tkáň, břišní aorta, patologie aorty, jednoosé tahové testy, Yeoh model, hyperelasticita, nelineární chování, silnostěnná dvojvrstvá trubice, inflačně-extenzní simulace, axiální předpětí.

Acknowledgement

I would like to thank my supervisor doc. Lukáš Horný for his leadership, valuable advice and his working deployment. Furthermore, I would like to thank and wish all the best colleagues from the Faculty of Mechanical Engineering with whom I still meet today. My big thanks go to my whole family, who have always stood behind me and surrounded me with love. Last but not least, I would like to thank my future husband, my love, for making me better.

This work has been financially supported by:

Grant Agency of the Czech Technical University in Prague, grant no. SGS13/176/OHK2/3T/12 "Biomechanika struktur lidského těla, jeho náhrad a interakce s blízkým okolím".

Grant Agency of the Czech Technical University in Prague, grant no. OHK2-033/16 " Biomechanika člověka - od buněk k náhradám".

Czech Science Foundation in the grant project no. GA18-26041S "Effect of axial prestretch on mechanical response of nonlinearly elastic and viscoelastic tubes".

Declaration

I declare, I composed this thesis individually and using the references quoted at the end of the thesis.

……

Contents

Nomenclature

Symbols

$\mathbf{B}$	left Cauchy-Green strain tensor	-
$\mathbf{C}$	right Cauchy-Green strain tensor	-
$\boldsymbol{C}$	dimensionless constant fourth-order tensor	-
c_1	stress-like material parameters	kPa
c_2	stress-like material parameters	kPa
$d\boldsymbol{f}$	infinitesimal resultant (actual) force	N
ds	spatial surface element	-
dS	surface element in reference configuration	-
e_I	unit base vector	-
$\mathbf{E}$	the Green-Lagrange strain tensor	-
F	force elongating	N
$\mathbf{F}$	deformation gradient	-
F_A	total deformation gradient of aorta	-
F_{A1}	deformation gradient expresses residual deformation	-
F_{A2}	deformation gradient expresses inflation-extension	-
F_{red}	axial force	N
H_{PT}	thickness of PVAT	mm
$\mathbf{I}$	second order unit tensor	-
I_1	first invariant	-
I_4	deformation invariant	-
I_6	deformation invariant	-
J	volume ratio	-
K_4	structural deformation invariants	-
K_6	structural deformation invariants	-
L	reference length	mm
l	deformed length	mm
$\boldsymbol{M}_1$	unit vector	-
$\boldsymbol{M}_2$	unit vector	-
n	number of observation points	-

$\boldsymbol{n}$	unit vector in deformed configuration	-
$\boldsymbol{N}$	unit vector in reference configuration	-
$\boldsymbol{N_i}$	eigenvectors	-
$\mathbf{P}$	the first Piola-Kirchhoff (nominal) stress tensor	kPa
P	internal pressure	kPa
p	indeterminate Lagrange multiplier	-
Q	quadratic forms of Green-Lagrange strains	-
Q	objective function	kPa
$\mathbf{R}$	tensor of rotation	-
R	radial coordinate (residual stress configuration)	-
r	radial coordinate (deformed configuration)	-
R_{iA}	reference inner radius of aorta	mm
R_{oA}	reference outer radius of aorta	mm
R_{iPT}	reference inner radius of PVAT	mm
R_{oPT}	reference outer radius of PVAT	mm
r_{iA}	deformed inner radius of aorta	mm
r_{oA}	deformed outer radius of aorta	mm
r_{iPT}	deformed inner radius of PVAT	mm
r_{oPT}	deformed outer radius of PVAT	mm
$\mathbf{S}$	the second Piola-Kirchhoff stress	kPa
S	reference cross-section area	mm^2
t	reference time	s
$\boldsymbol{t}$	the Cauchy (true) traction vector	-
$\boldsymbol{T}$	the first Piola-Kirchhoff (nominal) traction vector	-
$\boldsymbol{u}$	displacement vector	-
$\mathbf{U}$	right stretch tensor	-
$\mathbf{v}$	left stretch tensor	-
W	strain-energy function	kPa
W_A	strain energy stored in aorta	kPa
W_{PT}	strain energy stored in PVAT	kPa
$W_{\mathrm{isotropic}}$	isotropic part of W_A	kPa
$W_{\mathrm{anisotropic}}$	anisotropic part of W_A	kPa

$\widehat{W}$	denotes W during incompressibility condition	kPa
$\boldsymbol{X}$	position vector in reference configuration	-
$\boldsymbol{x}$	position vector in deformed configuration	-
Z	axial coordinate (residual stress configuration)	-
z	axial coordinate (deformed configuration)	-
α	opening angle of aorta	°
β	angle of collagen fibers	°
$\boldsymbol{\beta}$	deformed configuration	-
δ	axial stretch during close aorta	-
δ_{iJ}	Kronecker delta	-
ζ	axial coordinate (stress-free configuration)	-
θ	circumferential coordinate (deformed configuration)	-
Θ	circumferential coordinate (residual stresss configuration)	-
λ	principal stretch	-
λ_i	eigenvalues	-
λ_{11}	stretch in direction of loading force	-
$\lambda_{z\zeta}^{ini}$	initial axial stretch	-
λ_{zZ}	axial prestretch	-
μ	shear modulus	-
μ_p	material constant	-
α_p	material constant	-
∂	partial derivation	-
$\partial\Omega_0$	boundary surface	-
π	Ludolph number	-
Ω_0	reference configuration of the continuous body $\boldsymbol{\beta}$	-
Ω	deformed configuration	-
ρ	radial coordinate (stress-free configuration)	-
$\boldsymbol{\sigma}$	Cauchy (true) stress tensor	kPa
σ_{11}^{EXP}	experimental stress	kPa
σ_{11}^{MOD}	model stress	kPa

σ_{rr}	radial Cauchy stress tensor	kPa
$\sigma_{\theta\theta}$	circumferential Cauchy stress tensor	kPa
σ_{zz}	axial Cauchy stress tensor	kPa
ϑ	circumferential coordinate (stress-free configuration)	-

Indexes

A	abdominal aorta
det	determinant
I	unit base vector
i	unit base vector
K	unit base vector
PT	perivascular adipose tissue
T	transpose
tr	trace of the second-order tensor

1 Introduction

1.1 State of the art and motivation

Cardiovascular diseases are still the most frequent cause of death in developed countries, regardless of innovations that have appeared in last decades. New treatment approaches cannot be introduced without highly multidisciplinary research that combines knowledge from medical, biological, biochemical, and also engineering sciences. A way how engineering sciences can contribute to the progress in medicine are biomechanical simulations.

Biomechanical simulations can significantly reduce expensive and ethically problematic experiments determining an interaction between diseased tissues and therapeutic instruments. They make possible to predict whether some procedures, for example percutaneous intervention, will be successful or not (Fereidoonnezhad et al., 2017; Holzapfel et al., 2005). Computational simulations can also help to determine the optimal design of stents and prostheses (Kiousis et al, 2007) and to identify conditions leading to aneurysm rupture (Hejčl et al., 2017; Polzer and Gasser, 2015). Such simulations, however, have to be based on reliable data describing geometry, internal structure, mutual bonds, and the constitutive properties of interacting bodies.

Despite significant progress that has been achieved in arterial biomechanics, there are still topics that seem to have been overlooked for a long time. In the author's opinion, one of these is the role of perivascular adipose tissue (PVAT); see Figure 1 for detailed view of the infrarenal abdominal region (the aorta surrounded with adipose tissue). It may have been a widely accepted idea that perivascular tissue provides mechanical support to an artery, but it has led to a clear oversimplification in which one imagines the role of perivascular adipose tissue in the way that it merely fills the space between the external surface of the artery and neighboring organs. The current anatomical and physiological view of the role of PVAT is, however, quite different.

Similar to the endothelium, PVAT can modulate vascular tone by releasing vasoactive molecules (the adipocyte-derived relaxing factor, NO, prostacyclin, and H_2O_2; Zaborska et al., 2017) which has a direct impact on the mechanical state of the artery. In contrast to the endothelium, PVAT consists of multiple cell types. Besides adipocytes, macrophages, fibroblasts, lymphocytes, and adipocyte progenitor cells are also present in perivascular adipose tissue. The presence of these types of cells suggests the complex endocrine function of PVAT and its contribution to inflammatory processes occurring in the arterial wall (Zaborska et al., 2017; Brown et al., 2014; Králová Lesná et al., 2015). Considering this, one sees that PVAT is not merely a mechanical support mechanism, nor a simple energy-storing tissue, but it is an element with its own complex mechanobiological role that can affect the onset of various cardiovascular diseases (Huang Cao et al., 2017).

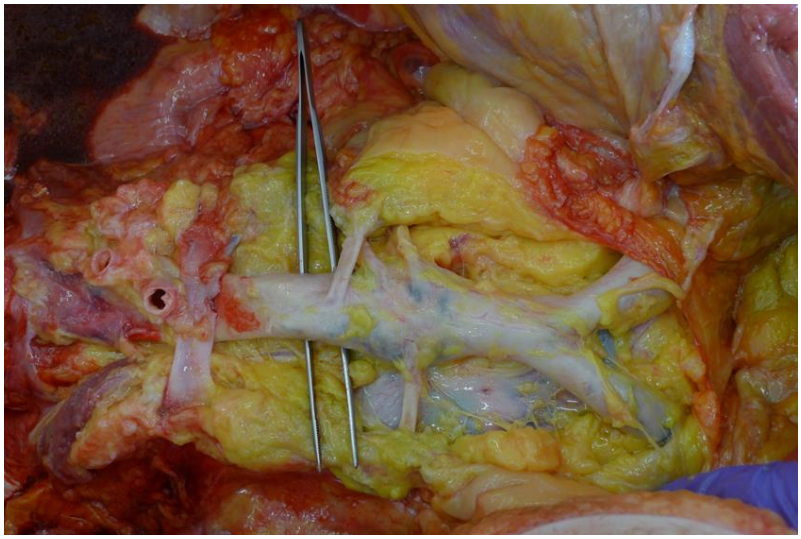

Figure 1. Infrarenal abdominal aorta surrounded by perivascular adipose tissue. Renal arteries stem from the aorta on the left side of the figure, and common iliac arteries continue from the aorta on right part of the figure. The picture from author's personal archive.

Nevertheless, it is not only the biological function of PVAT that seems to be underrated in the scientific literature. Computational simulations describing arterial biomechanics considering the effect of perivascular tissue are also rare. If the effect of perivascular tissue is considered, it is most frequently reduced to a form of the boundary condition imposed at the external surface of the artery and the most of studies even simplify a situation to a state in which the external pressure is considered to be zero. Thus no force acting between modeled artery and its surroundings is included to the model. This simplification may be adopted when pure tissue mechanics is studied. However, when one wants to study in vivo behavior to obtain predictions suitable for medical or treatment decisions, like in case of risk of aneurysm rupture evaluation, so in this case one should be as close to the reality as it is possible and in the real body, the abdominal aorta is surrounded by adipose tissue.

The approach expressing mechanical interaction between an artery and surrounding tissue by means of external pressure has been adopted by Zhang et al. (2004) and Moireau et al. (2012) who investigated the effect of the surrounding tissue on hemodynamics in the aorta. Hodis and Zamir (2009, 2011) investigated the effect of external tethering of the arterial wall on the dynamics of pressure pulse transmission. Their simulations were based on a 3D linearized viscoelastic model and showed that the surrounding tissue can have an important effect, again accounted for by means of the external boundary condition, on wall stress variation, and pulse wave velocity. Stress and strain variation and pulse velocity were reduced when external support was considered in their simulations (Hodis and Zamir, 2009, 2011).

With regard to elastostatics, Liu et al. (2007) obtained pressure-radius experimental data from swine carotid and femoral arteries in the tethered state and after PVAT excision. They showed that arteries with surrounding tissue sustain lower strains and stresses during inflation than their untethered counterparts, Figure 2. Masson et al. (2011) considered perivascular support in their computational model when estimating the constitutive parameters of human carotid arteries from in vivo data. They

used the model of the thick-walled tube for the artery; however, the perivascular tissue was again reduced only to its mechanical interaction with the wall by nonzero external pressure acting on the artery by means of the mathematical expression for perivascular pressure proposed by Humphrey and Na (2002).

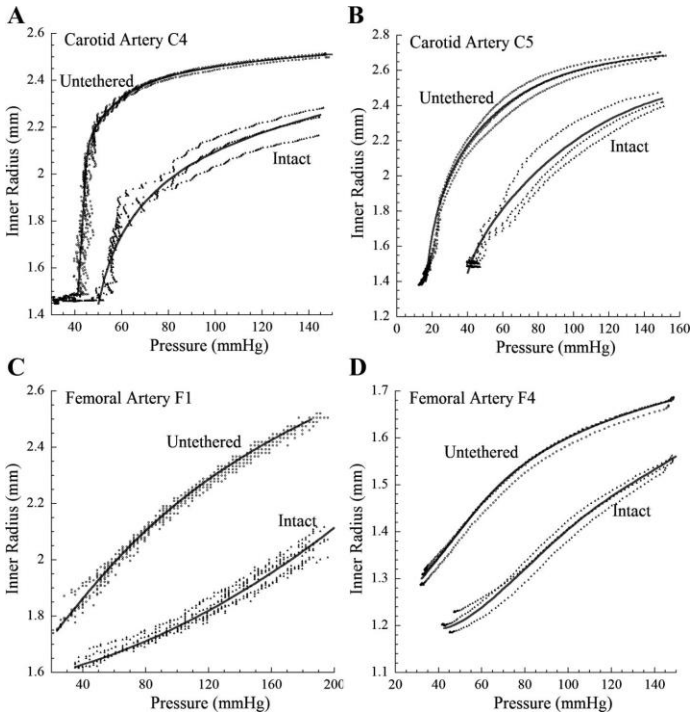

Figure 2. Pressure–radius relationships for swine carotid and femoral arteries obtained experimentally by Liu et al. (2007). Intact arteries contained adipose tissue envelop whereas in case of untethered samples the adipose tissue was dissected. Notice that untethered samples exhibit larger deformations and one also can say that their response shows higher degree of nonlinearity.

It is clear that approach implementing surrounding tissue as the boundary condition has its weak point in a fact that this pressure cannot be measured directly. To the best of author's knowledge, there are only two works where experiments focused on determining this pressure have been carried out. It is above mentioned study by Liu et al. (2007) where swine arteries were used and Misra and Singh (1983) who modeled perivascular tissue as linearly elastic material. Impossibility to measure perivascular pressure directly suggests that modeling PVAT as a real body could be more reliable approach.

One obvious barrier to considering PVAT in computational simulations as a 3D object is the fact that such an object has to be characterized with a constitutive equation to mathematically express its mechanical behavior. However, current scientific literature describing the elastic properties of PVAT at finite strains is very poor. In fact, we have not found any experimental study involving perivascular adipose tissue from human donors where mechanical tests aimed at describing the nonlinear elastic properties of PVAT at large strains has been carried out. It is worth noting that this finding is the main source of motivation for present study.

The many experiments available in the literature have been conducted with subcutaneous adipose tissue, usually from the abdominal region or from the breast, because their primary goal was to provide data suitable for computational simulations focused on plastic and reconstructive surgery (Sommer et al., 2013; Omidi et al., 2014). Moreover, most of these studies adopted the linear model and describe the elasticity of adipose tissue by means of the Young modulus (Geerligs et al., 2008; Comley and Fleck, 2010). The framework of nonlinear elasticity was adopted by Sommer et al. (2013), Omidi et al. (2014), and Calvo-Galleo et al. (2018), but they did not focus on perivascular tissue. Figure 3 and 4 show a typical response obtained in unconfined compression (Comley and Fleck, 2010) and shear test (Sommer et al., 2013).

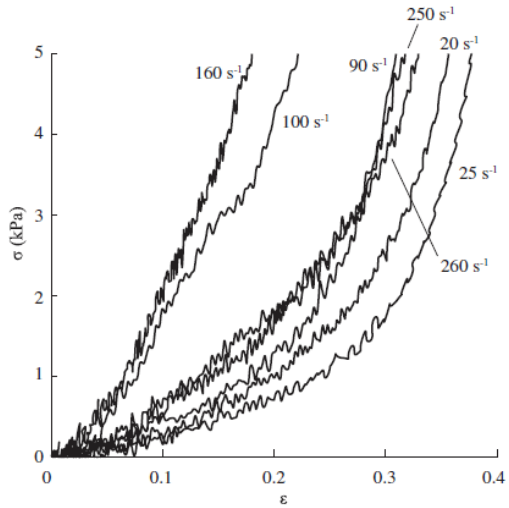

Figure 3. Data from unconfined compression tests carried out with porcine subcutaneous adipose tissue at different strain rates. Adopted from Comley and Fleck (2010).

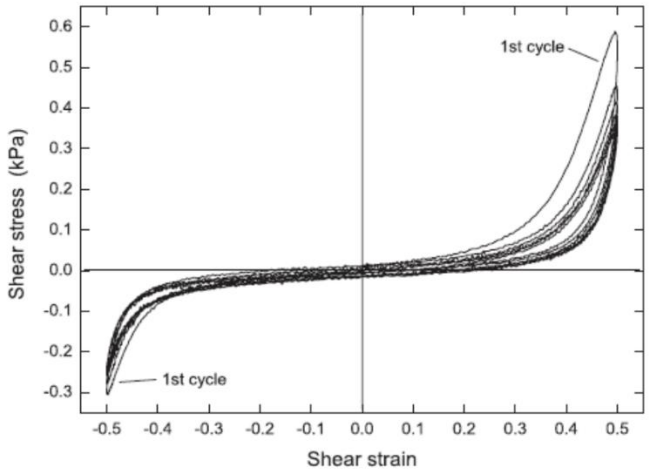

Figure 4. Data from cyclic shear test obtained with the human subcutaneous abdominal adipose tissues. Adopted from Sommer et al. (2013).

1.2 Brief outline the thesis goals and methods

From above mentioned it is clear that mechanical properties of the human perivascular tissue at the level of experimental observation as well as at the level of nonlinear constitutive modeling remain to large extent not well described at present. Thus the main goal of the present study is to extend our knowledge of the mechanical behavior of perivascular adipose tissue and its role in the biomechanics of the human abdominal aorta.

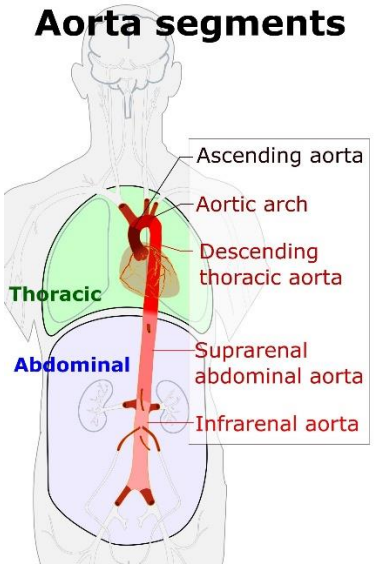

Figure 5. Segments of the human aorta. Adopted from Nataf and Lansac (2006).

To this end, uniaxial tensile tests with adipose tissue, which surround infrarenal part of the abdominal aorta (Figure 5) in the retropenitoneum, were carried out. Subsequently, the bi-layer, thick-walled tube analytical model was employed to simulate the effect of the thickness of PVAT on the mechanical response of the aorta. The inner layer modeled the human infrarenal aorta in accordance with data presented by Horný et al. (2014a). The outer layer of the computational model represented perivascular adipose tissue. The inflation behavior of the infrarenal aorta was computed with and without axial prestretch (Horný et al., 2014), and the existence of circumferential residual strain in the aorta was also considered (Horný et al., 2014b; Labrosse et al., 2013).

Figure 6. An evidence of the axial prestretch in abdominal aorta. Adopted from Horný et al. (2014).

Since elastic arteries are significantly prestretched in axial direction in their in situ positions (Horný et al.; 2011, 2013, 2014b, 2017), the author feels that a work spent in the simulations presented in the thesis would not deliver realistic results if the longitudinal prestretch was neglected (Figure 6 depicts how axial prestretch is manifested and Figure 7 details statistics of age-related changes in the axial prestretch of the human abdominal aorta). To the best of author's knowledge, there is no study considering both effect of nonlinearly elastic perivascular tissue and axial prestretching on the inflation-extension response of the human abdominal aorta.

Thus including the effect of the prestretching is the second goal of the study. From this point of view, one could see the study as the thesis that in general sense of a ward evaluates the effects of boundary conditions of the inflation response and stress state of the human abdominal aorta.

1.3 Why abdominal aorta

This thesis deals with human perivascular adipose tissue surrounding the abdominal aorta. The abdominal aorta is a prominent site where many kinds of often serious pathological conditions are manifested. Typically at old age, it suffers with large atherosclerotic lesions that may obstruct blood flow (see a segment of infrarenal aorta excised in autopsy in Figure 8), by elastocalcinosis of medial layer that adversely affects pressure pulse transition (Greenwald, 2007; Persy and D'Haese, 2009), and it also may be weakened by an aneurysm (Atul et al., 2016). Vu et al. (2014) present that the The AAA growth rate is correlated to its diameter and to the risk of rupture. Abdominal aorta aneurysms of more than 4 cm tend to have a greater growth rate of 3 mm per year. With every 5 mm increase in diameter, there is a 0.5 mm per year increase in growth rate and a doubling of rupture risk. When the aneurysm growth rate exceeds 1 cm per year, the increased rupture risk justifies elective AAA repair (Figure 9). From these reasons, the abdominal aorta is in the center of my biomechanical attention.

Another reason that affected the scope of the thesis is a fact that this location is well-documented with respect not only to available constitutive models for arterial tissue, but there are also papers that document specific values of the axial prestretch of the abdominal aorta. From this point of view my work can be understood as a continuation of the scientific interest for abdominal aorta biomechanics that at the Faculty of Mechanical Engineering of the Czech Technical University lasts more than 10 years.

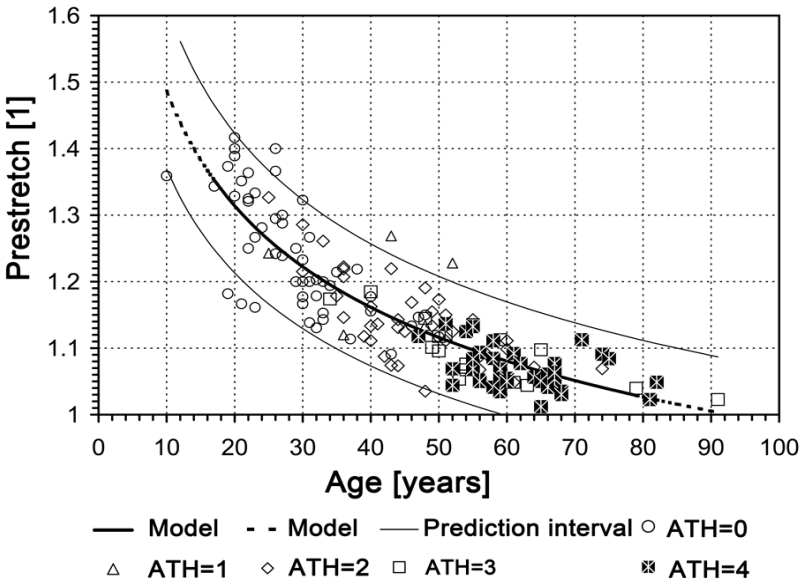

Figure 7. Age-related changes in axial prestretch of the human abdominal aorta with highlighted degree of atherosclerotic lesions. The legend for atherosclerotic changes is as follows: 0 – intact artery and fatty streaks; 1 – fibro-fatty plaques; 2 – advanced plaques; 3 – calcified plaques; 4 – ruptured plaques. Adopted from Horný et al. (2011).

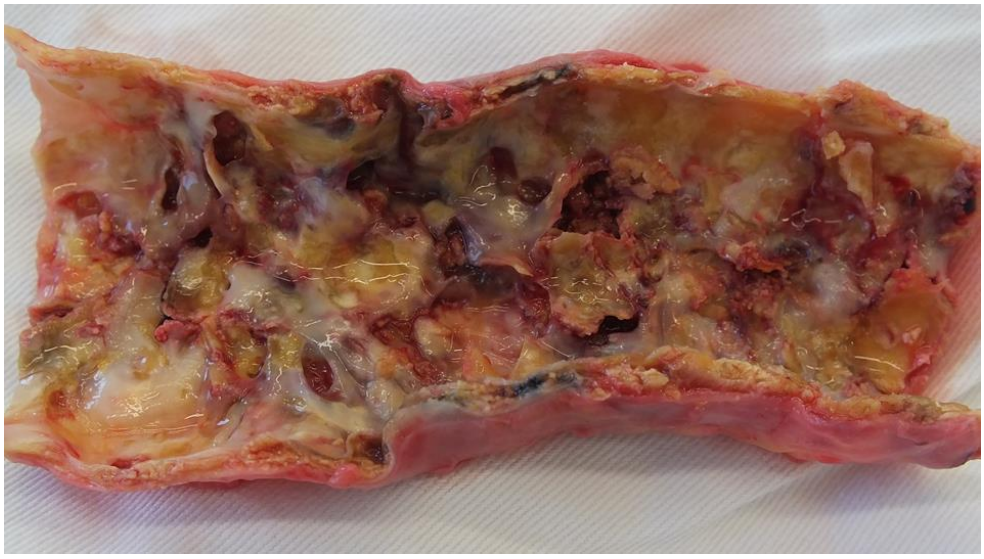

Figure 8. Luminal side of the abdominal aorta of the 70 years old male individual. The sample is totally calcified and ruptured atherosclerotic plaques are clearly distinguishable. The picture was provided by Lukáš Horný (author's advisor) from his personal archive.

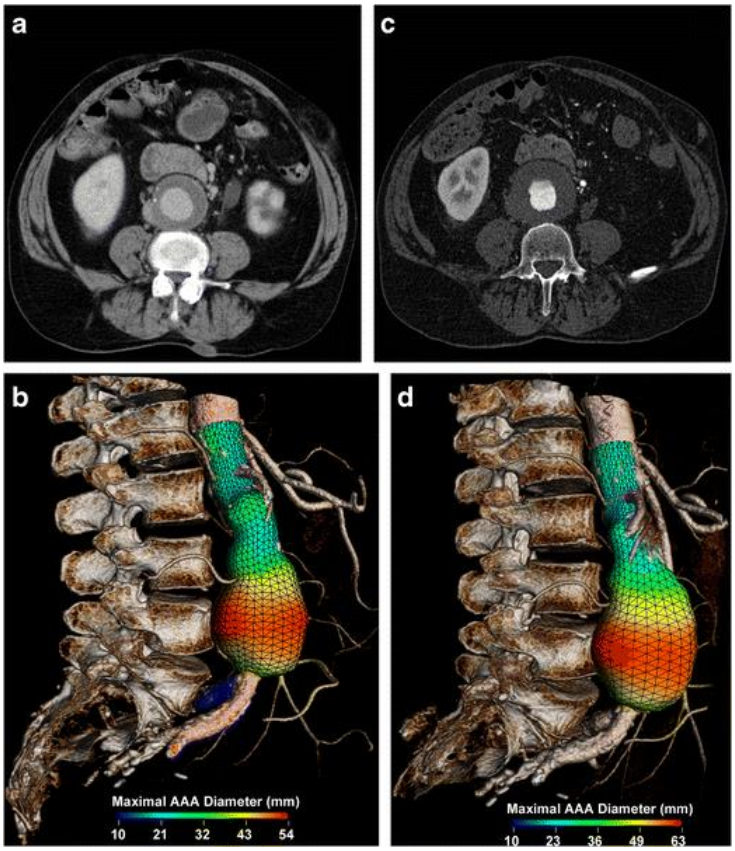

Figure 9. Illustration of the abdominal aorta aneurys growth rate.

a Axial enhanced CT and **b** 3D rendering image with a colour parametric map

c Axial enhanced CT and **d** 3D rendering image with a colour parametric map of the same patient performed a year later shows a 1 cm increase in diameter. Adopted from Vu et al. (2014).

2 Anatomy of the blood vessel and its surroundings

2.1 Individual parts of aorta

The aorta is the largest artery of the human body, with a diameter of 20–30 mm (Figure 10). The aorta distributes oxygenated blood from the left ventricle of the heart to the whole body using a branching artery system. Its four principal divisions are ascending aorta, arch of the aorta, thoracic aorta, abdominal aorta (Čihák, 2004).

2.2 The layers of aorta

The aorta is an elastic tube that transmits blood under high pressure from the heart. The aorta wall includes three structurally different layers (unlike the perivascular space that is filled with thin PVAT lamellas). The aorta layers are adapted to a high pressure (Figure 10; Figure 11; Brown et al., 2014; Paulsen, 2010; Loscalzo, 2010) and are divided to:

- *Tunica externa (tunica adventitia)* is outer layer of the aorta that is composed of a network bundles of collagen fibers, elastic fibers, and fibroblasts. The largest arteries (e.g. aorta and its branches) are containing vasa vasorum. Vasa vasorum is a network of small blood vessels that supply of the walls and serve to provide blood supply and nourishment for tunica adventitia and outer parts of tunica media.

- *External elastic membrane* (for large arteries) is the membrane which separates the tunica externa from the tunica media.

- *Tunica media* is an intermediate layer of arteries which is made of smooth muscle cells that can have both contractile and synthetic phenotype, elastic fibers that are arranged in roughly circular layers, and collagen fibers.

- *Internal elastic membrane* (for large arteries) is the membrane between the tunica media and the tunica intima.

- *Tunica intima* is the innermost layer of the elastic arteries. The layer is made up of endothelial cells which are in direct contact with the blood flow. The endothelium is acting as a semi-permeable membrane (the expression of adhesion molecules and pro-inflammatory cytokines) and affects the vascular tone.

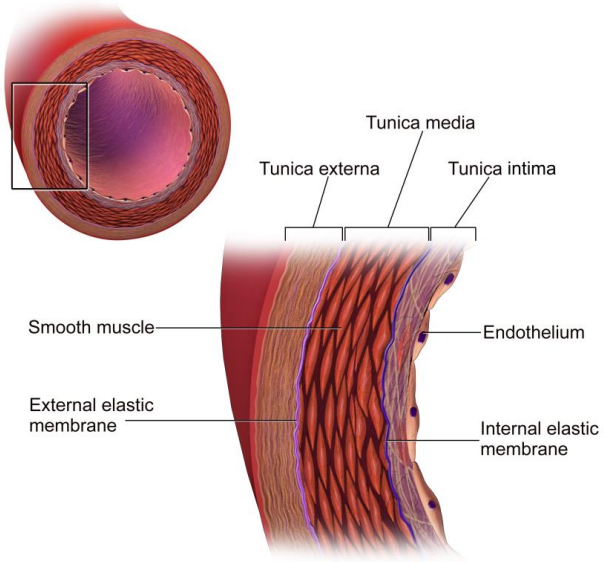

Figure 10. Illustration of the individual layers of the aorta wall. Adopted from https://en.wikiversity.org/wiki/WikiJournal_of_Medicine/Medical_gallery_of_Blausen_Medical_2014

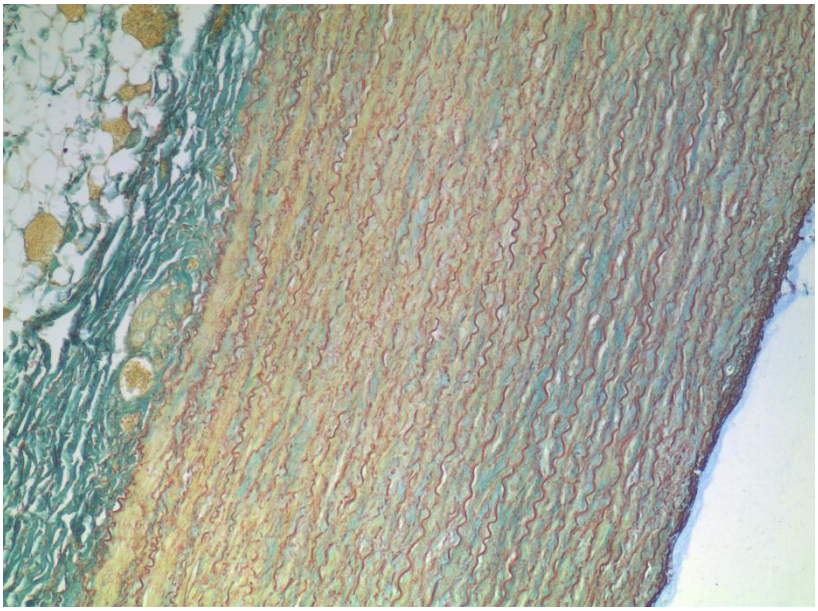

Figure 11. Histologic section of abdominal aorta stained with orcein. On the right is the tunica intima (one row of cells). In the middle is the tunica media. On the left (blue-green color) is the tunica adventitia. Next to tunica adventitia (on the far left), there are adipocyte remains (empty honeycombs) in the fat cover. Honeycombs of yellow color are the remains of red blood cells. The picture was adopted from personal archive.

2.3 Human adipose tissue

The adipose tissue is not only a passive place for energy storage in the form of triglycerides, but is the active organ with producing hormones with paracrine or endocrine activity take place inside. These hormones play an important role in regulating metabolism, control of food intake, inflammatory processes and other phenomena. The adipose tissue is one of the largest endocrine organs in the human body. In the case of obesity and its complications, as is atherosclerosis, type 2 diabetes mellitus, etc., its endocrine function changes significantly (Brown et al., 2014). In the human body existence several types of adipose tissue (Brown et al., 2014).

2.4 Distribution of adipose tissue by location in the human body

Subcutaneous adipose tissue is found in the subcutis and accounts for about 80 % of the total body fat in body (Figure 12 - left). This fat tissue serves as the thermal insulation of the organism and represents a source of energy during fasting (depot fat) and also performs metabolic and endocrine functions. Tissue has an ethological function (secondary sexual features in a woman, etc.). The subcutaneous tissue is less bloody and less innervated than visceral adipose tissue (Brown et al., 2014).

Visceral adipose tissue surrounds all the organs in the abdominal cavity (Figure 12 - left). This adipose tissue is metabolically more active than the subcutaneous fat and produces more adiponectin and less leptin. A higher amount of visceral fat in the abdominal space negative affects functioning of the organs and is associated with cardiovascular complications (Brown et al., 2014).

Perivascular adipose tissue (Figure 12 - right) is surrounding all blood vessels. Its properties will be discussed in 2.7 and 2.8.

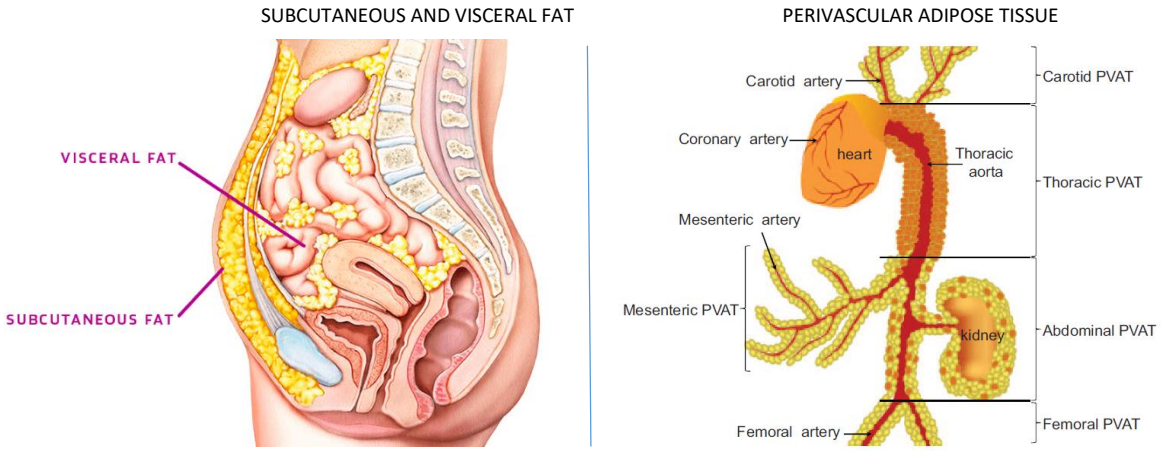

Figure 12. Types of adipose tissue and distribution in the human body.
Left side of figure, adopted from: https://makeyourbodywork.com/how-to-reduce-visceral-fat/.
Right side of figure, adopted from Brown et al., 2014.

2.5 Distribution of adipose tissue according to its composition

Figure 13 show the types of adipose tissue, which are different in composition (Brown et al., 2014).

White adipose tissue (WAT) or subcutaneous and visceral fat. White fat tissue is made up of fat cells with large fat droplets surrounded by a cytoplasmic ring (fat vacuole). The nucleus is located on the periphery of the cell. The stored fat is semi-liquid consistency and consists predominantly of triacylglycerols and cholesterol esters. WAT serves as thermal insulation, protection of internal organs and the energy reservoir. The fatty tissue is not a rigid part of the organism, but is highly metabolic, endocrine and paracrine active. Adipocytes synthesize fats and store them in the form of one large fat drop.

Brown adipose tissue (BAT). This fat is located mainly in neonates and rodents in the interscapular region of the spine, along the spinal cord and towards the shoulders. BAT forms up to 5% of the total weight. In adults people (with the exception of obese individuals), BAT occurs in the upper thorax and neck area. BAT contains several smaller fat droplets. The adipocytes (fat cells) have a high number of mitochondria and cytochromes, but little ATP (adenosine triphosphate) synthase activity. This means that ATP does not occur in the oxidation of glucose, but heat is released. The results is non-shivering thermogenesis. Over time, mitochondria disappear from the brown fat cells and their function begins to resemble the function of white fat tissue. The adipocytes are richly bloody therefore has BAT brown color.

Beige adipose tissue. This mixture of white and brown adipocytes has been classified only recently (Brown et al., 2014). The beige fat cells were recorded in rodents as first. The adipocytes are programmed to be flexible with the ability to store fat and produce heat under various circumstances. The presence of beige and brown fat in humans is still under debate.

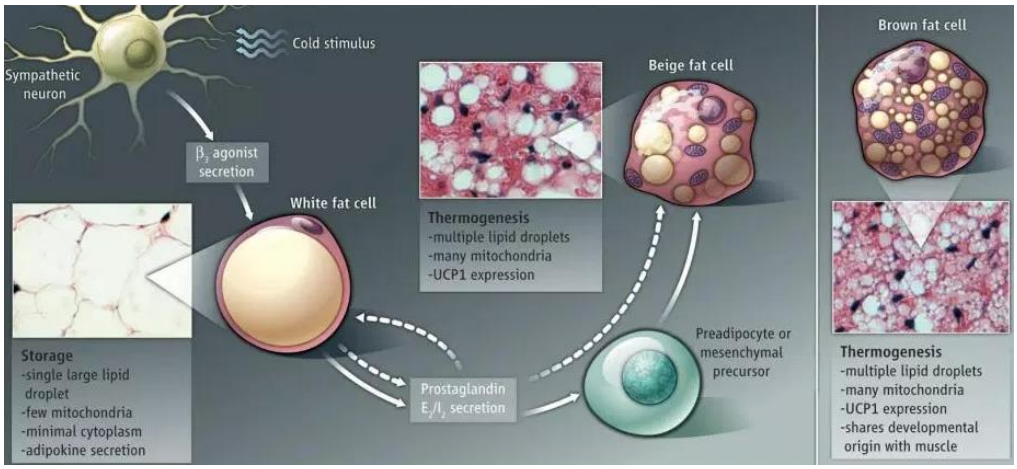

Figure 13. White, brown and beige adipose tissue with their function.
Adopted from http://brownadipose.com/beige-fat/.

2.6 Histology of adipose tissue

The adipose tissue is a complex set of cell types including (Figure 14):

- *Adipocytes (fat cells).* Adipocytes are the main component of adipose tissue and serve as a homeostatic control of whole body metabolism. They check energy balance by storing triglycerol during excess energy and mobilize it during energy deprivation. Triglycerides are the main constituents of body fat and present in the blood to allow glucose move from the liver and are also the main component of human skin (Lampe et al., 1983). Further, they excrete numerous lipid and protein factors. Adipocytes are considered to be the major endocrine organ that has a profound effect on the metabolism of other tissues, appetite regulation, insulin sensitivity, immunological responses, and vascular disease. Fat cells are surrounded by basal lamina and reticular fibers that produce adipokine and cytokine proteins. Adipokins affect the basic processes in the human body - intermediate metabolism, insulin sensitivity, hemocoagulation, immune processes, etc. (Paniagua, 2016).

- *Preadipocytes*, during adipogenesis as fibroblasts, differentiate into mature adipocytes. Adipogenesis can lead to central obesity (abdominal fat) or peripheral obesity (fat in the subcutaneous tissue) (Ali et al., 2018).

- *T-lymfocytes* is a type of lymphocyte (a subtype of white blood cell) that plays a central role in cell-mediated immunity (Alberts et al., 2002).

- *Fibroblast* is the basic cell of the connective tissue dispersed in different parts of the human body that produces extracellular matrix (collagen, etc.).

- *Macrophages* (in every tissue) are actively involved in maintaining tissue homeostasis by clearing cellular debris (Boutens et al., 2016). Macrophages are cells of the immune system that significantly contribute to the functioning of adipose tissue. Macrophages in lean people make up around 5% of the cells in adipose tissue, during obesity they constitute up to 50% of all adipose tissue cells (Weisberg et al., 2003). This cells contribute to the pathophysiological consequences of obesity (insulin resistance, type 2 diabetes, etc.) (Lumeng et al., 2007).

- *Leukocytes* (also called *white blood cells*) are of the immune system cells that are involved in protecting the body against infectious disease and foreign invader (Maton et al., 1997).

- *Blood vessels*.

- *Capillaries.*

- *Collagen fiber network.*

- *Nerves.*

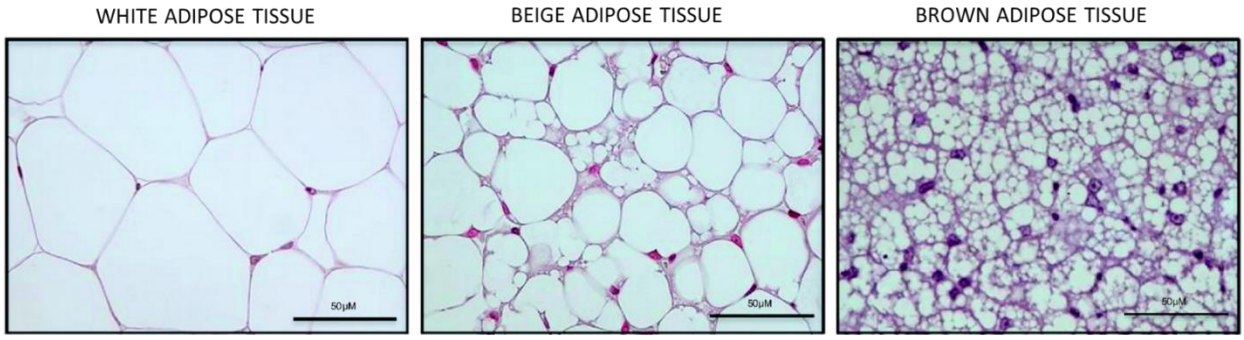

Figure 14. Histology of white, beige and brown adipose tissue (Keipert & Jastroch, 2014).

2.7 Perivascular adipose tissue (PVAT)

PVAT surrounding the aorta located in the retroperitoneal space is depicted in Figure 15 where anatomy of the retroperitoneum is displayed at the level of the kidneys. The anterior pararenal space (APRS) is located between the parietal peritoneum (PP) and the anterior renal fascia (ARF) and contains the pankreas (Pan), the ascending colon (AC), and the descending colon (DC). The posterior pararenal space (PPRS) is located between the posterior renal fascia (PRF) and the the transversalis fascia (TF). The perirenal space (PRS) is located between the anterior renal fascia and the posterior renal fascia. Ao is aorta, IVC is inferior vena cava, LCF is lateroconal fascia (Bhargavi et al., 2015).

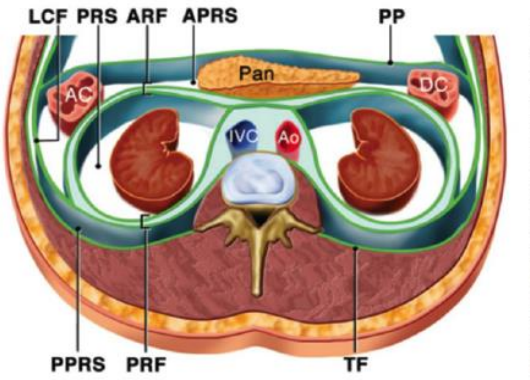

Figure 15. Anatomy of normal retroperitoneal space and structures (Bhargavi et al., 2015).

PVAT can be classified as white adipose tissue (WAT), brown adipose tissue (BAT) and beige adipose tissue. The classification is according to different anatomical locations (Figure 12 - Right). BAT surrounds the thoracic aorta, and WAT surrounds small arteries (mesenteric, carotid and femoral arteries). The abdominal aorta is surrounded by adipose tissue with a mixture of white and brown adipocytes (Brown et al., 2014).

Brown et al. (2014) conducted research on mouse models and found that PVAT may be considered as the fourth type of fat tissue that is different from white, beige and brown fat. Still, there are still no studies submitted to people. However, WAT acts as an endocrine organ and secretes cell signaling

proteins that mediate communication between visceral WAT or subcutaneous WAT and cardiovascular tissues. PVAT is an integral part of the vasculature, it can have immediate and direct effects on the blood vessels it covers.

PVAT secretes metabolically active substances - adipokines, chemokines and hormone-like factors. The adipokines include adiponectin, leptin, and inflammatory cytokines - interleukin-6 (IL-6) and tumor necrosis factor-α (TNF-α) (Brown et al., 2014).

PVAT is a complex, active organ with several functions not only as a mechanical protection of the underlying vascular berth.

2.8 Functions of PVAT

The main function of white adipose tissue (WAT) are shows in the Figure 16A and for brown adipose tissue (BAT) in the Figure 16B (Brown et al., 2014):

- *Mechanical protection* of organs and vessels during contraction (Sazs & Webb, 2012).
- *Vasodilation* caused by relaxation of smooth muscle cells in arteries causes an increase in blood flow. When blood vessels dilate, the blood flow is increased due to a decrease in vascular resistance. Therefore, dilation of arteries and arterioles leads to an immediate decrease in arterial blood pressure and heart rate (Aliya, 2011). Bioactive molecules influence contraction, proliferation and migration of cells. Leptin, resistin and TNF-α can directly affect endothelium function lead to relaxation of blood vessels. These factors are excreted under inflammatory conditions and can reduce vasodilatation (Okamoto et al., 2001).
- *Thermoregulation* has essential value in newborns. The heat production is increase to double. However, in adults is the mechanism significantly lower and allows increased heat production by 10 - 15 % (Chang L., 2012).
- *Modulation of vascular tone*. Similar to the endothelium, PVAT can modulate vascular tone by releasing vasoactive molecules (the adipocyte-derived relaxing factor, NO, prostacyclin, and H_2O_2; Zaborska et al., 2017) which has a direct impact on the mechanical state of the artery.
- *Autocrine and paracrine effect.* PVAT produces several molecules with autocrine or paracrine effects - adipokines such as leptin, adiponectin and resistin, visfatin, hepatic growth factor and others. Adipose tissue is closely associated with inflammation and PVAT releases several cytokines, including TNF-α and interleukin-6. Many of these molecules have effects on the development of atherosclerosis (Sazsz et al., 2013).
- *Endocrine function*. In contrast to the endothelium, PVAT consists of multiple cell types. Besides adipocytes, macrophages, fibroblasts, lymphocytes, and adipocyte progenitor cells are also present in PVAT. The presence of these types of cells suggests the complex endocrine

function of PVAT and its contribution to inflammatory processes occurring in the arterial wall (Zaborska et al., 2017; Brown et al., 2014; Králová Lesná et al., 2015). Considering this, one sees that PVAT is not merely a mechanical support mechanism, nor a simple energy-storing tissue, but it is an element with its own complex mechanobiological role that can affect the onset of various cardiovascular diseases (Huang Cao et al., 2017).

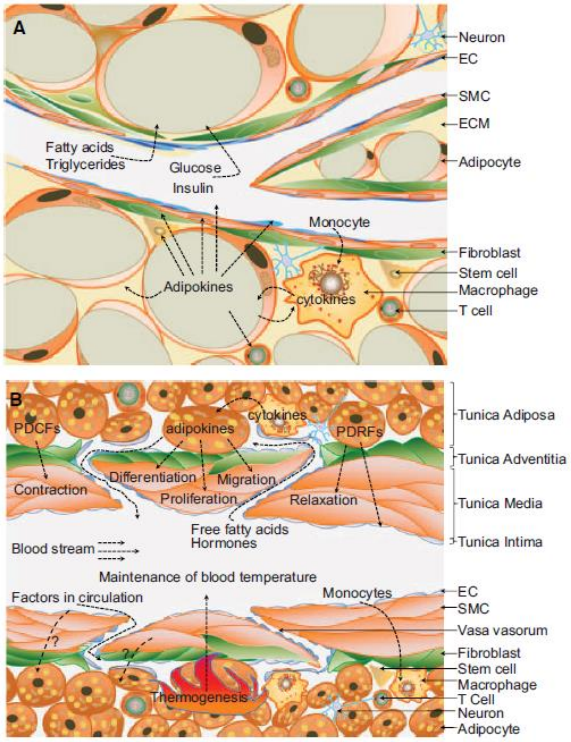

Figure 16. Function of PVAT (Brown et al., 2014). A - white adipose tissue; B - brown adipose tissue.

3 Theoretical foundations of adopted methods

This chapter is written with regard to continuity of definitions and nomenclature used in continuum mechanics. It is known that different authors define some variables differently or use differentnotations. At the same time, this chapter is also suitable for readers who are not familiar with nonlinear elasticity and mechanics at large deformations. The basic inspiration for writing this chapter were monographs of G. A. Holzapfel (Holzapfel, 2000), L. A. Taber (Taber, 2004), D. Humphrey (Humphrey, 2002), and R. W. Ogden (Ogden, 2009).

3.1 Kinematics of the deformation

Let Ω_0 be a reference configuration of the continuous body $\boldsymbol{\beta}$ that is stress-free (Figure 18). The reference configuration Ω_0 is described as a set of material points in three-dimensional space and their positions are given by the Vector $\boldsymbol{X}$. In Cartesian coordinates, the position vector $\boldsymbol{X}$ with components may be described as

$$\boldsymbol{X} = X_I e_I = \sum_{I=1}^{3} X_I e_I \tag{1}$$

where $e_I, I = 1, 2, 3$ are unit base vectors and the Einstein summation convention is used.

After loading each material point $\boldsymbol{X} \in \Omega_0$ of the continuous body $\boldsymbol{\beta}$, $\boldsymbol{X}$ is transformed to a new position $\boldsymbol{x} = \boldsymbol{\chi}(\boldsymbol{X}) \in \Omega$ in the deformed configuration. The position vector $\boldsymbol{x} \in \Omega$ in the deformed configuration is defined as

$$\boldsymbol{x} = x_i e_i, \qquad i = 1, 2, 3. \tag{2}$$

We introduce a displacement vector as a change between the reference and current configuration

$$\boldsymbol{u} = \boldsymbol{x} - \boldsymbol{X} = u_i e_i, \qquad i = 1, 2, 3. \tag{3}$$

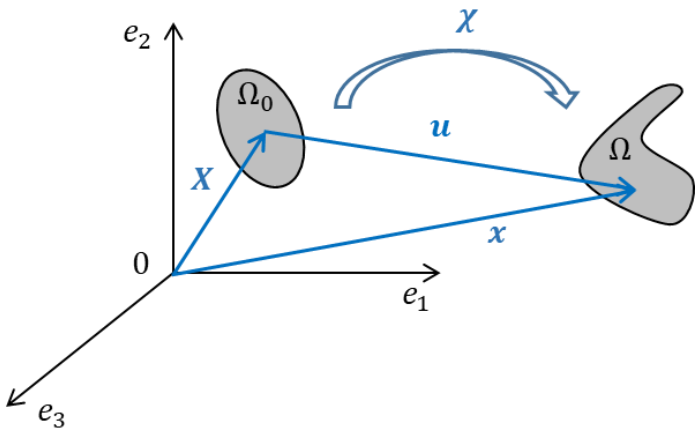

Figure 18. Example of kinematics of finite deformation. Each material point $\boldsymbol{X} \in \Omega_0$ after deformation move to the new position $\boldsymbol{x} \in \Omega$.

A fundamental measure of deformation is described by the deformation gradient **F**. **F** as a second order tensor represents a linear mapping between two vector spaces.

$$\mathbf{F} = \frac{\partial \boldsymbol{\chi}}{\partial \boldsymbol{X}} = \frac{\partial \boldsymbol{x}}{\partial \boldsymbol{X}} = \mathbf{I} + \frac{\partial \boldsymbol{u}}{\partial \boldsymbol{X}}, \tag{4}$$

where **I** is the second order unit tensor. The deformation gradient has nine independent components

$$F_{iJ} = \frac{\partial x_i}{\partial X_J} = \delta_{iJ} + \frac{\partial u_i}{\partial X_J}, \qquad i, J = 1, 2, 3, \tag{5}$$

where δ_{iJ} is the Kronecker delta with cases

$$\delta_{iJ} = 1 \qquad \text{if } i = J$$

$$\delta_{iJ} = 0 \qquad \text{if } i \neq J. \tag{6}$$

The deformation gradient **F** includes rotation and deformation. The polar decomposition of deformation gradient **F** is

$$\mathbf{F} = \mathbf{RU} = \mathbf{vR}, \tag{7}$$

where **R** is the tensor of rotation (a proper orthogonal tensor) , **U** and **v** is the right and left stretch tensor, respectively. **U** and **v** are positive definite ($\boldsymbol{X}.\mathbf{U}\boldsymbol{X} > 0$ and $\boldsymbol{x}.\mathbf{v}\boldsymbol{x} > 0$ for every nonzero $\boldsymbol{X}$ and $\boldsymbol{x}$) and symmetric tensors ($\mathbf{U} = \mathbf{U}^T$ and $\mathbf{v} = \mathbf{v}^T$).

In cylindrical coordinates considering an orthonormal base, the deformation gradient is defined as

$$\mathbf{F} = \begin{pmatrix} \frac{\partial r}{\partial R} & \frac{1}{R}\frac{\partial r}{\partial \Theta} & \frac{\partial r}{\partial Z} \\ r\frac{\partial \theta}{\partial R} & \frac{r}{R}\frac{\partial \theta}{\partial \Theta} & r\frac{\partial \theta}{\partial Z} \\ \frac{\partial z}{\partial R} & \frac{1}{R}\frac{\partial z}{\partial \Theta} & \frac{\partial z}{\partial Z} \end{pmatrix}. \tag{8}$$

3.2 Invariants of the second order tensor

The eigenvalues of **U** (material stretch tensor) and **v** (spatial stretch tensor) are the principal stretches, $\lambda_i (i = 1, 2, 3)$. The principal stretches can be calculated by finding the roots of the characteristic equations

$$\det(\lambda \mathbf{I} - \mathbf{U}) = 0, \qquad \det(\lambda \mathbf{I} - \mathbf{v}) = 0. \tag{9}$$

Let λ_i be the eigenvalues of **U** corresponding to the eigenvectors $\boldsymbol{N_i}$, such that

$$\mathbf{U}\boldsymbol{N_i} = \lambda_i \boldsymbol{N_i}, \qquad i = 1, 2, 3. \tag{10}$$

From (7) it follows

$$\mathbf{v}\mathbf{R}\boldsymbol{N_i} = \mathbf{R}\mathbf{U}\boldsymbol{N_i} = \lambda_i \mathbf{R}\boldsymbol{N_i}, \tag{11}$$

λ_i are also the eigenvalues of **v**, corresponding to the eigenvectors $\mathbf{R}\boldsymbol{N_i}$.

The right (left) Cauhy-Green deformation tensor $\mathbf{C}$ ($\mathbf{B}$) are defined as

$$\mathbf{C} = \mathbf{F}^T\mathbf{F} = \mathbf{U}^2, \qquad \mathbf{B} = \mathbf{F}\mathbf{F}^T = \mathbf{v}^2. \tag{12}$$

where ^{T} is the transpose of the second-order tensor.

The principle invariants of the right Cauchy-Green deformation tensor $\mathbf{C}$ are written in the form (13).

$$I_1 = tr(\mathbf{C}) = \lambda_1^2 + \lambda_2^2 + \lambda_3^2,$$

$$I_2 = \frac{1}{2}\left[\left(tr(\mathbf{C})\right)^2 - tr(\mathbf{C}^2)\right] = \lambda_1^2\lambda_2^2 + \lambda_2^2\lambda_3^2 + \lambda_3^2\lambda_1^2,$$

$$I_3 = det(\mathbf{C}) = \frac{1}{6}\left[\left(tr(\mathbf{C})\right)^3 - 3tr(\mathbf{C})tr(\mathbf{C}^2) + 2tr(\mathbf{C}^3)\right] = \lambda_1^2\lambda_2^2\lambda_3^2. \tag{13}$$

In (13) tr denotes the trace of the second-order tensor.

3.3 Stress

The stress is generated when the body is deformed and is a physical quantity that expresses the internal forces that neighbouring particles of a continuous material exert on each other. The stress has physical dimension force per unit of area.

A deformable continuum body $\boldsymbol{\beta}$ occupying an arbitrary region Ω of physical space with boundary surface $\partial\Omega$ at time t is exposed to arbitrary external loading (Figure 19). An arbitrary external forces act on parts or the whole of the boundary surface, and on surface within the interior of that body (internal forces) in some distributed manner.

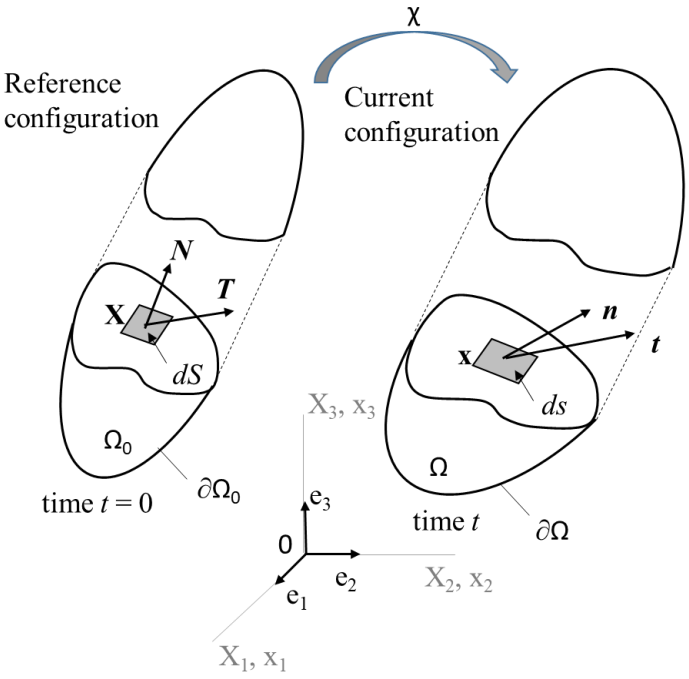

Figure 19. Traction vectors acting on infinitesimal surface elements with outward unit normal. Adopted from Holzapfel (2000).

The body is cut by a plane surface which passes any given point $\mathbf{x} \in \Omega$ with a normal unit vector $\boldsymbol{n}$ (Figure 19). The plane surface separetes the deformable body into two parts. Since we consider interaction of the two portions, forces are transmitted across the internal plane surface. The infinitesimal resultant (actual) force $d\boldsymbol{f}$ is introduced into point $\mathbf{x}$ and action on spatial surface element $ds \in \partial\Omega$ lying on the cut plane. Before motion occured, the continuum body $\boldsymbol{\beta}$ was in the reference (undeformed) configuration at the reference time $t = 0$ and has occupied the region of physical space with boundary surface. The quantities $\mathbf{x}$, ds, and $\boldsymbol{n}$ which are associated with the current (deformed) configuration of the body are denoted by $\mathbf{X}$, dS, and $\boldsymbol{N}$ when they are referred to the reference (undeformed) configuration. It applies to each surface element

$$d\boldsymbol{f} = \boldsymbol{t}ds = \boldsymbol{T}dS, \tag{14}$$

$$\boldsymbol{t} = \boldsymbol{t}(\mathbf{x}, t, \boldsymbol{n}), \qquad \boldsymbol{T} = \boldsymbol{T}(\mathbf{X}, t, \boldsymbol{N}). \tag{15}$$

Here, $\boldsymbol{t}$ is the Cauchy (true) traction vector, exerted on ds with outward normal $\boldsymbol{n}$. The Cauchy traction vector is force measured per unit surface area defined in the current configuration. $\boldsymbol{T}$ represents the first Piola-Kirchhoff (nominal) traction vector, and points in the same direction as the Cauchy traction vector $\boldsymbol{t}$. The first Piola-Kirchhoff traction vector is force measured per unit surface area defined in the reference configuration. The first Piola-Kirchhoff traction vector $\boldsymbol{T}$ act on the region Ω and is a function of the referential position **X** and the outward normal $\boldsymbol{N}$ to boundary surface $\partial\Omega_0$.

Cauchy´s stress theorem. There exist unique second-order tensor fields $\boldsymbol{\sigma}$ and **P** so that

$$\boldsymbol{t}(\mathbf{x}, t, \boldsymbol{n}) = \boldsymbol{\sigma}(\mathbf{x}, t)\boldsymbol{n}, \qquad \boldsymbol{T}(\mathbf{X}, t, \boldsymbol{N}) = \mathbf{P}(\mathbf{X}, t)\boldsymbol{N}, \tag{16}$$

where $\boldsymbol{\sigma}$ represents a symmetric spatial tensor field, the Cauchy (true) stress tensor (or the Cauchy stress). **P** denotes the first Piola-Kirchhoff (nominal) stress tensor (ort he Piola stress).

Cauchy´s stress theorem in the matrix notation is

$$[\boldsymbol{t}] = [\boldsymbol{\sigma}][\boldsymbol{n}], \tag{17}$$

$$[\boldsymbol{t}] = \begin{bmatrix} t_1 \\ t_2 \\ t_3 \end{bmatrix}, \qquad [\boldsymbol{\sigma}] = \begin{bmatrix} \sigma_{11} & \sigma_{12} & \sigma_{13} \\ \sigma_{21} & \sigma_{22} & \sigma_{23} \\ \sigma_{31} & \sigma_{32} & \sigma_{33} \end{bmatrix}, \qquad , \tag{18}$$

where $[\boldsymbol{\sigma}]$ is the Cauchy stress matrix.

The relation between the Cauchy stress tensor $\boldsymbol{\sigma}$ and the first Piola-Kirchhoss stress tensor **P** is expressed as

$$\boldsymbol{t}(\mathbf{x}, t, \boldsymbol{n})ds = \boldsymbol{T}(\mathbf{X}, t, \boldsymbol{N})dS,$$

$$\boldsymbol{\sigma}(\mathbf{x}, t)\boldsymbol{n}ds = \mathbf{P}(\mathbf{X}, t)\boldsymbol{N}dS. \tag{19}$$

Using Nanson's formula ($ds = J\mathbf{F}^{-T}dS$) which shows how the vector element of the infinitesimally small area ds and dS on the current and reference configuration are related, we can obtain the direct relationship between $\boldsymbol{\sigma}$ and **P** as

$$\mathbf{P} = J\boldsymbol{\sigma}\mathbf{F}^{-T}, \tag{20}$$

$$\boldsymbol{\sigma} = J^{-1}\mathbf{P}\mathbf{F}^{T}, \tag{21}$$

$$\mathbf{S} = \mathbf{F}^{-1}\boldsymbol{\sigma}\mathbf{F}^{-T}, \tag{22}$$

where J is volume ratio defined as $J = \det \mathbf{F}$. In equation (22), **S** is the second Piola-Kirchhoff stress.

3.4 Elasticity

For a hyperelastic material, the relationship between an isothermal reversible deformationand the stress response, the stress-strain relationship, is dened through, W, which is a scalar function of the deformation measure. Given W, stresses (the first Piola-Kirchhoff stress **P,** the Cauchy stress tensor **σ,** the second Piola-Kirchhoff stress **S**) are computed by taking a derivatives, for example,

$$\mathbf{P} = \frac{\partial W(\mathbf{F})}{\partial \mathbf{F}}, \tag{23}$$

$$\boldsymbol{\sigma} = 2J^{-1}\frac{\partial W(\mathbf{B})}{\partial \mathbf{B}}\mathbf{B}, \tag{24}$$

$$\mathbf{S} = 2\frac{\partial W(\mathbf{C})}{\partial \mathbf{C}}. \tag{25}$$

Incompressible hyperelasticity. Materials which keep the volume constant throughout a motion are characterized by the incompressibility constraint $J = 1$, for the volume ratio J. In general, a material which is subjected to an internal constraint is referred to as a constrained material.

In order to derive general constitutive equations for incompressible hyperelastic material, we may postulate the strain-energy function

$$W = W(\mathbf{F}) - p(J - 1), \tag{26}$$

the scalar p serve as an indeterminate Lagrange multiplier, which can be identified as a hydrostatic pressure. p may be determined only from boundary conditions. It represents a workless reaction to the kinematic constrain on the deformation field.

The constitutive equations (the first Piola-Kirchhoff stress **P,** the Cauchy stress tensor **σ,** the second Piola-Kirchhoff stress **S**) used to define incompressible hyperelastic materials at finite strains are

$$\mathbf{P} = -p\mathbf{F}^{-T} + \frac{\partial W(\mathbf{F})}{\partial \mathbf{F}}, \tag{27}$$

$$\boldsymbol{\sigma} = -p\mathbf{I} + \frac{\partial W(\mathbf{F})}{\partial \mathbf{F}}\mathbf{F}^{T}, \tag{28}$$

$$\mathbf{S} = -p\mathbf{C}^{-1} + 2\frac{\partial W(\mathbf{C})}{\partial \mathbf{C}}. \tag{29}$$

3.5 Models of the strain energy density

The hyperelastic material models are used for predicting the nonlinear stress-strain behavior of materials undergoing large deformations.

The neo-Hooke model. The basic model in rubber elasticity is the neo-Hooke model. The strain energy density function is linear function of the first invariant and for an incompressible neo-Hookean material is

$$W = c_1(I_1 - 3), \tag{30}$$

where $c_1 = \frac{\mu}{2}$. μ is a positive constant representing the shear modulus of the material in the reference configuration. I_1 is the first invariant of the right Cauchy-Green deformation tensor.

The Mooney-Rivlin model. The Mooney-Rivlin model is a hyperelastic material model where the strain energy density function $W = W(I_1, I_2)$ is linear combination of two strain invariants

$$W = c_1(I_1 - 3) + c_2(I_2 - 3), \tag{31}$$

with constants $c_1 = \frac{\mu_1}{2}$, $c_2 = -\frac{\mu_2}{2}$. The shear modulus μ has the value $\mu_1 - \mu_2$.

The Ogden model. The strain energy function of the principal stretches $\lambda_i (i = 1, 2, 3)$ plays crucial role in the theory of finite elasticity. The Ogden model describes the change of the principal stretches from the reference to the current configuration and has form

$$W = W(\lambda_1, \lambda_2, \lambda_3) = \sum_{p=1}^{N} \frac{\mu_p}{\alpha_p} \left(\lambda_1^{\alpha_p} + \lambda_2^{\alpha_p} + \lambda_3^{\alpha_p} - 3\right), \tag{32}$$

where N, μ_p, and α_p are material constants with condition

$$2\mu = \sum_{p=1}^{N} \mu_p \alpha_p \qquad \text{with} \qquad \mu_p \alpha_p > 0, \qquad p = 1, \dots, N, \tag{33}$$

where the parameter μ denotes the classical shear modulus in the reference configuration. N is a positive integer which determines the number of terms in the strain-energy function. μ_p are shear moduli and α_p are dimensionless constant.

The Fung-type exponential models. The strain-energy functions are based directly on the Green-Lagrange strain tensor $\mathbf{E}$ $\left(\mathbf{E} = \frac{\mathbf{C}-\mathbf{I}}{2}\right)$ rather than on invariants. These are all special cases of the strain-energy function given by

$$W = \frac{1}{2} c(e^Q - 1), \tag{34}$$

where typically Q is quadratic forms of Green-Lagrange strains, which may be written in the general form

$$Q = (\boldsymbol{C}\mathbf{E}).\mathbf{E} = C_{ijkl} E_{ij} E_{kl}, \tag{35}$$

c (>0) is a material constant with dimensions of stress, and $\boldsymbol{C}$ is a dimensionless constant fourth-order tensor having the major and minor symmetries

$$C_{ijkl} = C_{klij} = C_{ijlk}. \tag{36}$$

3.6 Equilibrium equations

In the absence of body forces, the local form of equilibrium equations is

$$\text{div}\,(\boldsymbol{\sigma}) = 0, \tag{37}$$

where div $(\bullet)$ denotes the spatial divergence of the spatial field $(\bullet)$. From the momentum balance equation implies the law of coupled shear stresses. Local equations of equilibrium in cylindrical coordinates (r, θ, z) can be written in components as follows

$$\frac{\partial \sigma_{rr}}{\partial r} + \frac{1}{r}\frac{\partial \sigma_{r\theta}}{\partial \theta} + \frac{\partial \sigma_{rz}}{\partial z} + \frac{\sigma_{rr} - \sigma_{\theta\theta}}{r} = 0,$$

$$\frac{\partial \sigma_{r\theta}}{\partial r} + \frac{1}{r}\frac{\partial \sigma_{\theta\theta}}{\partial \theta} + \frac{\partial \sigma_{\theta z}}{\partial z} + 2\frac{\sigma_{r\theta}}{r} = 0,$$

$$\frac{\partial \sigma_{rz}}{\partial r} + \frac{1}{r}\frac{\partial \sigma_{\theta z}}{\partial \theta} + \frac{\partial \sigma_{zz}}{\partial z} + \frac{\sigma_{rz}}{r} = 0. \tag{38}$$

Equilibrium equations for thick-walled tube. Assuming zero shear stress and independence of the solution from the axial coordinate and the azimuthal coordinate, the equilibrium equation considering the boundary conditions $(\sigma_{rr}(r_i) = -P, \sigma_{rr}(r_o) = 0)$ can be integrated into the form

$$P = \int_{r_i}^{r_o} \lambda_{\theta\Theta} \frac{\partial \widehat{W}}{\partial \lambda_{\theta\Theta}} \frac{dr}{r}, \tag{39}$$

$$F_{red} = \pi \int_{r_i}^{r_o} \left(2\lambda_{zZ} \frac{\partial \widehat{W}}{\partial \lambda_{z\mathrm{Z}}} - \lambda_{\theta\Theta} \frac{\partial \widehat{W}}{\partial \lambda_{\theta\Theta}}\right) r dr, \tag{40}$$

here $\widehat{W}$ denotes W with radial stretch being substituted from the incompressibility condition. Here P denotes internal pressure and F_{red} is the reduced axial (prestretching) force acting on the closed end of the tube additionally to the force generated by the pressure acting on the end. Proves of the equation (39) and (40) can be found for instance in Horný (2015) and Matsumoto and Hayashi (1996). The analytical model of a thick-walled tube can be used for closing a cut ring of an artery into cylidrical geometry and subsequent inflation and extension of such a tube. This will form a theoretical basis of the model used in following chapters.

4 Aim of the Study

It is clear from above mentioned that the abdominal aorta is a prominent site where various diseases can develop. They can change blood flow in the aorta substantially or even can threaten patient's life due to purely mechanical events like aneurysm rupture. **Thus from biomechanical point of view, the abdominal aorta still needs scientific attention. Particularly, its boundary conditions – perivascular tissue-aorta force interaction and axial prestretch – seem to be scientifically undervalued. This thesis is written with an aim to contribute to fill this gap.** Its objectives are as follow.

This work aims to confirm the significant influence of boundary conditions on the mechanical condition of the abdominal aorta. To confirm this hypothesis was considered:

1. mechanical interaction of the abdominal aorta with human perivascular adipose tissue on its outer radius in order to obtain that it is necessary

- **to identify mechanical properties by perform experiments with human perivascular adipose tissue,**

- **to identify constitutive model of perivascular adipose tissue and then it is necessary to create analytical model by simulation of inflation-extension test of bilayer tube (abdominal aorta surrounded by perivascular adopise tissue).**

2. application of axial prestretch on ends of the abdominal aorta which is surrounding by perivascular adipose tissue in order to achieve investigation under realistic conditions.

5 Materials and Methods

5.1 Tensile testing of adipose tissue

Samples. Specimens were obtained from cadavers autopsied in the Department of Forensic Medicine of Královské Vinohrady University Hospital in Prague. The post-mortem usage of human tissue was approved by the Ethics Committee of the Third Faculty of Medicine of Charles University in Prague. Figure 20 shows the aorta surrounded by adipose tissue. Approximately rectangular strips with typical dimensions of 10 mm x 10 mm x 50 mm were prepared using a scalpel. The reference dimensions of the samples were determined by an image analysis of digital photographs (NIS-Elements, Nikon Instruments). Due to high compliance and the slipperiness of the tissue, it was not possible to perfectly align the strips in either circumferential or longitudinal directions [Voňavková and Horný, 2020; Vonavkova et al., 2015; Voňavková et al., 2014].

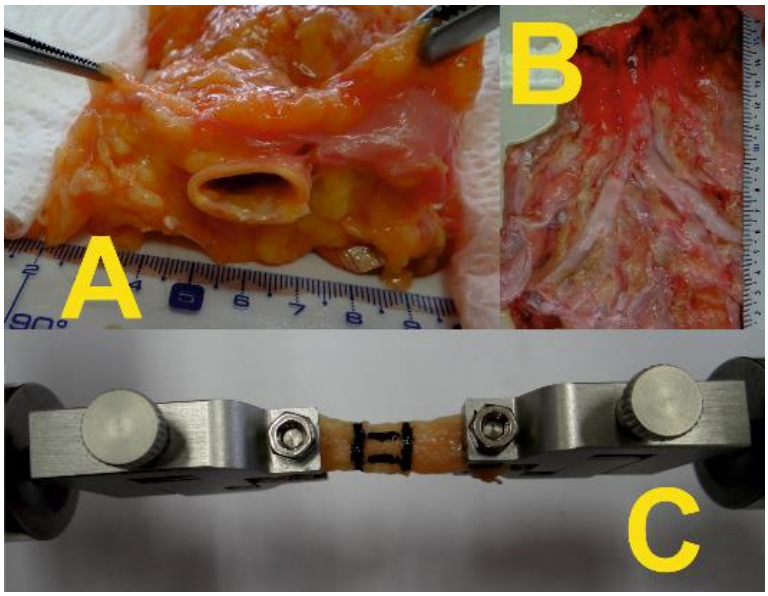

Figure 20. Perivascular tissue surrounds infrarenal aorta – transversal plane (panel A), frontal plane (panel B). A sample of PVAT in uniaxial tension (panel C).
Adopted from [Voňavková and Horný, 2020; Vonavkova et al., 2015; Voňavková et al., 2014].

Testing procedure. A multipurpose tensile testing machine (Zwick/Roell, Germany) was used (Figure 21). The testing machine used electromechanical actuators with a displacement resolution of ± 1 μm and U9B force transducers (HBM, Germany, ± 25 N). During the test, the deformation of samples was determined with a built-in videoextensometer by means of contrasting marks created on a sample with liquid eyeliner. The experimental protocol consisted of four cycles as a preconditioning of tissue behavior, and the fifth cycle was used in the subsequent determination of the material parameters. The loading part of the force–elongation response was used for this purpose. All tests were conducted at room temperature with the velocity of clamps set to 0.2 mms^{-1} [Voňavková and Horný, 2020; Vonavkova et al., 2015; Voňavková et al., 2014].

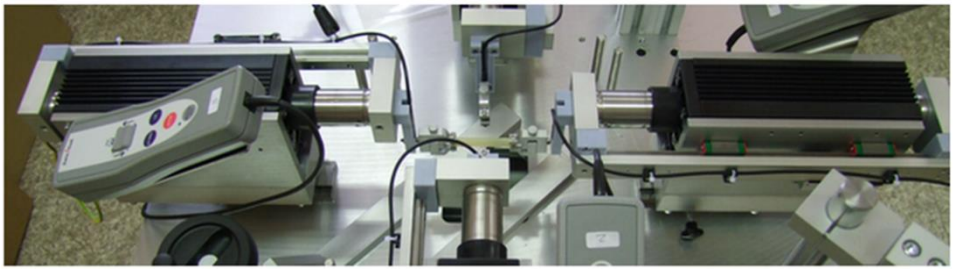

Figure 21. The multipurpose testing machine for uniaxial tensile test.
Adopted from [Vonavkova et al., 2015].

5.2 PVAT constitutive model and its parameters

Kinematics. It was assumed that during the uniaxial tensile test, the portion of the sample restricted by marks undergoes homogenous dilatation expressed in Cartesian coordinates as $x_i = \lambda_{iK} X_K$ for $i, K = 1, 2, 3$ where $\lambda_{iK} = 0$ for $i \neq K$. Here $\boldsymbol{X} = (X_1, X_2, X_3)^T$ and $\boldsymbol{x} = (x_1, x_2, x_3)^T$ respectively denote the position vector in the reference and in the deformed configuration. Due to high lipid content in the adipose tissue, it is assumed that PVAT is incompressible (Comley and Fleck, 2010; Sommer et al., 2013), thus $det(\mathbf{F}) = 1$ holds during the deformation. During uniaxial tensile test, the deformation gradient **F** of isotropic material undergoing isochoric deformation has a form as follows [Voňavková and Horný, 2020; Vonavkova et al., 2015; Voňavková et al., 2014].

$$\mathbf{F} = \begin{pmatrix} \lambda_{11} & 0 & 0 \\ 0 & \lambda_{22} & 0 \\ 0 & 0 & \lambda_{33} \end{pmatrix} = \begin{pmatrix} \lambda_{11} & 0 & 0 \\ 0 & 1/\sqrt{\lambda_{11}} & 0 \\ 0 & 0 & 1/\sqrt{\lambda_{11}} \end{pmatrix} \tag{41}$$

Constitutive model. Since our aim was to use data characterizing PVAT in time-independent (quasi-static) simulations of the inflation-extension behavior of the abdominal aorta, we restricted our attention to the elastic response of PVAT. This means that viscoelastic effects like stress relaxation and creep, which may accompany in vivo pressure wave propagation, are neglected here. Thus perivascular adipose tissue was considered to be hyperelastic (Sommer et al., 2013; Omidi et al., 2014). It was characterized with the strain energy density function expressed in (42). Here c_1, and c_2 denote stress-like material parameters, and I_1 is the first invariant of the right Cauchy-Green deformation tensor **C**. The isotropic elastic potential (41) was chosen in accordance with Omidi et al. (2014). An assumption of isotropy was adopted, because we were not able to perfectly align samples with their anatomical directions [Voňavková and Horný, 2020].

$$W_{\mathrm{PT}} = c_1(I_1 - 3) + c_2(I_1 - 3)^2 \tag{42}$$

The hyperelastic constitutive equation for incompressible material is given by (43), cf. with (28). Here σ denotes the Cauchy stress tensor, and **I** is the second order unit tensor. The symbol p denotes the

indeterminate multiplier related to the hydrostatic part of the stress tensor [Voňavková and Horný, 2020].

$$\boldsymbol{\sigma} = \frac{\partial W_{\mathrm{PT}}}{\partial \mathbf{F}} \mathbf{F}^{\mathrm{T}} - p\mathbf{I} \tag{43}$$

Regression analysis. Experimental stress was obtained as $\sigma_{11}^{EXP} = F\lambda_{11}/S$, where S denotes the reference cross-section area and F is the force elongating the sample from reference length L to deformed length l; $\lambda_{11} = l/L$. The stress predicted by the model, σ_{11}^{MOD}, is obtained from (43), and its final expression is given in (44) [Voňavková and Horný, 2020].

$$\sigma_{11}^{MOD} = 2\left(c_1 + 2c_2\left(\lambda_{11}^2 + \frac{2}{\lambda_{11}} - 3\right)\right)\left(\lambda_{11}^2 - \frac{1}{\lambda_{11}}\right) \tag{44}$$

5.3 Constitutive model for abdominal aorta

The abdominal aorta wall was modeled as a homogenous, anisotropic, incompressible and hyperelastic continuum characterized by the strain energy density function W_A proposed by Gasser et al. (2006). It is expressed in (45) [Voňavková and Horný, 2020; Vonavkova et al., 2016].

$$W_A = W_{\mathrm{isotropic}} + W_{\mathrm{anisotropic}} = \frac{\mu}{2}(I_1 - 3) + \sum_{i=4,6}\left(\frac{k_1}{2k_2} e^{k_2(K_j-1)^2} - 1\right) \tag{45}$$

$$K_j = \kappa I_1 + (1 - 3\kappa)I_i, \;\; i = 4, 6 \tag{46}$$

The elastic potential (45) consists of an isotropic part, it is a neo-Hookean term depending on the first invariant of $\mathbf{C}$, and an anisotropic exponential part that depends on generalized structural deformation invariants denoted K_4 and K_6. The isotropic part is related to the elastic energy stored in the non-collagenous part of the arterial wall, whereas the anisotropic part is linked to the energy stored in bundles of collagen fibers. Since these fibers have a stochastic wavy pattern, their recruitment into the load-bearing process results in the strain-stiffening response, which is well described by an exponential function (Holzapfel et al., 2000). The model is based on the assumption that bundles of collagen fibers are arranged in the arterial wall with two dominant helices wound around the longitudinal axis at angles of $\pm(90° - \beta)$ (Figure 22). These helices can be in cylindrical coordinates (R, Θ, Z) characterized with unit vectors $\boldsymbol{M}_1 = \left(0, cos(\beta), sin(\beta)\right)^T$, $\boldsymbol{M}_2 = \left(0, cos(-\beta), sin(-\beta)\right)^T$. These preferred directions give rise to deformation invariants I_4 and I_6 according to (47) [Voňavková and Horný, 2020; Vonavkova et al., 2016].

$$I_4 = M_1(CM_1) = M_2(CM_2) = I_6 \tag{47}$$

In fact, however, the collagen fibers are not perfectly aligned with the directions $\boldsymbol{M}_1$ and $\boldsymbol{M}_2$. Rather, they exhibit some dispersion around the predominant directions. The used strain energy function takes

this into account by using generalized structural invariants K_4 and K_6 that also include a contribution from invariant I_1. Nevertheless, it is worth noting that, although the model (45) enables structural interpretation, in fact it is a phenomenological model, and its parameters should not be confused with the exact internal architecture of the arterial wall [Voňavková and Horný, 2020; Vonavkova et al., 2016].

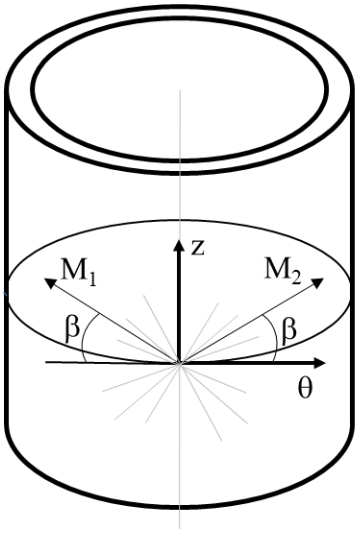

Figure 22. Two preferred directions of collagen fibers $\boldsymbol{M}_1$ and $\boldsymbol{M}_2$ with angles β.

5.4 Simulation of the inflation-extension behavior of the abdominal aorta with PVAT

Geometry and kinematics. The abdominal aorta was modeled as a homogenous thick-walled tube with the reference geometry corresponding to an open cylinder to take into account circumferential residual strains (Horný et al., 2014 a, b). Hence in the first step, the reference stress-free opened cylinder is closed to form a hollow cylinder. The kinematics in polar cylindrical coordinates is expressed in equations (48a, b, c). (ρ, ϑ, ζ) are coordinates defined in the stress-free configuration, whereas (R, Θ, Z) are defined in the residually stressed but unpressurized state. In equations (48b) and (48c), α is the opening angle, and δ is the axial stretch accompanying closing into a cylindrical geometry [Voňavková and Horný, 2020; Vonavkova et al., 2016].

$$R = R(\rho) \tag{48a}$$

$$\Theta = 2\pi/(2\pi - 2\alpha)\vartheta \tag{48b}$$

$$Z = \delta\zeta \tag{48c}$$

Subsequently, the aorta is elongated by axial force F_{red} to reach its in situ length, and inflation by internal pressure P follows. During pressurization, the aorta can further elongate or shorten, and that is governed by equilibrium equations. In (49a, b, c), the deformed configuration is expressed in the polar cylindrical coordinates (r, θ, z) [Voňavková and Horný, 2020].

$$r = r(R) \tag{49a}$$

$$\theta = \Theta \tag{49b}$$

$$z = \lambda Z \tag{49c}$$

The total deformation gradient of the aorta F_A is then given as $F_A = F_{A2}F_{A1}$, where F_{A1} is linked to the residual deformation and F_{A2} expresses subsequent inflation and extension. The matrices of the gradients are given in (50), (51) and (52) [Voňavková and Horný, 2020; Vonavkova et al., 2016].

$$F_A = F_2F_1 = \begin{pmatrix} \lambda_{r\rho} & 0 & 0 \\ 0 & \lambda_{\theta\vartheta} & 0 \\ 0 & 0 & \lambda_{z\zeta} \end{pmatrix} = \begin{pmatrix} \frac{\partial r}{\partial \rho} & 0 & 0 \\ 0 & \frac{\pi r}{[\rho(\pi-\alpha)]} & 0 \\ 0 & 0 & \lambda\delta \end{pmatrix} \tag{50}$$

$$F_{A1} = \begin{pmatrix} \lambda_{R\rho} & 0 & 0 \\ 0 & \lambda_{\Theta\vartheta} & 0 \\ 0 & 0 & \lambda_{Z\zeta} \end{pmatrix} = \begin{pmatrix} \frac{\partial R}{\partial \rho} & 0 & 0 \\ 0 & \frac{\pi R}{[\rho(\pi-\alpha)]} & 0 \\ 0 & 0 & \delta \end{pmatrix} \tag{51}$$

$$F_{A2} = \begin{pmatrix} \lambda_{rR} & 0 & 0 \\ 0 & \lambda_{\theta\Theta} & 0 \\ 0 & 0 & \lambda_{zZ} \end{pmatrix} = \begin{pmatrix} \frac{\partial r}{\partial R} & 0 & 0 \\ 0 & \frac{r}{R} & 0 \\ 0 & 0 & \lambda \end{pmatrix} \tag{52}$$

To account for the effect of perivascular tissue on the mechanics of the aorta, it is assumed that during its inflation and extension the aorta is surrounded by an external cylindrical layer composed of PVAT. $R_{oA} = R_{iPT}$ and $r_{oA} = r_{iPT}$ hold during the deformation. Here R_{iPT} and r_{iPT} denote the reference and deformed inner radius of the PVAT cylinder, Figure 23. It is assumed that the PVAT cylinder retains its cylindrical shape in the deformation, thus its deformation gradient has a form similar to F_{A2} [Voňavková and Horný, 2020; Vonavkova et al., 2016].

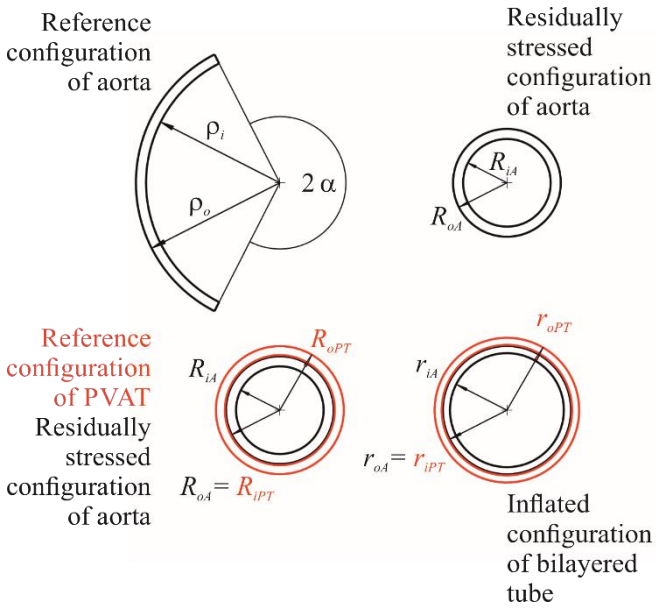

Figure 23. Reference and deformed configurations.
Adopted from [Voňavková and Horný, 2020].

Equilibrium equations. Equilibrium equations for the bi-layered tube can be written in the forms (53), (54). For the convenience of readers, the author remind that $\widehat{W}$ denotes W with radial stretch being substituted from the incompressibility condition. W_A represents the strain energy stored in the aorta (45), and W_{PT} denotes the energy stored in PVAT (42) [Voňavková and Horný, 2020; Vonavkova et al., 2016].

$$P = P_A + P_{PT} = \int_{r_{iA}}^{r_{oA}} \lambda_{\theta\vartheta} \frac{\partial \widehat{W}_A}{\partial \lambda_{\theta\vartheta}} \frac{dr}{r} + \int_{r_{iPT}}^{r_{oPT}} \lambda_{\theta\Theta} \frac{\partial \widehat{W}_{PT}}{\partial \lambda_{\theta\Theta}} \frac{dr}{r} \tag{53}$$

$$F_{red} = F_{red\,A} + F_{red\,PT} =$$

$$= \pi \int_{r_{iA}}^{r_{oA}} \left(2\lambda_{z\zeta} \frac{\partial \widehat{W}_A}{\partial \lambda_{z\zeta}} - \lambda_{\theta\vartheta} \frac{\partial \widehat{W}_A}{\partial \lambda_{\theta\vartheta}} \right) r dr + \pi \int_{r_{iPT}}^{r_{oPT}} \left(2\lambda_{zZ} \frac{\partial \widehat{W}_{PT}}{\partial \lambda_{zZ}} - \lambda_{\theta\Theta} \frac{\partial \widehat{W}_{PT}}{\partial \lambda_{\theta\Theta}} \right) r dr \tag{54}$$

Equations (53) and (54) assume that the boundary conditions $\sigma_{rr}(r_{iA}) = -P \wedge \sigma_{rr}(r_{oPT}) = 0$ hold. The tube is considered to be closed, and F_{red} is an additional axial force which ensures the initial axial stretch $\left(\lambda_{z\zeta}^{ini}\right)$ and which the aorta sustains independently of internal pressure P (Horný et al., 2013, 2014b, 2017) [Voňavková and Horný, 2020; Vonavkova et al., 2016].

5.5 Stress distribution through the wall

To evaluate stress distribution through the wall, equations (55-60) have been adopted. To be accurate, it has to be noted that the form expressed in (55), (56), and (57) applies for the stress within the aorta. The equations (58), (59), and (60) show stresses acting in PVAT [Voňavková and Horný, 2020; Vonavkova et al., 2016].

$$\sigma_{rrA}(r) = -\int_r^{r_{oA}} \lambda_{\theta\vartheta} \frac{\partial \widehat{W}_A}{\partial \lambda_{\theta\vartheta}} \frac{dx}{x} - \int_{r_{iPT}}^{r_{oPT}} \lambda_{\theta\Theta} \frac{\partial \widehat{W}_{PT}}{\partial \lambda_{\theta\Theta}} \frac{dx}{x} \tag{55}$$

$$\sigma_{\theta\theta A}(r) = \lambda_{\theta\vartheta} \frac{\partial \widehat{W}_A}{\partial \lambda_{\theta\vartheta}} + \sigma_{rrA} \tag{56}$$

$$\sigma_{zzA}(r) = \lambda_{z\zeta} \frac{\partial \widehat{W}_A}{\partial \lambda_{z\zeta}} + \sigma_{rrA} \tag{57}$$

$$\sigma_{rrPT}(r) = -\int_r^{r_{oPT}} \lambda_{\theta\Theta} \frac{\partial \widehat{W}_{PT}}{\partial \lambda_{\theta\Theta}} \frac{dx}{x} \tag{58}$$

$$\sigma_{\theta\theta PT}(r) = \lambda_{\theta\Theta} \frac{\partial \widehat{W}_{PT}}{\partial \lambda_{\theta\Theta}} + \sigma_{rrPT} \tag{59}$$

$$\sigma_{zzPT}(r) = \lambda_{zZ} \frac{\partial \widehat{W}_{PT}}{\partial \lambda_{zZ}} + \sigma_{rrPT} \tag{60}$$

5.6 Thickness of PVAT, loading conditions and material parameters

***PVAT thickness*.** With regard to the amount of fat tissue, anatomical variations in the human population are rather large. To take this fact into account, three representative thicknesses of the PVAT layer were considered in the present simulations. These cases were chosen with reference to the thickness of the aorta such that:

(I) represents a very thin fat layer with 0.20 mm $= H_{PT} << R_{oA} - R_{iA}$,
(II) 1.22 mm $= H_{PT} = R_{oA} - R_{iA}$ is the middle case, and
(III) $R_{oA} - R_{iA} << H_{PT} =$ 40 mm represents a situation in which the movement of aorta is significantly restricted by surrounding tissue.

Loading. External loading during the inflation-extension response of the aorta is represented by internal pressure P and the initial axial stretch $\lambda_{z\zeta}^{ini}$ that the aorta sustains independently of pressure. To account for prestretch, F_{red} necessary to elongate the aorta to $\lambda_{z\zeta}^{ini}$ was computed at $P = 0$. In the subsequent pressurization from 0 up to 16 kPa, F_{red} was held constant, which ensured that $\lambda_{z\zeta}$ would vary during inflation. Values where $\lambda_{z\zeta}^{ini} = 1, 1.1,$ and 1.2 were considered in study [Voňavková and Horný, 2020].

***Material parameters for the aorta and PVAT*.** The material parameters for the abdominal aorta were adopted from Horný et al. (2014a). Two representative samples, one of a 38-year-old male donor (denoted M38), and another of a 63 year-old female donor (denoted F63), were considered. The specific values of the material parameters are provided in Table 1. In contrast to aortic tissue, the PVAT parameters are based on author's experiments. In the inflation-extension simulation, average perivascular tissue behavior was considered. Since the constitutive equation for PVAT is nonlinear, the

material parameters used in the study were fitted to all the data to obtain a mean model. Such an approach takes into account the effects of all observed responses and naturally produces a model which can be considered an average model [Voňavková and Horný, 2020; Vonavkova et al., 2016].

Table 1. Constitutive parameters and geometry of the human abdominal aorta. Adopted from Horný et al. (2014a).

	Sex	Age [years]	μ [kPa]	k_1 [kPa]	k_2 [–]	κ [–]	β [°]	ρ_i [mm]	ρ_o [mm]	α [°]	R_{iA} [mm]	R_{oA} [mm]
M38	Male	38	15.9	78.49	4.99	0.19	41.41	16.2	17.24	117	5.3	6.52
F63	Female	63	28.78	113.8	5.953	0.17	38.99	12.10	13.06	96	5.4	6.36

5.7 W_{PT} parameters of PVAT estimation

The experimental data of PVAT was used in the nonlinear regression to obtain estimates of material parameters c_1 and c_2 for W_{PT} (42). The material parameters were obtained by the method of least squares applied to the sum of squared residuals (61). The objective function Q (61) was minimized in Maple (Maplesoft, Waterloo, Canada) employing the NLPSolve command.

$$Q = \sum_n \left(\sigma_{11,n}^{MOD} - \sigma_{11,n}^{EXP}\right)^2, \tag{61}$$

where n is the number of observation points. $\sigma_{11,n}^{MOD}$ and $\sigma_{11,n}^{EXP}$ are listed in Chapter 5.2.

5.8 Simulation of inflation-extension test

The material and reference geometrical parameters of abdominal aorta (μ, k_1, k_2, κ and β for W_A; ρ_i, ρ_o, α, R_{iA} and R_{oA} for geometry) are presented in Table 1 and will be used to generate mechanical response. The material parameters of PVAT (c_1 and c_2) were obtained as described in the chapter 5.7. The reference geometrical parameters (H_{PT}) are listed in the chapter 5.6.

The simulation of inflation-extension test was performed in several steps:

1. The simulation of circumferential residual strains of aorta. The reference stress-free opened cylinder is closed to form a hollow cylinder at $P_A = 0$ and $F_{red_A} = 0$.

2. The closed tube is now considered together with the second outer layer (with PVAT), i.e. arises bilayer tube. The outer layer has no effect on stress and strain. The layers are only attached together without loading and $R_{oA} = R_{iPT}$ is applies.

3. Determination F_{red} ($F_{red_A} + F_{red_{PT}}$), which is necessary to stretch of the bilayer tube to $\lambda_{zZ} = 1, 1.1, 1.2$. F_{red} is determined from the equilibrium equations (54), where $P = 0$ and F_{red} are searched for the given λ_{zZ}.

4. Inflating of the bilayer tube with pressure P under acting of F_{red}.

6 Results

6.1 Constitutive behavior of PVAT

The fifteen uniaxial tensile tests were conducted with samples of PVAT obtained from seven cadaveric donors (1 female and 6 male donors). Table 2 summarizes age, sex, and number of samples (n) obtained from each donor [Voňavková and Horný, 2020].

Table 2. PVAT samples summary.
Adopted from [Voňavková and Horný, 2020].

Donor	Sex {M,F}	Age [years]	n [–]
1	M	71	3
2	M	41	3
3	M	67	2
4	M	71	1
5	F	53	1
6	M	29	3
7	M	69	2

The fifteen experimental curves are depicted as blue points in Figure 24. Large variance of experimental data is typical for biological tissues in general. The all samples exhibited nonlinear response at large strains. At higher deformations, PVAT has a stiffer response than at the beginning of loading.

The model curves (red lines in Figure 24) were computed by means of least square optimization for (a) the most compliant case, (c) the stiffest case, and finally (b) with all measured data pooled together which resulted in the set of material parameters that represents average mechanical behavior. The estimated material parameters $(c_1,\ c_2)$ for these three cases are summarized in Table 3 [Voňavková and Horný, 2020].

Since constitutive equation for PVAT is nonlinear, material parameters were fitted to all the data to obtain mean material model. Such an approach takes into account effects of all observed responses and naturally gives the model which can be considered as average model or the model representing expected behavior as is defined in the theory of statistics.

Difficult handling with PVAT made impossible to get samples with constant orientation during their separation. For these reasons, the anisotropic behavior of adipose tissue can not be determined. Our subjective impression was that the bending stiffness at small strains, necessary to an object exhibit stable geometrical shape, was in case of the PVAT the lowest in comparison with materials with which we had had experimental experience so far (artery walls, vein walls, heart valves, pericardium).

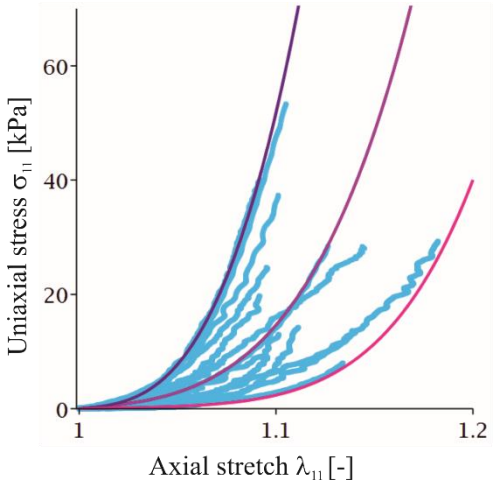

Figure 24. Results from uniaxial tensile tests of PVAT. The experimental data was fitted with the hyperelastic model (41). Mean, the stiffest, and the most compliant model curves are shown (red lines). For estimated parameters, see Table 3.
Adopted from [Voňavková and Horný, 2020].

Table 3. The material parameters of PVAT computed by means of least square optimization from the model curves for: (a) the most compliant case, (b) with all measured data, and (c) the stiffest case.
Adopted from [Voňavková and Horný, 2020].

	c_1 [kPa]	c_2 [kPa]
(a)	0.1	89.7
(b)	0.723	418
(c)	5.46	1439

The uniaxial tensile tests confirmed that the elastic response of PVAT, similar to subcutaneous fatty tissue, is highly nonlinear (Sommer et al., 2013; Calvo-Gallego et al., 2018). Unfortunately, in contrast to Sommer et al. (2013), we cannot conclude that the observed behavior suggests anisotropic material properties, because we were not able to ensure the constant orientation of the samples during their separation. The highly compliant response of the tissue complicated manual preparation.

6.2 Inflation-extension response of abdominal aorta surrounded with PVAT

The inflation behavior of bilayer tube in terms deformed radius is shown in the Figure 25. The mechanical response of M38 abdominal aorta (AA) will be studied depending on increasing wall thickness of PVAT (H_{PT}) and axial prestretch ($\lambda_{z\zeta}^{ini} = 1, 1.1, 1.2$).

The top three graphs in the Figure 25 show a deformed radius of M38 abdominal aorta during pressurization 0-16 kPa without application of axial prestretching $\lambda_{z\zeta}^{ini} = 1$. The middle (bottom) three panels display a deformed radius with axial prestretching $\lambda_{z\zeta}^{ini} = 1.1$ ($\lambda_{z\zeta}^{ini} = 1.2$). The left, middle, and right column of plots present inner radius of AA, radius at interface of AA-PVAT, and outer radius of PVAT, respectively. Three different wall thicknesses of PVAT ($H_{PT} = 0.2,\ 1.22\ (= H_A)$, and 40 mm) are also considered in the simulations.

The influence of PVAT thickness (H_{PT}) on deformability of bilayer tube during pressurization and with $\lambda_{z\zeta}^{ini} = 1$, $\lambda_{z\zeta}^{ini} = 1.1$:

- Deformability decreases on the inner radius of the AA (r_i^A). The internal aortic radius increases during pressurization.

- Deformability decreases on the AA-PVAT interface ($r_o^A = r_i^{PT}$).

- The outer PVAT radius (r_o^{PT}) is almost constant for all 3 PVAT thicknesses.

The influence of PVAT thickness (H_{PT}) on deformability of bilayer tube during pressurization and with application $\lambda_{z\zeta}^{ini} = 1.2$:

- Deformability decreases on the inner radius of the AA (r_i^A) and on the AA-PVAT interface ($r_o^A = r_i^{PT}$). The pressure curves trend changes from convex to concave at a PVAT thickness of 40 mm. During pressurization, the inner radius of the aorta increases.

- The outer radius of the PVAT (r_o^{PT}) is almost constant for all 3 PVAT thicknesses.

Comparison of bilayer tube withnout axial prestretch ($\lambda_{z\zeta}^{ini} = 1$) and with axial prestretch ($\lambda_{z\zeta}^{ini} = 1.1, 1.2$):

- On the inner radius of the AA (r_i^A) and on the AA-PVAT interface ($r_o^A = r_i^{PT}$) with application axial prestretch is the aorta more flexible than without prestretch. Axial prestretch has compensatory character for thickness of PVAT $H_{PT} = 0.2$ and 1.22. With PVAT thickness $H_{PT} = 40$ mm, deformability decreases.

- On the outer radius of the PVAT (r_o^{PT}), negligible radius changes occur during the pressurization for both non-prestressed and prestressed cases.

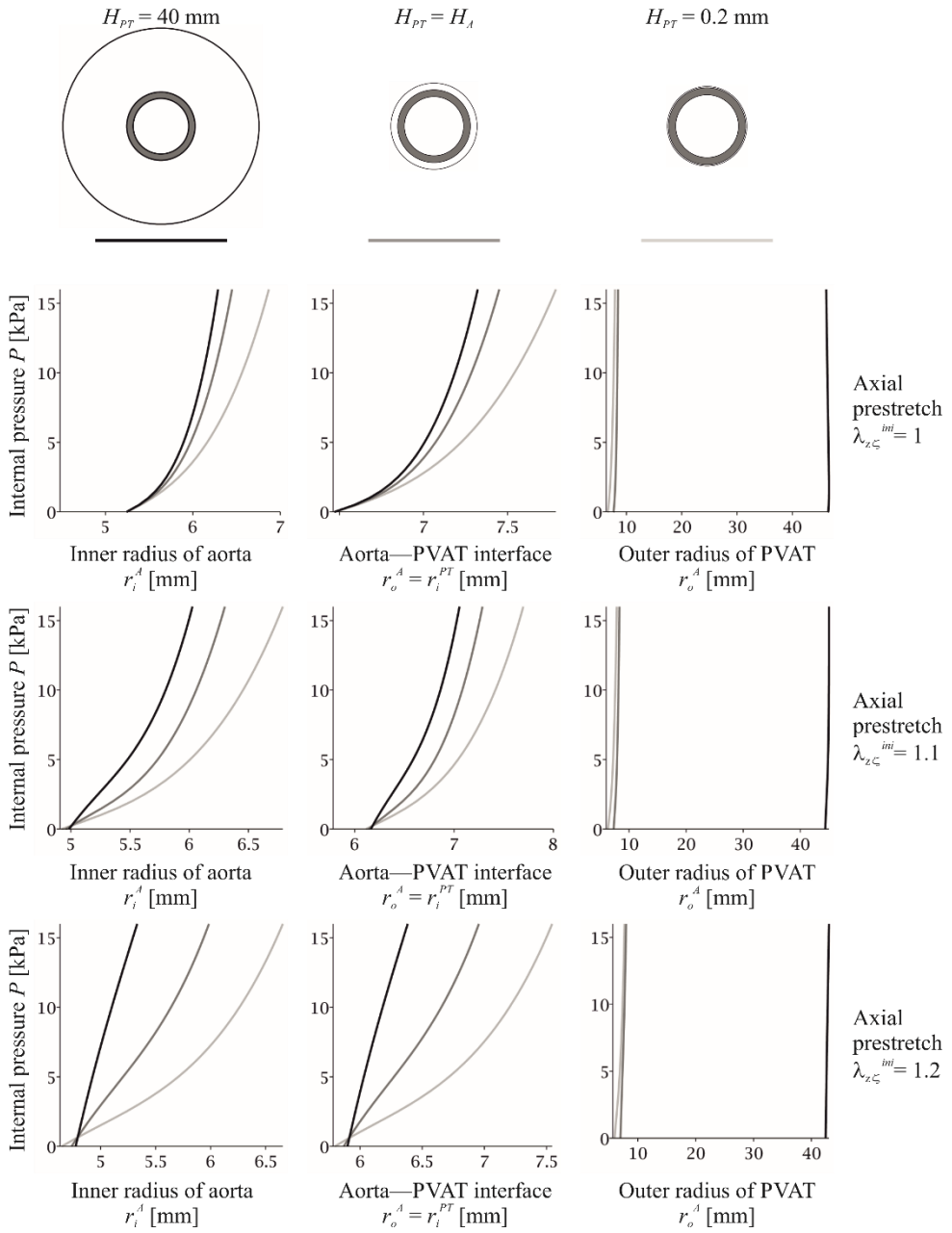

Figure 25. Inflation response of abdominal aorta (donor M38) surrounded by PVAT with wall thickness $H_{PT} = 0.2$, 1.22, and 40 mm.
Adopted from [Voňavková and Horný, 2020].

The extension behavior of bilayer tube in terms deformed radius of M38 abdominal aorta is shown in the Figure 26. The non-prestretched tube ($\lambda_{z\zeta}^{ini} = 1$) is the most prolonged in case $H_{PT} = 0.2$ mm. If prestretch is applied ($\lambda_{z\zeta}^{ini} = 1.1$, 1.2), the tube is shortened during the pressurization. The tube is the most shorter in the case of $H_{PT} = 40$ mm.

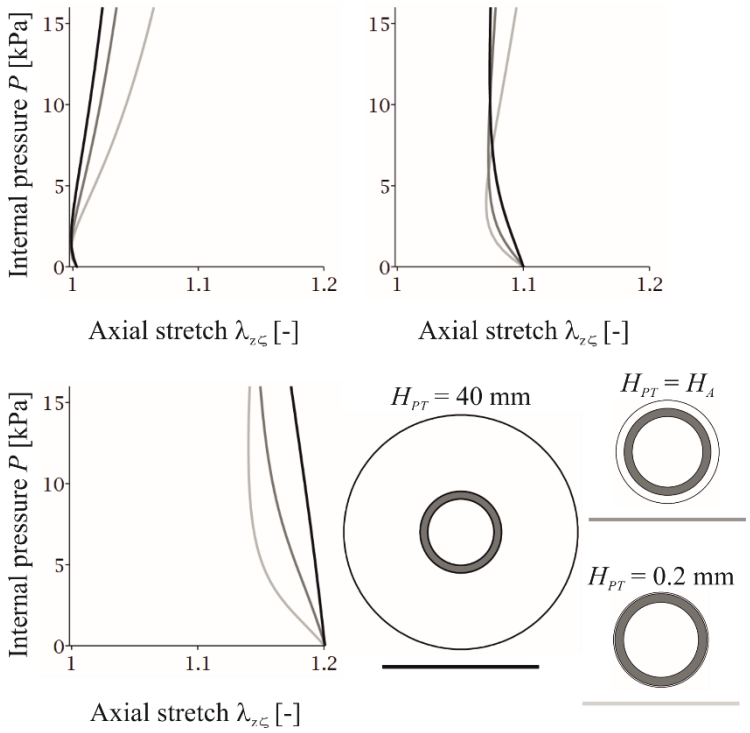

Figure 26. Extension response of abdominal aorta M38 surrounded by thick-walled tube of PVAT with $H_{PT} = 0.2$, 1.22, and 40 mm.
Adopted from [Voňavková and Horný, 2020].

Figure 27 depicts dependence between circumferential stretch (computed at r_i^A) and inflating internal pressure of M38 abdominal aorta. In the case of a non-prestretched tube ($\lambda_{z\zeta}^{ini} = 1$), the circumferential stretch is decreased (or also reduced internal circumference/aortic radius) with increasing PVAT thickness. If we compare results with ($\lambda_{z\zeta}^{ini} = 1.1, 1.2$) and without applying axial prestretch, we conclude that axial prestretch causing enlargement of the aortic circumference in case of a thin PVAT layer. Thick PVAT layer ($H_{PT} = 40$ mm) prevents the aorta of expanding circumferentially, thus causing opposite effect to thin PVAT layer.

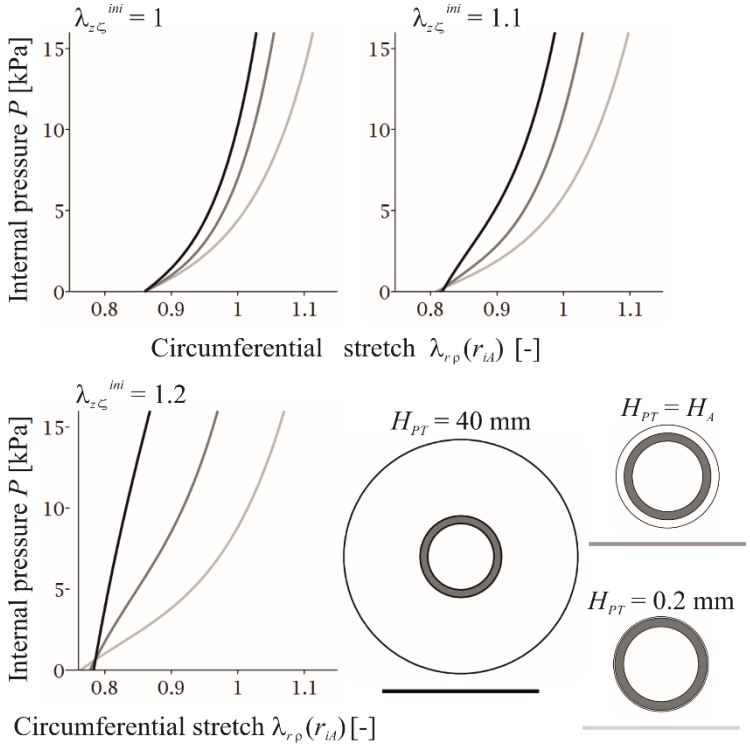

Figure 27. Dependence of the circumferential stretch at inner radius of aorta during inflation of M38 on the axial prestretch.
Adopted from [Voňavková and Horný, 2020].

The response obtained for F63 abdominal aorta was qualitatively similar as M38. The specific results in the form of pictures are presented in the Appendix A of this work.

6.3 Distribution of in-wall stresses in bilayer tube

Figure 28 and Figure 29 present distribution of radial, circumferential and axial stress ($\sigma_{rr}, \sigma_{\theta\theta}, \sigma_{zz}$) throught the wall thickness of bilayer tube at systolic pressure ($P = 16$ kPa). The radial, circumferential and axial stress is depicted on the first, second and third line, respectively. The model has 3 different value of PVAT thickness and axial prestretch. The thickness of the PVAT has different grey color from the lightest to the darkest ($H_{PT} = 0.2,\ 1.22,$ and 40 mm, respectively). The axial prestretch ($\lambda_{z\zeta}^{ini} = 1, 1.1, 1.2$) are displayed on the first, second, and third column, respectively. The plots are divided, for greater clarity, into the distribution of the stress inside aorta wall M38 (Figure 28) and distribution of the stress in PVAT wall (Figure 29).

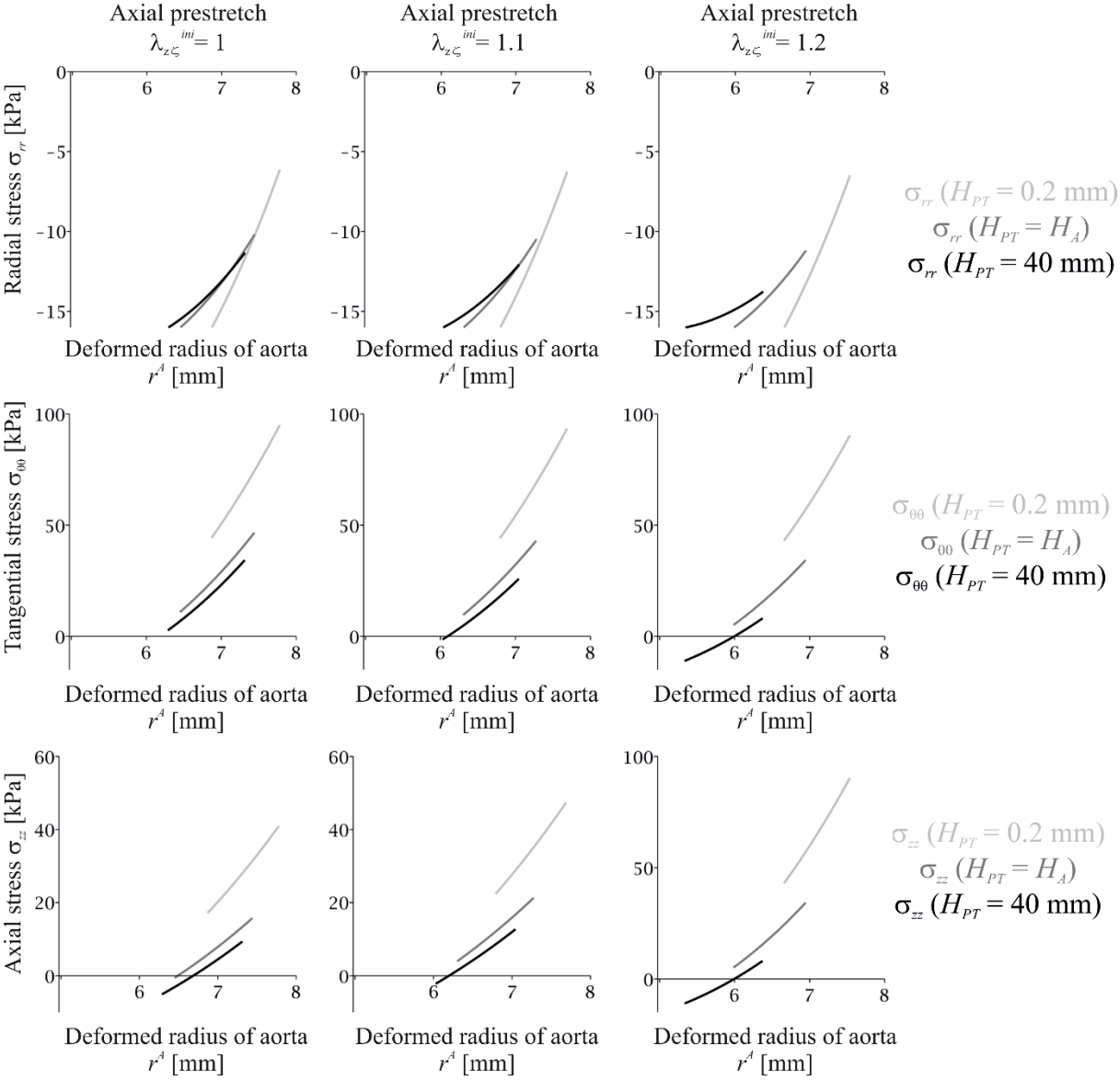

Figure 28. Distribution of in-wall stresses in aorta M38 pressurized to 16 kPa and surrounded by PVAT with $H_{PT} = 0.2$, 1.22, and 40 mm.
Adopted from [Voňavková and Horný, 2020].

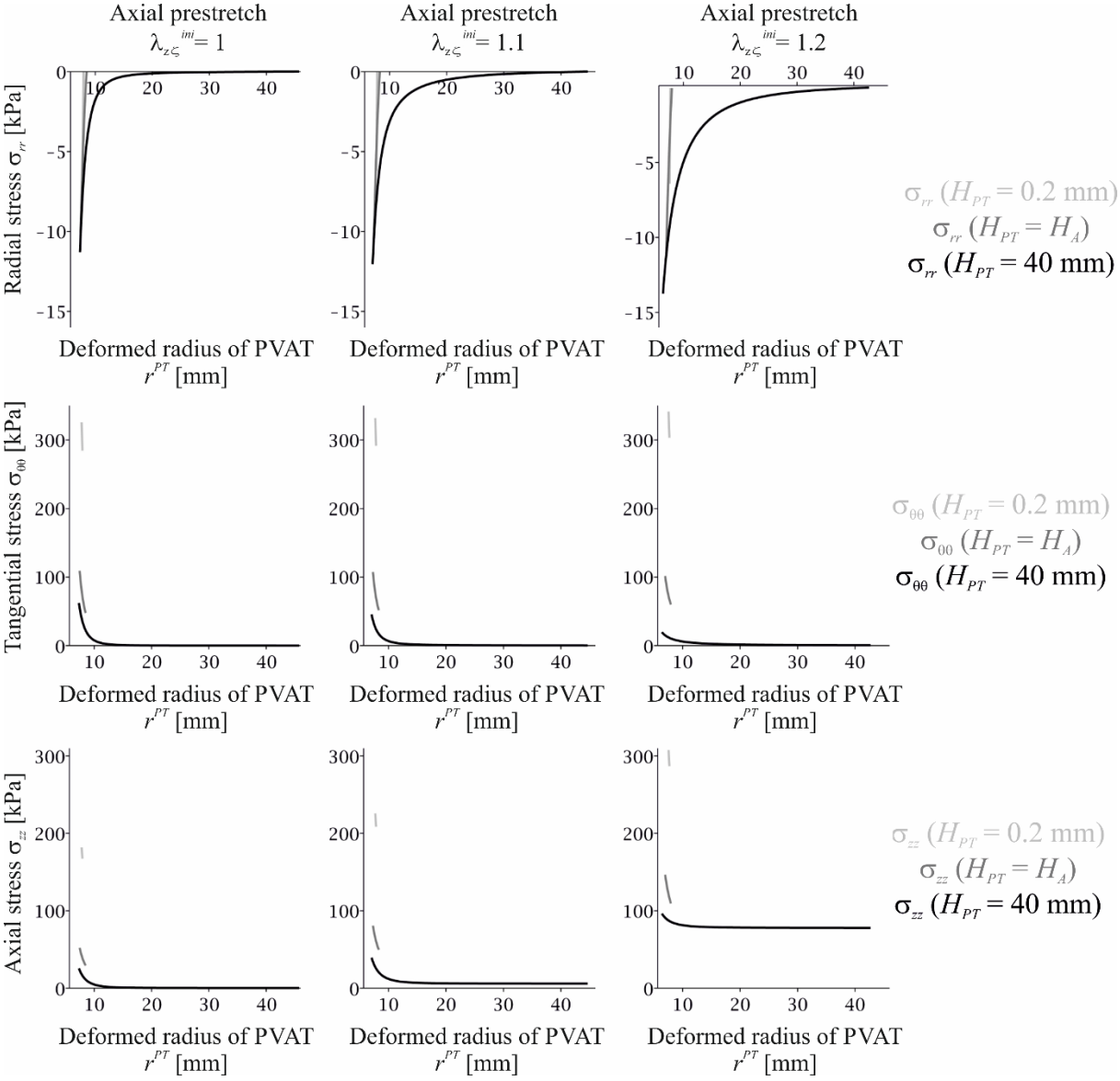

Figure 29. Distribution of in-wall stresses in PVAT at $P = 16$ kPa. PVAT tube thickness was $H_{PT} = 0.2$, 1.22, and 40 mm.
Adopted from [Voňavková and Horný, 2020].

Also in this chapter, the distribution of in-wall stresses in aorta F63 was qualitatively similar as M38. The specific results in the form of pictures are presented in the Appendix A of this work.

7 Discussion

7.1 Constitutive behavior of PVAT

Omidi et al. (2014) studied the mechanical behavior of adipose tissue in subcutaneous abdominal region by means of an indentation test. They employed the Yeoh hyperelastic model (third order polynomial in $\boldsymbol{I_1}$) to express the constitutive properties of the tissue. They arrived at values of the material parameters that seems to be somewhat lower than found in our study. $c_1 = 0.16$ kPa, $c_2 = 0.018$ kPa, and $c_3 = 1.1 \cdot 10^{-7}$ kPa are typical values estimated by Omidi et al. (2014). However, herein obtained results presented in Table 3 show that $c_1 = 0.723$ kPa, $c_2 = 418$ kPa (for all measured data) [Voňavková and Horný, 2020]. This discrepancy may be partially attributed to a different experimental technique used in Omidi et al. (2014), but the most important difference seems to be the fact that Omidi et al. (2014) decellularized the tissue before testing, which can significantly change the mechanical properties of tissues (Bielli et al., 2018; Liao et al., 2008).

Although adipose tissue is very compliant and small values of an acting force can deform such an object to a state which requires employing the finite strain theory, small strain approximations are sometimes used in the literature. In this approach, the framework of linear elasticity is appropriate, and one can find studies reporting values for the Young elastic modulus for adipose tissue. Restricting our attention to the small strain theory, we can substitute the nonlinear model (41) with the slope of the tangent computed to a stress–strain curve at the beginning of the deformation. This slope is referred to as the initial elastic modulus.

A consideration of the material parameters presented in Table 3 leads to initial elastic modulus of 0.6 kPa, for the most compliant material response, of 4.3 kPa for average response, and of 32.7 kPa for the stiffest case [Voňavková and Horný, 2020]. Omidi et al. (2014) reported 3.4 kPa for the Young modulus obtained for abdominal subcutaneous tissue. Comley and Fleck (2010, 2012), Nightingale et al. (2003), and Miller-Young et al. (2002) reported a Young modulus in the range of 1 – 14 kPa depending on the source of the tissue and applied strain rate. Geerligs et al. (2008) reported the shear elastic modulus of subcutaneous tissue to be of 7.5 kPa that implies a elastic modulus of about 22 kPa. Thus, we conclude that our data suggest somewhat stiffer behavior for perivascular adipose tissue than is known for subcutaneous tissue; however, under small strains they do not differ significantly.

7.2 Inflation-extension response of abdominal aorta surrounded with PVAT

The effect of perivascular adipose tissue on the mechanics of the abdominal aorta was simulated by means of an analytical model based on the bi-layered thick-walled tube problem formulated within a framework of nonlinear elasticity and numerically solved in Maple (Maplesoft, Waterloo, Canada). Figures 25 and 26 show the resulting inflation and extension behavior in terms of deformed radius and axial stretch obtained for the 38-year-old male individual (M38). To highlight the effect of PVAT and axial prestretch on the circumferential response of the aorta, Figure 27 depicts the dependence between circumferential stretch (computed at r_{iA}) and the inflating pressure. Figures 28 (aorta) and 29 (PVAT)

show the stress distribution through the thickness of the wall computed at loading pressure $P = 16$ kPa for tubes with different H_{PT} and $\lambda_{z\zeta}^{ini}$ [Voňavková and Horný, 2020].

With regard to inflation behavior, the figures document that PVAT restricts the radial motion of an artery. It is exhibited in each studied position (r_{iA}, $r_{oA} = r_{iPT}$, and r_{oPT}; see Figure 25). Where r_{oPT} for $H_{PT} = 40$ mm, the movement is almost negligible in comparison with the thickness of the fatty tissue [Voňavková and Horný, 2020]. Thus, one could hypothetically conclude that the presence of the fatty surrounding is mechanically disadvantageous for the human body, because it prevents an artery from functioning as an elastic capacitor in the Windkessel effect. Later, we will see that this is just one side of the coin.

In contrast to PVAT, axial prestretch has, in the range of physiological pressure, the absolutely opposite effect. Figure 25 document that the $P - r$ responses are more compliant when longitudinal pretension is applied. Perhaps it is most clearly depicted in Figure 27, where circumferential stretch at the inner radius of the aorta is presented. In accordance with our previous study, Horný et al. (2014b), it can be said that the axial prestrain of the tube leads to higher circumferential distensibility in the inflation carried out at physiological pressures. Since the distensibility may not be easily recognized from the figure, Table 4 includes the specific results obtained for H_{PT} and $\lambda_{z\zeta}^{ini}$. The distensibility is quantified as $(r_{iA}(16\text{kPa}) - r_{iA}(10\text{kPa}))/r_{iA}(10\text{kPa})$. From Table 4, we can conclude that, although increasing H_{PT} leads to decreasing distensibility, axial preloading balances this influence [Voňavková and Horný, 2020].

Table 4. Specific values of distensibility, $(r_{iA}(16\text{kPa}) - r_{iA}(10\text{kPa}))/r_{iA}(10\text{kPa})$, obtained from the curves in Figure X27.
Adopted from [Voňavková and Horný, 2020].

M38	$H_{PT} = 0.2$ mm	$H_{PT} = H_A = 1.22$ mm	$H_{PT} = 40$ mm
$\lambda_{z\zeta}^{ini} = 1$	0.0469	0.0333	0.0279
$\lambda_{z\zeta}^{ini} = 1.1$	0.0521	0.0340	0.0390
$\lambda_{z\zeta}^{ini} = 1.2$	0.0631	0.0612	0.0454

The axial response is depicted in Figure 26. We again observe that including perivascular tissue into the model has, similar to circumferential behavior, an immobilization effect. The dark curves corresponding to $H_{PT} = 40$ mm exhibit a lower stretch variation, $\lambda_{z\zeta}(P_2) - \lambda_{z\zeta}(P_1)$ for $P_1 < P_2$, than the light curves obtained for the thinner PVAT layers. At typical physiological pressures, $P_2 = 16$ kPa and $P_1 = 10$ kPa, it is also visible for $\lambda_{z\zeta}^{ini} = 1.1$. In this case, the curve corresponding to $H_{PT} = 40$ mm is almost perpendicular to the horizontal axis of the graph, which suggests that the prestretched tube does not move axially during the pressure pulse [Voňavková and Horný, 2020]. It has been hypothesized in the literature that minimization of the axial movement during the pressure pulse transmission is

advantageous for arteries (Schulze-Bauer et al., 2003). Our results show that PVAT contributes to the minimization of axial movement of the aorta.

On the other hand, comparing the panels created for $\lambda_{z\zeta}^{ini} = 1.2$ with panels for $\lambda_{z\zeta}^{ini} = 1.1$ indicates that this behavior is not monotonic. It does not hold true in the sense that the higher the prestretch the lower the axial movement would generally be. Where $\lambda_{z\zeta}^{ini} = 1.2$, the lowest variation of axial deformation is obtained for $H_{PT} = 0.2$ mm. However, human arteries are not prestrained without limits. Rather, the internal fiber structure (elastin, collagen) could be subject to shortening. The plots show that the PVAT layer compensates for elongation and shortening [Voňavková and Horný, 2020].

For the abdominal aorta, typical values can be found in Horný et al. (2014b, 2017). These studies suggest $\lambda_{z\zeta}^{ini} = 1.179$ for M38 is to be expected. The value come from the studied interval $\lambda_{z\zeta}^{ini} = 1 - 1.2$. Computations show that somewhere inside this interval the longitudinal response changes from pressure-induced elongation to pressure-induced shortening. Our results suggest that the expected values of prestretch, presented in Horný et al. (2014b), fall close to a hypothetical optimal point not only in the case of bare aortas but also when the existence of PVAT and its mechanical role are considered [Voňavková and Horný, 2020].

The only study, to the author's knowledge, that experimentally worked with an artery enveloped by a perivascular tissue, is listed in the article Liu et al. (2007). As mentioned in the introduction, they found that the presence of perivascular tissue significantly immobilizes of the vessel in its inflation-extension response. In contrast to this dissertation thesis, Liu et al. (2007) did not search for a constitutive model for perivascular adipose tissue and worked with porcine, not human arteries.

7.3 Distribution of in-wall stresses in bilayer tube

In accordance with a solution known from the classical theory of elasticity for the bi-layered thick-walled tube, the computed distribution of radial stress confirms that PVAT bears some portion of the pressure load. Transmural pressure loading PVAT, $-\Delta P_{PT} = \sigma_{rr}(r_{iPT}) - \sigma_{rr}(r_{oPT}) = \sigma_{rr}(r_{iPT})$, increases when the thickness of PVAT increases (Figure 28 and 29). Reciprocally, the thicker the PVAT layer is, the lower is the loading of the aorta, $-\Delta P_A = \sigma_{rr}(r_{iA}) - \sigma_{rr}(r_{oA}) = P - \Delta P_{PT}$. As a consequence of the decreasing loading of the aorta, the increasing thickness of PVAT causes a decrease in circumferential and axial stresses [Voňavková and Horný, 2020]. This is another example showing that the existence of PVAT is advantageous from a mechanical point of view. It bears some portion of the loading and thus decreases the load acting on the aorta itself.

The role of axial prestretch is very interesting. The middle row in Figure 28 show that increasing axial pretension leads to a decrease in circumferential stress in the aorta. Where $\lambda_{z\zeta}^{ini} = 1.2$ and $H_{PT} = 40$ mm, negative values for $\sigma_{\theta\theta}$ at r_{iA} are even reached. Interestingly, in the PVAT layer, an increase in circumferential stress at r_{iPT} is observed for $H_{PT} = 0.2$ mm (Figure 29). However, the

maximum value of circumferential stress decreases with increasing $\lambda_{z\zeta}^{ini}$ for $H_{PT} = H_A$ mm and $H_{PT} = 40$ mm. This documents that the effect of axial pretension is not monotonic with respect to the simultaneous effect of the thickness [Voňavková and Horný, 2020].

To the best of the author's knowledge, there is no study in the literature that deals with the simultaneous influence of axial prestress and perivascular tissue on the distribution of stress and strain within the artery wall.

8 Conclusion

This thesis combines experimental and computational approach. To the best of author's knowledge, there was no experimental study carried out with perivascular adipose tissue surrounding the abdominal aorta to obtain its constitutive description. Seven abdominal aortas with surrounding PVAT were removed in autopsy. Total number of 15 PVAT samples was prepared from these 7 pieces. Uniaxial tensile tests were performed with pre-cycling to eliminate the viscoelastic effects of the tissue. Subsequently, the sample was stretched to the failure. Experimental data show a rather large dispersion in the stress-strain curves when all 15 samples are considered. Axial stretching at maximum stress ranges from approximately 1.07 to 1.17 [Voňavková and Horný, 2020]. Despite the large variance in the stress-strain curves, it can be said that the behavior at infinitesimal deformations corresponds to the values for other adipose tissues, which can be found in the literature.

Basic experiments, in the form of tensile tests, made it possible to describe the mechanical behavior of human perivascular tissue. PVAT response was found to be highly nonlinear, thus hyperelastic description was adopted for large deformation domain. In the nonlinear constitutive model, the variability of the observations was taken into account by making three estimates of the sets of material parameters, for (a) the most compliant case, (b) with all measured data, and (c) the stiffest case [Voňavková and Horný, 2020]. The aim of this thesis was to use data characterizing PVAT under time-independent and equilibrium conditions and to focus purely on the elastic behavior of the tissue. For these reasons, the viscoelastic effects, such as relaxation and creep, which accompany the propagation of the pressure wave in vivo have been neglected. The isotropic model was chosen due to difficult sample handling.

The next part of the thesis dealt with computational simulations. The analytical model of a two-layer, thick-walled, closed, homogeneous cylindrical tube with a constant radius was created [Voňavková and Horný, 2020]. In a human body, no blood vessel (separate and enveloped surrounding tissue) has the same radius at any point. The author of this thesis would like to point out that it is only a simplified model so that the results can be better interpreted and generalized.

The inner layer of the model captured properties corresponding to the human abdominal aorta. The material parameters of the abdominal aorta, as already mentioned, were adopted from the literature. The outer layer of the model tube corresponded to PVAT.

All blood vessels are circumferentially and axially prestressed in the human body. In this work, aortic prestretches were considered. To the best of author's knowledge, no information has been available in the scientific literature about the existence of the prestretch. During autopsy, the author tried to observe and to measure residual strains exhibited when PVAT is excised form a body. However, she arrived at conclusion that it is unmeasurable by methods available at autopsy room. It seems that adipose tissue somewhat spreads when one makes an incision into the tissue by a scalpel. It suggests that there may be some force that was released by the cut. However, when one excises PVAT from a body or from the aorta, PVAT doesn't change its dimension on scale measureable by a rule. Thus it is possible that small

spreading of the incision made by scalpel is the consequence of some momentum transfer accompanying movement of the scalpel through the tissue. Hence from observations made in autopsy, it was concluded residual stresses in PVAT are not measurable by our methods. Under these conditions, the model does not include prestressed PVAT.

The two-layer tube model was subjected to an inflation-extension. The pressure was applied in the range of $P = 0 - 16$ kPa at the inner surface of the tube. The most important pressure values are in the physiological range - from diastole to systole (10 kPa and 16 kPa).

Axial prestretch (extension) was evaluated for cases $\lambda_{z\zeta}^{ini} = 1, 1.1, 1.21$. The non-prestressed tube has the initial axial stretch prestretching equal to 1. Axial prestretching was applied to both tube layers because the aorta and PVAT are firmly attached to each other and deform together [Voňavková and Horný, 2020].

Each person has a different amount of PVAT in the abdominal area, so 3 models with different PVAT layer thicknesses were created ($H_{PT} = 0.22$ mm, 1.22 mm, and 40 mm) [Voňavková and Horný, 2020].

After simulation of inflation-extension tests, with different additional axial prestressing and different PVAT thickness, a stress-strain analysis was performed. The results of the simulations showed the significant effect of PVAT on the abdominal aorta.

It was found that presence of the PVAT reduces distensibility of the abdominal aorta (Figure 25, 26). Axial prestretch applied to the aorta had an opposite effect than PVAT. Axially prestrained aorta exhibited higher distensiblity than non-prestrained aorta (Figure 27). It was also showed that perivascular tissue carries some of the pressure load and reduces mechanical stresses inside the wall of aorta by approximately twice (Figure 28) [Voňavková and Horný, 2020]. Similar effect was found for axial prestetch. The results suggest that PVAT is mechanically advantageous due to reducing wall stresses and decreased arterial distensibilty is compensated by the axial prestretch in the aorta.

In biomechanical simulations is no doubt that the PVAT layer surrounding of the abdominal aorta plays an irreplaceable role. Most authors neglect surrounding tissue and simulate aorta by itself with internal overpressure (external pressure is zero), or replace the PVAT with a boundary condition in the form of the applied pressure (it should be noted that it is difficult to determine the exact value of external pressure). However, the simulations do not correspond with real state in the human body. The abdominal aorta works in cooperation with the PVAT. The analytical model of bilayer tube (abdominal aorta with PVAT) more closely matches the configuration in the abdominal cavity. If we modeled only the aorta, the results of stress-strain inside the aorta wall would be inaccurate.

9 References

Alberts B., Johnson A., Lewis J., Raff M., Roberts K., Walter P. (2002). T cells and B cells derive their names from the organs in which they develop. T cells develop in the thymus, and B cells, in mammals, develop in the bone marrow in adults or the liver in fetuses. Molecular Biology of the Cell. Garland Science: New York, NY pg 1367.

Ali, A. T., Hochfeld, W. E., Myburgh R., and Pepper M. S. (2013). Adipocyte and adipogenesis. European Journal of Cell Biology. 92(6-7), 229-236. doi: 10.1016/j.ejcb.2013.06.001.

Aliya S (2011) Effects of Vasodilation and Arterial Resistance on Cardiac Output. J Clinic Experiment Cardiol 2:170. doi: 10.4172/2155-9880.1000170.

Atul M., Varun M., Deepak A. et al. (2016). Aortic aneurysm. J Transl Int Med. 2016 Apr 1; 4(1): 35–41. doi: 10.1515/jtim-2016-0008.

Bhargavi D. V., Avantsa R., Kala P. (2015). MDCT signs differentiating retroperitoneal and intraperitoneal lesions- diagnostic pearls. ECR Congress. doi:10.1594/ecr2015/C-0987

Bielli, A., Bernardini, R., Varvaras, D., Rossi, P., Di Blasi, G., Petrella, G., Buonomo, O. C., Mattei, M., Orlandi, A. (2018). Characterization of a new decellularized bovine pericardial biological mesh: Structural and mechanical properties. Journal of the Mechanical Behavior of Biomedical Materials, 78, 420-426. doi:10.1016/j.jmbbm.2017.12.003.

Blausen.com staff (2014). "Medical gallery of Blausen Medical 2014". *WikiJournal of Medicine* **1** (2): 10. doi:10.15347/wjm/2014.010. ISSN 2002-4436.

Boyle, C. J., Lennon, A. B., Prendergast, P. J. (2011). In silico prediction of the mechanobiological response of arterial tissue: application to angioplasty and stenting. J. Biomech. Eng. 133, 081001.

Braverman A. C. (2010). Acute Aortic Dissection: Clinician Update. J Circulation. 122:184-188. doi: 10.1161/circulationaha.110.75.

Brown, N. K., Zhou, Z., Zhang, J., Zeng, R., Wu, J., Eitzman, D. T., Chen, Y. E., Chang, L. (2014). Perivascular adipose tissue in vascular function and disease: A review of current research and animal models. Arteriosclerosis, Thrombosis, and Vascular Biology, 34(8), 1621-1630. doi:10.1161/ATVBAHA.114.303029.

Brynskov J., Foegh P., Pedersen G., Ellervik C., Kirkegaard T., Bingham A., Saermark T. (2002). Tumour necrosis factor alpha converting enzyme (TACE) activity in the colonic mucosa of patients with inflammatory bowel disease. Gut. 51 (1): 37–43. doi:10.1136/gut.51.1.37.

Calvo-Gallego, J. L., Domínguez, J., Gómez Cía, T., Gómez Ciriza, G., & Martínez-Reina, J. (2018). Comparison of different constitutive models to characterize the viscoelastic properties of human abdominal adipose tissue. A pilot study. Journal of the Mechanical Behavior of Biomedical Materials, 80, 293-302.

Comley, K., & Fleck, N. A. (2010). A micromechanical model for the young's modulus of adipose tissue. International Journal of Solids and Structures, 47(21), 2982-2990. doi:10.1016/j.ijsolstr.2010.07.001.

Comley, K., & Fleck, N. (2012). The compressive response of porcine adipose tissue from low to high strain rate. International Journal of Impact Engineering, 46, 1-10. doi:10.1016/j.ijimpeng.2011.12.009.

Čihák, R. *Anatomie 3*. Praha: Grada, 2004.

Deanfield J. E., Halcox J. P., and Rabelink T. J. (2007) Endothelial Function and Dysfunction: Testing and Clinical Relevance**.** Circulation.115:1285–1295.

Dowlati Y., Herrmann N., Swardfager W., Liu H., Sham L., Reim E. K., Lanctôt K. L. (2010). A meta-analysis of cytokines in major depression. Biol Psychiatry. 67 (5): 446–457. doi:10.1016/j.biopsych.2009.09.033.

Fereidoonnezhad, B., Naghdabadi, R., Sohrabpour, S., & Holzapfel, G. A. (2017). A mechanobiological model for damage-induced growth in arterial tissue with application to in-stent restenosis. Journal of the Mechanics and Physics of Solids, 101, 311-327. doi:10.1016/j.jmps.2017.01.016.

Ferguson-Smith A. C., Chen Y. F., Newman M. S., May L. T., Sehgal P. B., Ruddle F. H. (1988). Regional localization of the interferon-beta 2/B-cell stimulatory factor 2/hepatocyte stimulating factor gene to human chromosome 7p15-p2. Genomics. 2 (3): 203–8. doi:10.1016/0888-7543(88)90003-1.

Filippone, G., Caruana, G. G., Calia, C., Moscaritolo, V., and Argano, V.(2018. Evidence of intimal tear in type A intramural hematoma of the aorta: A case series. International Journal of Surgery Case Report. 179-181 (42). doi: 10.1016/j.ijscr.2017.12.018.

Flammer AJ, Anderson T, Celermajer DS, Creager MA, Deanfield J, Ganz P, Hamburg NM, Lüscher TF, Shechter M, Taddei S, Vita JA, Lerman A (Aug 2012). The assessment of endothelial function: from research into clinical practice. Circulation. 126 (6):75.67.doi:10.1161/circulationaha.112.093245.

Gasser, T. C., Ogden, R. W., & Holzapfel, G. A. (2006). Hyperelastic modelling of arterial layers with distributed collagen fibre orientations. Journal of the Royal Society Interface, 3(6), 15-35. doi:10.1098/rsif.2005.0073.

Geerligs, M., Peters, G. W. M., Ackermans, P. A. J., Oomens, C. W. J., & Baaijens, F. P. T. (2008). Linear viscoelastic behavior of subcutaneous adipose tissue. Biorheology, 45(6), 677-688. doi:10.3233/BIR-2008-0517.

Greenwald, S. E. (2007). Ageing of the conduit arteries. Journal of Pathology, 211(2), 157-172. doi:10.1002/path.2101.

Hejčl, A., Švihlová, H., Sejkorová, A., Radovnický, T., Adámek, D., Hron, J., Dragomir-Daescu, D., Málek, J., Sameš, M. (2017). Computational fluid dynamics of a fatal ruptured anterior communicating artery aneurysm. Journal of Neurological Surgery, Part A: Central European Neurosurgery, 78(6), 610-616. doi:10.1055/s-0037-1604286.

Hodis, S., Zamir, M. (2001) Mechanical events within the arterial wall under the forces of pulsatile flow: A review. J Mechan Behav Biomed Mater 2011; 4:1595-1602.

Hodis, S., & Zamir, M. (2009). Mechanical events within the arterial wall: The dynamic context for elastin fatigue. Journal of Biomechanics, 42(8), 1010-1016. doi:10.1016/j.jbiomech.2009.02.010.

Hodis S. Zamir M. (2011). Coupled radial and longitudinal displacements and stresses within the arterial wall in pulsatile flow under tethered and free-wall conditions. Physical Review E 83, 051923(1)-(8). doi: 10.1103/PhysRevE.83.051923.

Holzapfel, G. A. (2000). Nonlinear Solid Mechanics: A Continuum Approach for Engineering. Wiley. ISBN: 13: 9780471823049.

Holzapfel, G. A., Gasser, T. C., & Ogden, R. W. (2000). A New constitutive framework for arterial wall mechanics and a comparative study of material models. Journal of Elasticity and the physical science of solids 61:1-48.

Holzapfel, G. A., Stadler, M., & Gasser, T. C. (2005). Changes in the mechanical environment of stenotic arteries during interaction with stents: Computational assessment of parametric stent designs. Journal of Biomechanical Engineering, 127(1), 166-180. doi:10.1115/1.183536.

Holzapfel, G. A., Gasser, T. C. (2007). Computational stress–deformation analysis of arterial walls including high-pressure response. Int. J. Cardiol. 116, 78–85.

Horny, L., Adamek, T., Gultova, E., Zitny, R., Vesely, J., Chlup, H., & Konvickova, S. (2011). Correlations between age, prestrain, diameter and atherosclerosis in the male abdominal aorta. Journal of the Mechanical Behavior of Biomedical Materials, 4(8), 2128-2132. doi:10.1016/j.jmbbm.2011.07.011.

Horny, L., Adamek, T., & Zitny, R. (2013). Age-related changes in longitudinal prestress in human abdominal aorta. Archive of Applied Mechanics, 83(6), 875-888. doi:10.1007/s00419-012-0723-4.

Horný L, Netušil M, Daniel M. (2014a). Limiting extensibility constitutive model with distributed fibre orientations and ageing of abdominal aorta. J Mechan Behav Biomed Mater; 38:39-51.

Horný L, Netušil M, Voňavková T. (2014b). Axial prestretch and circumferential distensibility in biomechanics of abdominal aorta. Biomech Model Mechanobiol;13:783-799.

Horný L. (2015) Axial prestretch and biomechanics of abdominal aorta. Habilitation thesis, Czech Technical University in Prague.

Horný L, Adámek T, Kulvajtová M. (2017). A comparison of age-related changes in axial prestretch in human carotid arteries and in human abdominal aorta. Biomech Model Mechanobiol; 16:375-383.

Huang Cao, Z. F., Stoffel, E., & Cohen, P. (2017). Role of perivascular adipose tissue in vascular physiology and pathology. Hypertension, 69(5), 770-777. doi:10.1161/HYPERTENSIONAHA.116.08451.

Humphrey, J. D., & Na, S. (2002). Elastodynamics and arterial wall stress. Annals of Biomedical Engineering, 30(4), 509-523. doi:10.1114/1.1467676.

Humphrey, J. D., Eberth, J. F., Dye, W. W., & Gleason, R. L. (2009). Fundamental role of axial stress in compensatory adaptations by arteries. Journal of Biomechanics, 42(1), 1-8. doi:10.1016/j.jbiomech.2008.11.011.

Hülsmann, J., Grün, K., El Amouri, S., Barth, M., Hornung, K., Holzfuß, C., Lichtenberg, A., Akhyari, P. (2012). Transplantation material bovine pericardium: Biomechanical and immunogenic characteristics after decellularization vs. glutaraldehyde-fixing. Xenotransplantation, 19(5), 286-297. doi:10.1111/j.1399-3089.2012.00719.x.

Chang L., Villacorta L., Li R., Hamblin M., Xu W., Dou C., Zhang J., Wu J., Zeng R., Chen Y. E. (2012). Loss of perivascular adipose tissue on peroxisome proliferator-activated receptor-γ deletion in smooth muscle cells impairs intravascular thermoregulation and enhances atherosclerosis. Circulation. 126:1067–1078.

Insull, W. (2009). The Pathology of Atherosclerosis: Plaque Development and Plaque Responses to Medical Treatment. *The American Journal of Medicine*. 122 (1 Suppl): S3–S14. doi:10.1016/j.amjmed.2008.10.013.

Keipert, S. & Jastroch, M. (2014). Brite/beige fat and UCP1 — is it thermogenesis? Biochimica et Biophysica Acta (BBA) – Bioenergetics. 1837(7), 1075-1082. doi: 10.1016/j.bbabio.2014.02.008.

Kent, K. C. (2014). Clinical practice. Abdominal aortic aneurysms. The New: England Journal of Medicine. 371 (22):2101-8. doi:10.1056/NEJMcp1401430.

Kiousis, D. E., Gasser, T. C., & Holzapfel, G. A. (2007). A numerical model to study the interaction of vascular stents with human atherosclerotic lesions. Annals of Biomedical Engineering, 35(11), 1857-1869. doi:10.1007/s10439-007-9357-z.

Králová Lesná, I., Tonar, Z., Malek, I., Maluskova, J., Nedorost, L., Pirk, J., Pitha, J., Lanska, V., Poledne, R. (2015). Is the amount of coronary perivascular fat related to atherosclerosis? Physiological Research, 64, S435-S443.

Labrosse, M. R., Gerson, E. R., Veinot, J. P., & Beller, C. J. (2013). Mechanical characterization of human aortas from pressurization testing and a paradigm shift for circumferential residual stress. Journal of the Mechanical Behavior of Biomedical Materials, 17, 44-55. doi:10.1016/j.jmbbm.2012.08.004.

Lampe, M. A., Burlingame, A. L., Whitney, J., Williams, M. L., Brown, B. E., Roitman, E., Elias, M. (1983). Human stratum corneum lipids: characterization and regional variations. J. Lipid Res. 24 (2): 120–130. PMID 6833889.

Lansman S. L., Saunders P. C., Malekan R., and Spielvogel D. (2010). Acute aortic syndrome. J Thorac Cardiovasc Surg. 140:S92-7. doi:10.1016/j.jtcvs.2010.07.062

Liao, J., Joyce, E. M., & Sacks, M. S. (2008). Effects of decellularization on the mechanical and structural properties of the porcine aortic valve leaflet. Biomaterials, 29(8), 1065-1074. doi:10.1016/j.biomaterials.2007.11.007.

Liu, Y., Dang, C., Garcia, M., Gregersen, H., & Kassab, G. S. (2007). Surrounding tissues affect the passive mechanics of the vessel wall: Theory and experiment. American Journal of Physiology - Heart and Circulatory Physiology, 293(6), H3290-H3300. doi:10.1152/ajpheart.00666.2007.

Locksley R. M., Killeen N., Lenardo M. J. (2001). The TNF and TNF receptor superfamilies: integrating mammalian biology. Cell. 104 (4): 487–501. doi:10.1016/S0092-8674(01)00237-9.

Loscalzo, J. (2010). Harrison's cardiovascular medicine. New York: McGraw-Hill Medical. ISBN 978-0-07-170291-1.

Lumeng CN, Bodzin JL, Saltiel AR. Obesity induces a phenotypic switch in adipose tissue macrophage polarization. J Clin Invest 2007; 117: 175-84.

Maeda K., Okubo K., Shimomura I., Funahashi T., Matsuzawa Y., Matsubara K. (1996). cDNA cloning and expression of a novel adipose specific collagen-like factor, apM1 (AdiPose Most abundant Gene transcript 1). Biochemical and Biophysical Research Communications. 221 (2): 286–9. doi:10.1006/bbrc.1996.0587. PMID 8619847.

Mancini M. C. (2019). Aortic Dissection Treatment & Management. *https://emedicine.medscape.com/article/2062452-treatment* [online]. [cit. 2019-12-25].

Masson, I., Beaussier, H., Boutouyrie, P., Laurent, S., Humphrey, J. D., & Zidi, M. (2011). Carotid artery mechanical properties and stresses quantified using in vivo data from normotensive and hypertensive humans. Biomechanics and Modeling in Mechanobiology, 10(6), 867-882. doi:10.1007/s10237-010-0279-6.

Maton D., Hopkins J., McLaughlin C. W., Johnson S., Warner M. Q., Lahart D., Wright J. D., Kulkarni D. V. (1997). Human Biology and Health. Englewood Cliffs, New Jersey, US: Prentice Hall. ISBN 0-13-981176-1.

Matsumoto, T., & Hayashi, K. (1996). Stress and strain distribution in hypertensive and normotensive rat aorta considering residual strain. *Journal of Biomechanical Engineering, 118*(1), 62-73. doi:10.1115/1.2795947.

Mélik-Parsadaniantz S., Rostène W. (2008). Chemokines and neuromodulation. *Journal of Neuroimmunology*. 198 (1–2): 62–8. doi:10.1016/j.jneuroim.2008.04.022.

Miller-Young, J. E., Duncan, N. A., & Baroud, G. (2002). Material properties of the human calcaneal fat pad in compression: Experiment and theory. Journal of Biomechanics, 35(12), 1523-1531. doi:10.1016/S0021-9290(02)00090-8.

Misra, J. C., & Singh, S. I. (1983). A large deformation analysis for aortic walls under a physiological loading. International Journal of Engineering Science, 21(10), 1193-1202. doi:10.1016/0020-7225(83)90083-6.

Moireau, P., Xiao, N., Astorino, M., Figueroa, C. A., Chapelle, D., Taylor, C. A., & Gerbeau, J. -. (2012). External tissue support and fluid-structure simulation in blood flows. Biomechanics and Modeling in Mechanobiology, 11(1-2), 1-18. doi:10.1007/s10237-011-0289-z.

Mussa F. F., Horton J. D., Moridzadeh R., et al. (2016). Acute Aortic Dissection and Intramural Hematoma: A Systematic Review. Published in JAMA. doi:10.1001/jama.2016.10026.

Nataf, P., Lansac, E. (2006) Dilation of the thoracic aorta: medical and surgical management. Heart, 92, 1345-1352. doi: 10.1136/hrt.2005.074781.

Nightingale, K., McAleavey, S., & Trahey, G. (2003). Shear-wave generation using acoustic radiation force: In vivo and ex vivo results. Ultrasound in Medicine and Biology, 29(12), 1715-1723. doi:10.1016/j.ultrasmedbio.2003.08.008.

Ogden R. W. (2009). Anisotropy and nonlinear elasticity in arterial wall mechanics. Biomechanical Modelling at the Molecular, Cellular and Tissue Levels, 179-258. doi:10.1007/978-3-211-95875-9.

Okamoto E., Couse T., De Leon H., Vinten-Johansen J., Goodman R. B., Scott N. A., Wilcox J. N. (2001). Perivascular inflammation after balloon angioplasty of porcine coronary arteries. Circulation. 104:2228–2235.

Omidi, E., Fuetterer, L., Reza Mousavi, S., Armstrong, R. C., Flynn, L. E., & Samani, A. (2014). Characterization and assessment of hyperelastic and elastic properties of decellularized human adipose tissues. Journal of Biomechanics, 47(15), 3657-3663. doi:10.1016/j.jbiomech.2014.09.035.

Pan H., Guo J., Su Z. (2014). Advances in understanding the interrelations between leptin resistance and obesity. Physiology & Behavior. 130: 157–69. doi:10.1016/j.physbeh.2014.04.003. PMID 24726399.

Paniagua, J. A. (2016). Nutrition, insulin resistance and dysfunctional adipose tissue determine the different components of metabolic syndrome. World Journal of Diabetes. 7(19). doi: 10.4239/wjd.v7.i19.483. ISSN 1948-9358.

Paulsen, D. F. (2010). Histology & Cell Biology: Examination & Board Review, 5e**.** McGraw-Hill Education / Medical. 432 p. ISBN-10: 0071476652.

Persy, V., & D'Haese, P. (2009). Vascular calcification and bone disease: The calcification paradox. Trends in Molecular Medicine, 15(9), 405-416. doi:10.1016/j.molmed.2009.07.001.

Polzer, S., & Gasser, T. C. (2015). Biomechanical rupture risk assessment of abdominal aortic aneurysms based on a novel probabilistic rupture risk index. Journal of the Royal Society Interface, 12(113) doi:10.1098/rsif.2015.0852.

Rubin, R., Strayer, D. S., Rubin, E. (2011). *Rubin's Pathology:Clinicopathologic Foundations of Medicine*. Lippincott Williams & Wilkins. ISBN 9781605479682.

Shah, R. G., DeVore, D., & Silver, F. H. (2018). Biomechanical analysis of decellularized dermis and skin: Initial in vivo observations using optical cohesion tomography and vibrational analysis. Journal of Biomedical Materials Research - Part A, 106(5), 1421-1427. doi:10.1002/jbm.a.36344.

Schechter A. N., Gladwin M. T. (2003). Hemoglobin and the paracrine and endocrine functions of nitric oxide. N Engl J Med. 348: 1483–1485.

Schulze-Bauer, C. A. J., Mörth, C., & Holzapfel, G. A. (2003). Passive biaxial mechanical response of aged human iliac arteries. Journal of Biomechanical Engineering, 125(3), 395-406. doi:10.1115/1.1574331.

Shah, R. G., DeVore, D., & Silver, F. H. (2018). Biomechanical analysis of decellularized dermis and skin: Initial in vivo observations using optical cohesion tomography and vibrational analysis. Journal of Biomedical Materials Research - Part A, 106(5), 1421-1427. doi:10.1002/jbm.a.36344.

Singh, R. S., Mengi, S. A., Xu, Y. J., Arneja, A. S., and Dhalla, N. S. (2002). Pathogenesis of atherosclerosis: A multifactorial process. Exp Clin Cardiol; 7(1):40-53.

Sitia, S., Tomasoni, L., Atzeni, F., Ambrosio, G., Cordiano, C., Catapano, A., Tramontana, S., Perticone, F., Naccarato, P. (2010). From endothelial dysfunction to atherosclerosis. Autoimmunity Reviews. 9 (12):830.834.doi:10.1016/j.autrev.2010.07.016.

Sommer, G., Eder, M., Kovacs, L., Pathak, H., Bonitz, L., Mueller, C., Regitnig, P., Holzapfel, G. A. (2013). Multiaxial mechanical properties and constitutive modeling of human adipose tissue: A basis for preoperative simulations in plastic and reconstructive surgery. Acta Biomaterialia, 9(11), 9036-9048. doi:10.1016/j.actbio.2013.06.011.

Swardfager W., Lanctôt K., Rothenburg L., Wong A., Cappell J., Herrmann N. (2010). A meta-analysis of cytokines in Alzheimer's disease. Biol Psychiatry. 68 (10): 930–941. doi:10.1016/j.biopsych.2010.06.012. PMID 20692646.

Szasz T., Webb R. C. (2012). Perivascular adipose tissue: more than just structuralsupport. Clin Sci (Lond). 122:1–12.

Szasz T., Bomfim G. F., Webb R. C. (2013). The influence of perivascular adipose tissue on vascular homeostasis. Vasc Health Risk Manag. 9:105–116.

Taber L. A. (2004). Nonlinear theory of elasticity: applications in biomechanics. World Scientific, 276. ISBN-10: 9812387358.

Van Loon, P., Klip, W., & Bradley, E. L. (1977). Length-force and volume-pressure relationships of arteries. Biorheology, 14(4), 181-201. doi:10.3233/BIR-1977-14405.

Victor F. C., Gottlieb A. B. (2002). TNF-alpha and apoptosis: implications for the pathogenesis and treatment of psoriasis. J Drugs Dermatol. 1 (3): 264–75.

Vita J. A., Keaney J. F. (2002). Endothelial function: a barometer for cardiovascular risk? Circulation. 106: 640–642.

Vu, K., Kaitoukov, Y., Morin-Roy, F. et al. Rupture signs on computed tomography, treatment, and outcome of abdominal aortic aneurysms. *Insights Imaging* 5, 281–293 (2014).doi: 10.1594/ecr2014/C-0789.

Weisberg S. P., McCann D., Desai M., Rosenbaum M., Leibel R. L., Ferrante A. W., Jr. (2003). Obesity is associated with macrophage accumulation in adipose tissue. J Clin Invest. 112:1796–1808. doi: 10.1172/JCI200319246.

Williams & Wilkins (2006). Cytokine" in Stedman's Medical Dictionary, 28th ed. ISBN 9780199549351.

Zaborska, K. E., Wareing, M., and Austin, C. (2017). Comparisons between perivascular adipose tissue and the endothelium in their modulation of vascular tone. British Journal of Pharmacology, 174(20), 3388-3397. doi:10.1111/bph.1364.

Zhang, W., Herrera, C., Atluri, S. N., & Kassab, G. S. (2004). Effect of surrounding tissue on vessel fluid and solid mechanics. Journal of Biomechanical Engineering, 126(6), 760-769. doi:10.1115/1.1824128.

10 Curriculum vitae

Personal data:

Name and surname: Ing. Tereza Voňavková
Date of birth: 22 April, 1988
Address: Nad Okrouhlíkem 17, 182 00 Praha 8, Czech Republic
Tel.: +420 720 245 523
E-mail: terezka.vonavkova@centrum.cz

Education:

2013 – now Czech Technical University in Prague, Czech Republic
Faculty: Faculty of Mechanical Engineering
Doctoral study program: Mechanical Engineering
Field of study: Biomechanics
Dissertation topic: Mechanical properties of perivascular adipose tissue and its effect on biomechanics of abdominal Aorta

2011 – 2013 Czech Technical University in Prague, Czech Republic
Faculty: Faculty of Mechanical Engineering
Master's degree in Biomechanics and medical devices
Diploma thesis: Stress and strain fields in non-uniformly loaded artery

2007 – 2011 Czech Technical University in Prague, Czech Republic
Faculty: Faculty of Mechanical Engineering
Bachelor's degree in Applied mechanics
Bachelor thesis: Experimental in vitro coronary stent implantation

2003 – 2007 Gymnasium J. A. Komenského (Grammar school)

Employment history:

2010 – 2017 Czech Technical University in Prague, Faculty of Mechanical Engineering
Position: Science and research
Job description:

- Experimental coronary stent implantation - implementation and evaluation of a series of experiments in vitro, determining deformation of an artery after stent implantation and the interaction of the stent and artery
- The effect of age on the elasticity of arteries - evaluation of histological sections of elastic arteries, statistical evaluation of ripple collagen fibers
- Mechanical tests of blood vessels, perivascular adipose tissue, prostates and the evaluation of mechanical properties
- Constitutive modeling of blood vessels and perivascular tissue

- FE modeling of abdominal aorta with existence of atherosclerotic plaque - analysis of stress and strain in the model of vessel
- Teaching the subject Elasticity and strength

2018 – now Motol University Hospital, Department of medical technology and investment
Position: Biomedical engineer
Job description:

- Ensuring proper operation of medical devices and technical support on clinical departments
- Service and control of medical devices
- Comunication between clinical department and companies distributing medical devices
- Determination of technical specifications for purchasing new medical devices

Computer skills:
MS Office, Maple, Matlab, Abaqus, NIS-Elements, AutoCAD, Syngovia.

Language skills:
Czech – native
English – intermediate

Other skills:
Driving license

Personal skills and hobbies:
Willing to learn, hard working, cooperative, easy-going, communicative.
Sport and healthy lifestyle, medicine, traveling, literature, music.

11 List of author´s publications

11.1 Publications on topic of the dissertation thesis

Voňavková and Horný (2020) Effect of axial prestretch and adipose tissue on the inflation-extension behavior of the human abdominal aorta. Computer Methods in Biomechanics and Biomedical Engineering 23(3):81-91.
Publisher link: https://doi.org/10.1080/10255842.2019.1699544.
Article in journal with WoS impact factor (IF2018 = 1.61).

Vonavkova, T., Horny, L., Vesely, J., Adamek, T., and Zitny, R. (2016) Effect of perivascular tissue on inflation-extension behavior of abdominal aorta. ECCOMAS Congress 2016: VII European Congress on Computational Methods in Applied Sciences and Engineering. p. 6616-6624.
Publisher link: https://doi.org/10.7712/100016.2283.10742.
Conference paper indexed in SCOPUS/WoS.

Vonavkova, T., Horny, L., Adamek, T., Kulvajtova, M.,Zitny, R. (2015) Constitutive modelling of human perivascular adipose tissue. A: COMPLAS XIII. "COMPLAS XIII: proceedings of the XIII International Conference on Computational Plasticity: fundamentals and applications". CIMNE ed. Barcelona: CIMNE, p. 463-470.
Conference paper indexed in SCOPUS/WoS.

Voňavková T., Horný L., Kulvajtová M., Žitný R. (2014). Uniaxial tensile test of perivascular adipose tissue. *Bulletin of Applied Mechanics* 10(36):11-14. ISSN 1801-1217.
Article in peer-reviewed journal.

11.2 Other publications

Suchý T., Šupová M., Klapková E., Adámková V., Závora J., Žaloudková M., Rýglová Š., Ballay R., Denk F., Pokorný M., Sauerová P., Hubálek Kalbáčová M., Horný L., Veselý J., Voňavková T., Průša R. (2017). The release kinetics, antimicrobial activity and cytocompatibility of differently prepared collagen/hydroxyapatite/vancomycin layers: Microstructure vs. Nanostructure. *Eur J Pharm Sci*, 100:219-229.
Publisher link: https://doi.org/10.1016/j.ejps.2017.01.032.
Article in jounral with WoS impact factor (IF2018 = 3.532).
Horny, L., Chlup, H., Zitny, R., Vonavkova, T., Vesely, J., & Lanzer, P. (2012). Ex vivo coronary stent implantation evaluated with digital image correlation. *Exp Mech* 52(9), 1555-1558.
Publisher link: https://doi.org/10.1007/s11340-012-9620-6.
Article in journal with WoS impact factor (IF2018 = 2.256).

Horny, L., Netusil, M., Vonavkova, T. (2014). Axial prestretch and circumferential distensibility in biomechanics of abdominal aorta. *Biomech Model Mechanobiol* 13(4):783-799.
Publisher link: https://doi.org/10.1007/s10237-013-0534-8.
Article in journal with WoS impact factor (IF2018 = 2.829).

Horny, L., Chlup, H., Vesely, J., Gultova, E., Kronek, J., Zitny, R., Vonavkova, T., Adamek, T., Lanzer, P., and Hromadka, D. (2011) In vitro Coronary Stent Implantation: Vessel Wall-Stent Interaction. 5th European Conference of the International Federation for Medical and Biological Engineering. IFMBE Proceedings, vol 37. Springer, Berlin, Heidelberg.
Publisher link: https://doi.org/10.1007/978-3-642-23508-5_207.
Confernece paper indexed in SCOPUS/WoS.

Appendix A

Inflation response of abdominal aorta (DONOR F63) surrounded by PVAT with 3 different wall thickness $H_{PT} = 0.2, 1.22, 40$ mm.

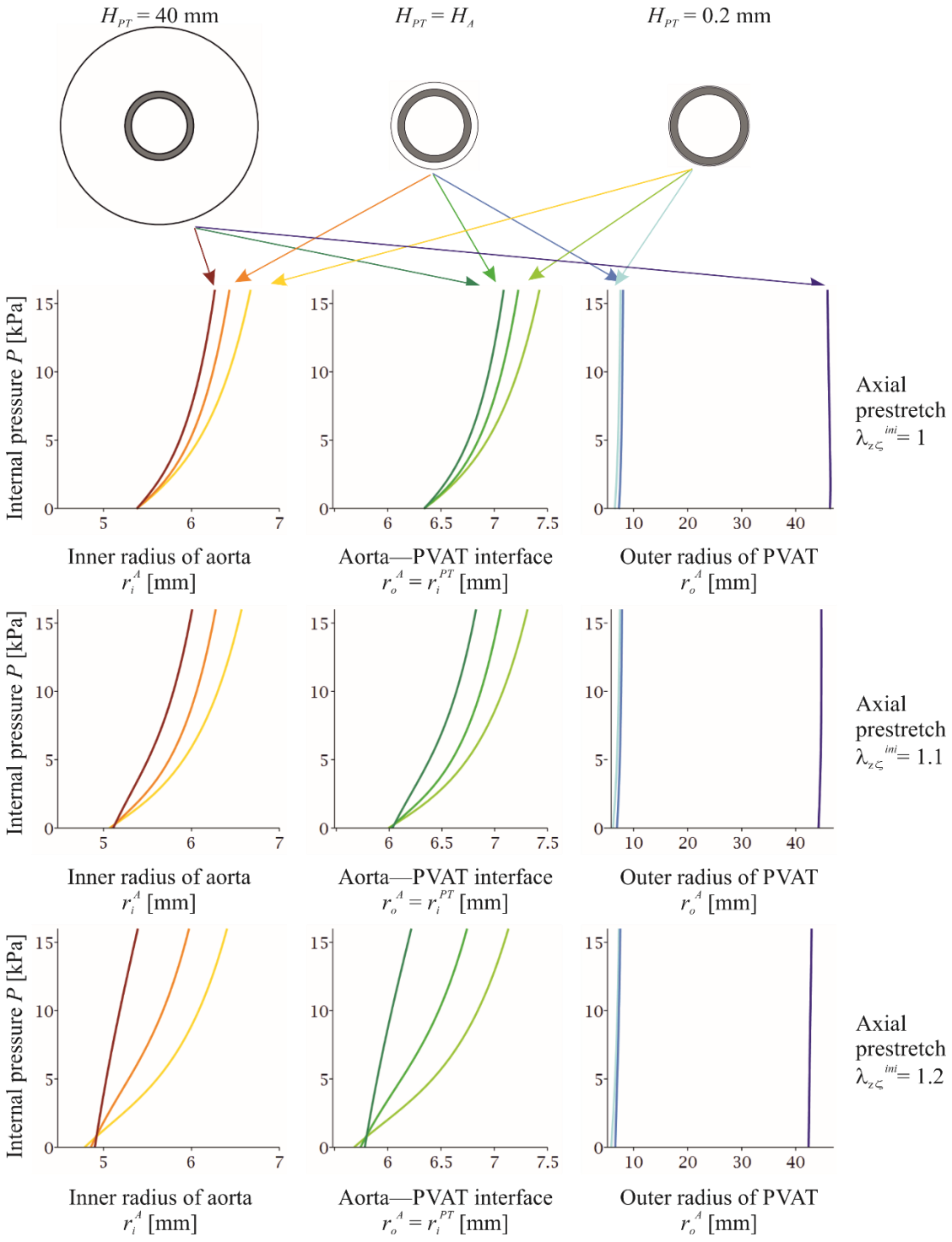

Extension response of abdominal aorta (DONOR F63) surrounded by PVAT with 3 different wall thickness $H_{PT} = 0.2, 1.22, 40$ mm

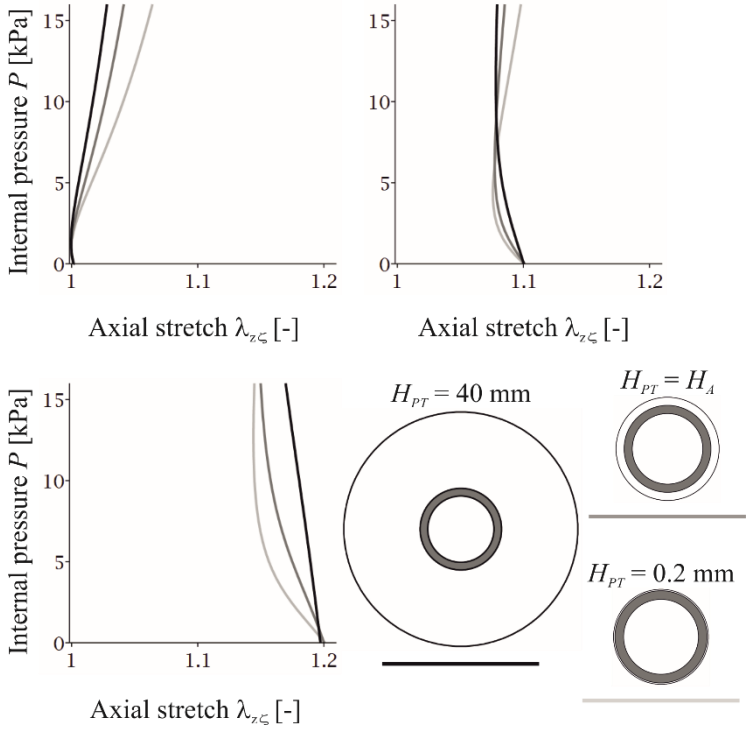

Results of circumferential stretch at aorta inner radius (DONOR F63) in dependence on the axial prestretch during inflation

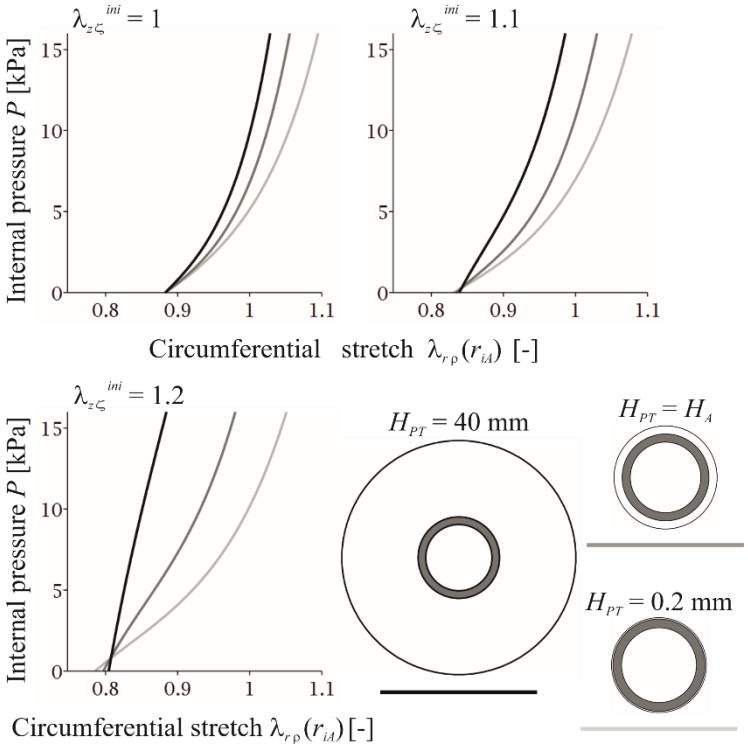

Distribution of in-wall stresses in aorta (DONOR F63) pressurized to 16 kPa and surrounded by PVAT with 3 different wall thickness $H_{PT} = 0.2, 1.22, 40$ mm

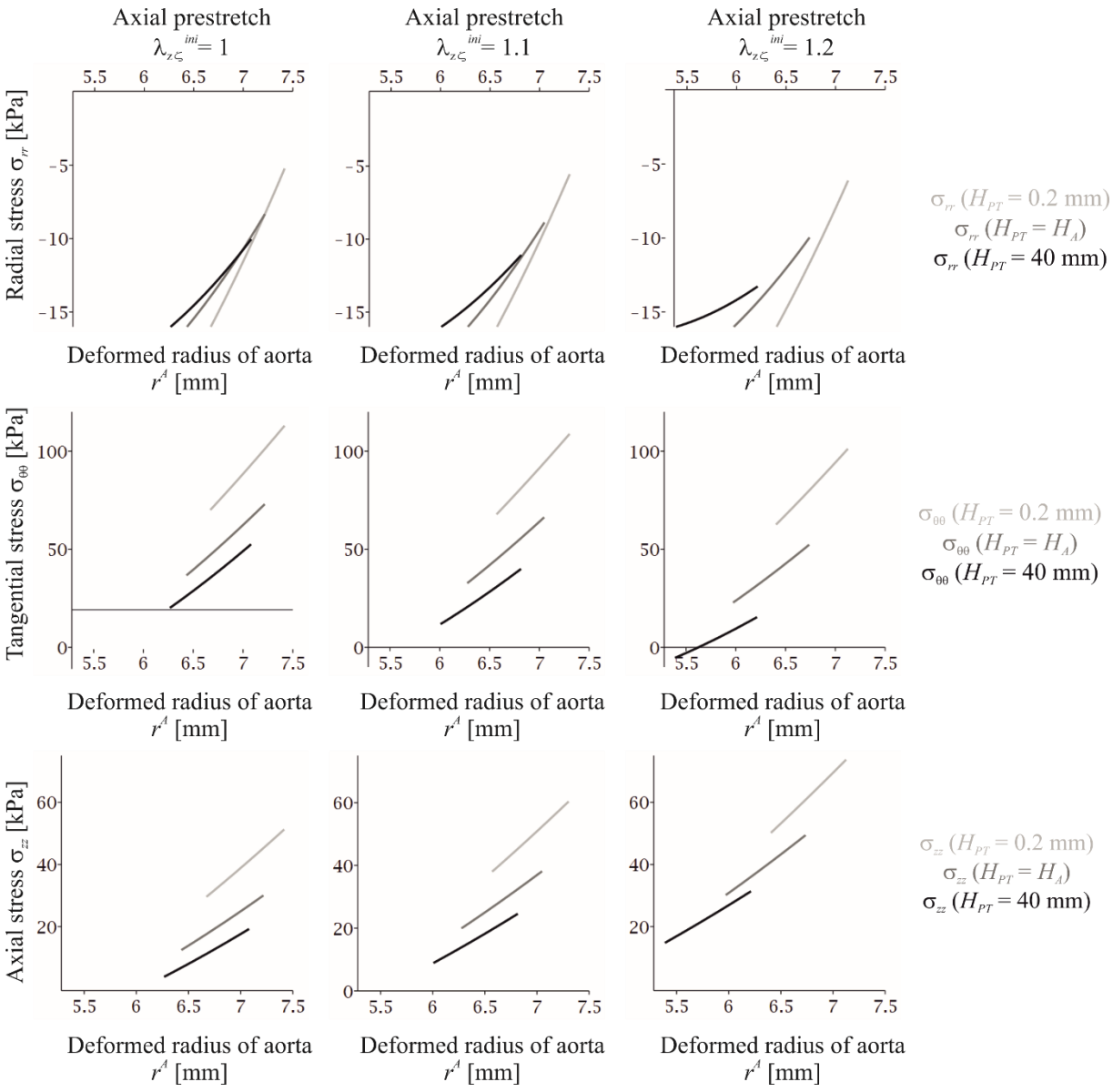

Distribution of in-wall stresses in PVAT inflated by aorta (DONOR F63) pressurized to 16 kPa. PVAT tube thickness was $H_{PT} = 0.2, 1.22, 40$ mm

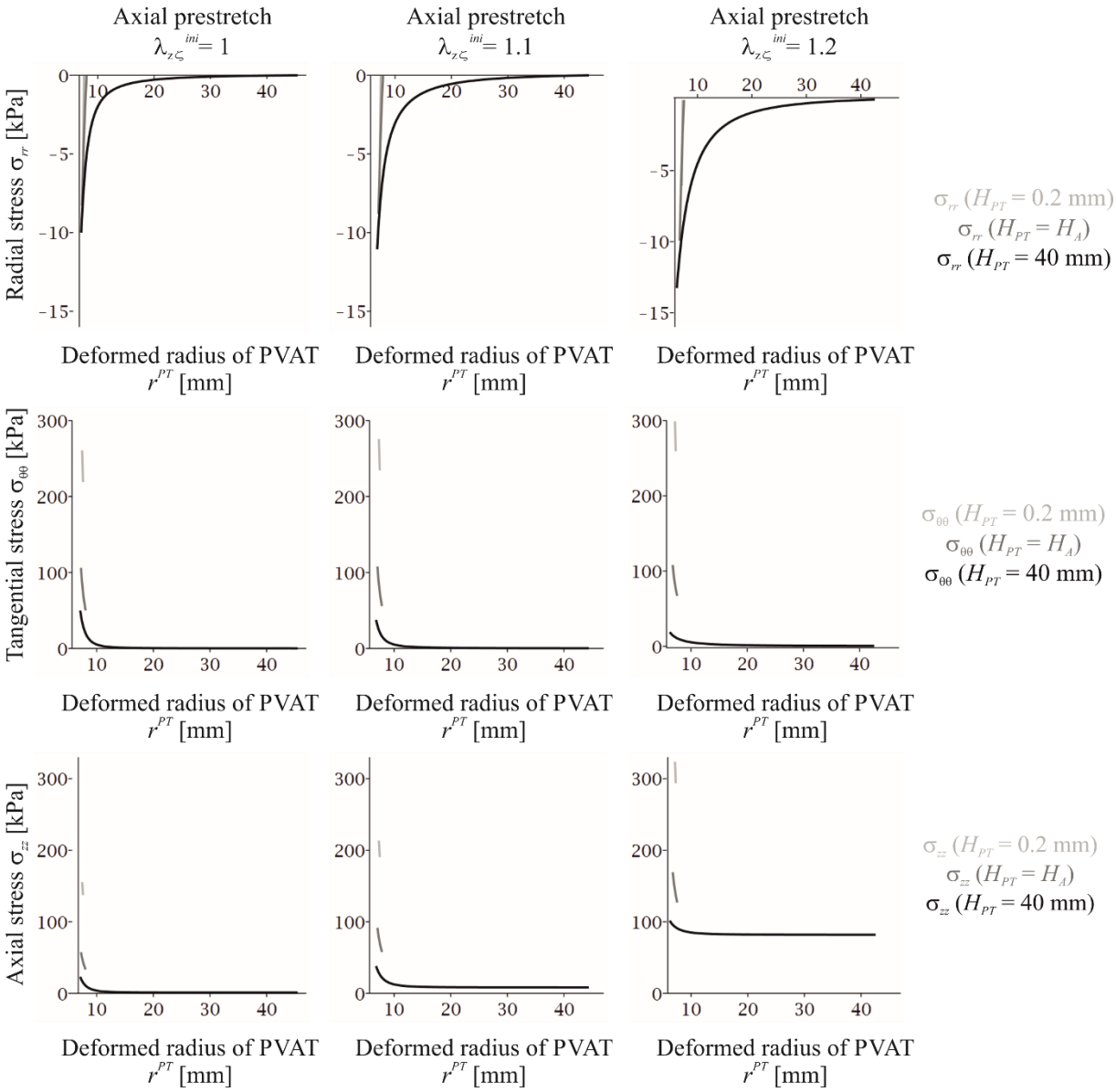

Appendix B

The article *"Effect of axial prestretch and adipose tissue on the inflation-extension behavior of the human abdominal aorta"* will follow on the next pages.

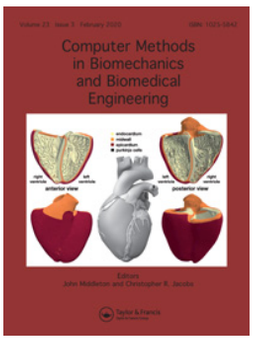

Computer Methods in Biomechanics and Biomedical Engineering

ISSN: 1025-5842 (Print) 1476-8259 (Online) Journal homepage: https://www.tandfonline.com/loi/gcmb20

Effect of axial prestretch and adipose tissue on the inflation-extension behavior of the human abdominal aorta

Tereza Voňavková & Lukáš Horný

To cite this article: Tereza Voňavková & Lukáš Horný (2020) Effect of axial prestretch and adipose tissue on the inflation-extension behavior of the human abdominal aorta, Computer Methods in Biomechanics and Biomedical Engineering, 23:3, 81-91, DOI: 10.1080/10255842.2019.1699544

To link to this article: https://doi.org/10.1080/10255842.2019.1699544

Published online: 09 Dec 2019.

COMPUTER METHODS IN BIOMECHANICS AND BIOMEDICAL ENGINEERING
2020, VOL. 23, NO. 3, 81–91
https://doi.org/10.1080/10255842.2019.1699544

Effect of axial prestretch and adipose tissue on the inflation-extension behavior of the human abdominal aorta

Tereza Voňavková and Lukáš Horný

Faculty of Mechanical Engineering, Czech Technical University in Prague, Prague, Czech Republic

ABSTRACT

Our study aims to show that perivascular adipose tissue may significantly change the mechanical state of the abdominal aorta. To this end, uniaxial tensile tests with perivascular fat tissue were carried out. In the subsequent regression analysis, stress-strain data were fitted by the polynomial strain energy density. A constitutive model of adipose tissue was used in the analytical simulation of the inflation-extension behavior of the human abdominal aorta. The computational model was based on the theory of the bi-layered thick-walled tube. In addition to the effect of perivascular tissue, the effect of axial prestretch was also studied. It was found that the presence of perivascular tissue reduces the distensibility of the aorta. Axial prestretch applied to the aorta embedded in adipose tissue had an effect opposite to that of adipose tissue. Axially prestrained aorta exhibited higher distensiblity than non-prestrained aorta. It was also shown that the perivascular envelope bears some portion of the pressure loading and thus reduces the mechanical stresses inside the wall of aorta. A similar effect was found for axial prestretch.

ARTICLE HISTORY
Received 17 April 2019
Accepted 27 November 2019

KEYWORDS
Adipose tissue; aorta; axial prestretch; constitutive model; hyperelasticity; thick-walled tube

1. Introduction

Despite significant progress that has been achieved in arterial biomechanics in the last few decades, there are still topics that seem to have been overlooked for a long time. In the authors' opinion, one of these is the role of perivascular adipose tissue (PVAT). It may have been a widely accepted idea that perivascular tissue provides mechanical support to an artery, but it has led to a clear oversimplification in which one imagines the role of perivascular adipose tissue in the way that it merely fills the space between the external surface of the artery and neighboring organs. The current anatomical view of the role of PVAT is, however, quite different. Similar to the endothelium, PVAT can modulate vascular tone by releasing vasoactive molecules (Zaborska et al. 2017) which has a direct impact on the mechanical state of the artery. In contrast to the endothelium, PVAT consists of multiple cell types. Besides adipocytes, macrophages, fibroblasts, lymphocytes, and adipocyte progenitor cells are also present in PVAT. The presence of these types of cells suggests the complex endocrine function of PVAT and its contribution to inflammatory processes occurring in the arterial wall (Zaborska et al. 2017; Brown et al. 2014). Considering this, one sees that PVAT is not merely a mechanical support, nor a simple energy-storing tissue, but it is an element with its own complex mechanobiological role.

Nevertheless, it is not only the biological function of PVAT that seems to be underrated in the scientific literature. Computational simulations describing arterial biomechanics considering the effect of perivascular tissue are also rare. If the effect of perivascular tissue is considered, it is most frequently reduced to a form of the boundary condition imposed at the external surface of the artery. This approach has been adopted by Moireau et al. (2012) who investigated the effect of the surrounding tissue on hemodynamics in the aorta, and by Hodis and Zamir (2011) who investigated the effect of external tethering of the arterial wall on the dynamics of pressure pulse transmission.

Liu et al. (2007) obtained pressure-radius experimental data from swine carotid and femoral arteries in the tethered state and after PVAT excision. They showed that arteries with surrounding tissue sustain lower strains and stresses during inflation than their untethered counterparts. Masson et al. (2011) considered perivascular support in their computational model when estimating the constitutive parameters of human carotid arteries from in vivo data. They used

CONTACT Lukáš Horný Lukas.horny@fs.cvut.cz

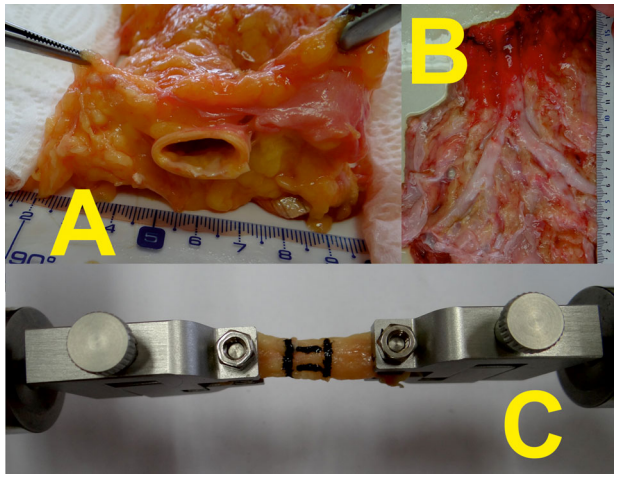

Figure 1. Perivascular tissue surrounds infrarenal aorta – transversal plane (panel A), frontal plane (panel B). A sample of PVAT in uniaxial tension (panel C).

the model of the thick-walled tube for the artery; however, the perivascular tissue was again reduced only to its mechanical interaction with the wall by a nonzero external pressure acting on the artery by means of the mathematical expression for perivascular pressure proposed by Humphrey and Na (2002).

One obvious barrier to considering PVAT in computational simulations as a 3 D object is the fact that such an object has to be characterized with a constitutive model. However, current scientific literature describing the elastic properties of PVAT at finite strains is very poor. Most of the available experiments have been conducted with subcutaneous adipose tissue, usually from the abdominal region or from the breast, because their primary goal was to provide data suitable for computational simulations focused on plastic and reconstructive surgery (Sommer et al. 2013; Omidi et al. 2014). Moreover, most of these studies adopted the linear model and describe the elasticity of adipose tissue by means of the Young modulus (Geerligs et al. 2008; Comley and Fleck 2010). The framework of nonlinear elasticity was adopted by Sommer et al. (2013), Omidi et al. (2014), and Calvo-Galleo et al. (2018), but they did not focus on perivascular tissue.

The goal of the present study is to extend our knowledge of the mechanical behavior of perivascular adipose tissue and its role in the biomechanics of the human abdominal aorta. To this end, uniaxial tensile tests with retropenitonal adipose tissue were carried out. Subsequently, the bi-layer, thick-walled tube analytical model was employed to simulate the effect of the thickness of PVAT and axial prestretch on the mechanical response of the aorta.

2. Materials and methods

2.1. Tensile testing of adipose tissue

2.1.1. Samples

Specimens were obtained from cadavers autopsied in the Department of Forensic Medicine of Královské Vinohrady University Hospital in Prague. The post-mortem usage of human tissue was approved by the Ethics Committee of the Third Faculty of Medicine of Charles University in Prague. Figure 1 shows the aorta surrounded by adipose tissue. Approximately rectangular strips with typical dimensions of 10 mm x 10 mm x 50 mm were prepared using a scalpel. The reference dimensions of the samples were determined by an image analysis of digital photographs (NIS-Elements, Nikon Instruments). Due to high compliance and the slipperiness of the tissue, it was not possible to perfectly align the strips in either circumferential or longitudinal directions.

2.1.2. Testing procedure

A multipurpose tensile testing machine (Zwick/Roell, Germany) was used. The testing machine used electromechanical actuators with a displacement resolution of ± 1 µm and U9B force transducers (HBM, Germany, ± 25 N). During the test, the deformation of samples was determined with a built-in videoextensometer by means of contrasting marks created on a sample with liquid eyeliner. The experimental protocol consisted of four cycles as a preconditioning of tissue behavior, and the fifth cycle was used in the subsequent determination of the material parameters. The loading part of the force–elongation response was used for this purpose. All tests were conducted at room temperature with the velocity of clamps set to 0.2 mms^{-1}.

2.2. PVAT constitutive model and its parameters

2.2.1. Kinematics

It was assumed that during the uniaxial tensile test, the portion of the sample restricted by marks undergoes homogenous dilatation expressed in Cartesian coordinates as $x_i = \lambda_{iK} X_K$ for i, $K = 1$, 2, and 3 where $\lambda_{iK} = 0$ for $i \neq K$. Here $\boldsymbol{X} = (X_1, X_2, X_3)^T$ and $\boldsymbol{x} = (x_1, x_2, x_3)^T$ respectively denote the position vector in the reference and in the deformed configuration. Deformation gradient $\mathbf{F}$ is defined in (1), and the right Cauchy-Green strain tensor $\mathbf{C}$ is given by $\mathbf{C} = \mathbf{F}^T\mathbf{F}$.

$$\mathbf{F} = \frac{\partial \boldsymbol{x}}{\partial \boldsymbol{X}} \tag{1}$$

Due to high lipid content in the adipose tissue, it is assumed that PVAT is incompressible (Comley and Fleck 2010; Sommer et al. 2013), thus $det(\mathbf{F}) = 1$ holds during the deformation.

2.2.2. Constitutive model

Since our aim was to use data characterizing PVAT in time-independent (quasi-static) simulations of the inflation-extension behavior of the abdominal aorta, we restricted our attention to the elastic response of PVAT. This means that viscoelastic effects like stress relaxation and creep, which may accompany in vivo pressure wave propagation, are neglected here. Thus perivascular adipose tissue was considered to be hyperelastic (Sommer et al. 2013; Omidi et al. 2014). It was characterized with the strain energy density function expressed in (2). Here c_1, and c_2 denote stress-like material parameters, and I_1 is the first invariant of the right Cauchy-Green deformation tensor $\mathbf{C}$. The isotropic elastic potential (2) was chosen in accordance with Omidi et al. (2014). An assumption of isotropy was adopted, because we were not able to perfectly align samples with their anatomical directions.

$$W_{PT} = c_1(I_1 - 3) + c_2(I_1 - 3)^2 \tag{2}$$

The hyperelastic constitutive equation for incompressible material is given by (3). Here $\boldsymbol{\sigma}$ denotes the Cauchy stress tensor, and $\mathbf{I}$ is the second order unit tensor. The symbol p denotes the indeterminate multiplier related to the hydrostatic part of the stress tensor.

$$\boldsymbol{\sigma} = \frac{\partial W}{\partial \mathbf{F}}\mathbf{F}^T - p\mathbf{I} \tag{3}$$

2.2.3. Regression analysis

Experimental stress was obtained as ${\sigma_{11}}^{EXP} = F\lambda_{11}/S$, where S denotes the reference cross-section area and F is the force elongating the sample from reference length L to deformed length l; $\lambda_{11} = l/L$. The stress predicted by the model, ${\sigma_{11}}^{MOD}$, is obtained from (3), and its final expression is given in (4).

$$\sigma_{11}^{MOD} = 2\left(c_1 + 2c_2\left(\lambda_{11}^2 + \frac{2}{\lambda_{11}} - 3\right)\right)\left(\lambda_{11}^2 - \frac{1}{\lambda_{11}}\right) \tag{4}$$

2.3. Constitutive model for abdominal aorta

The abdominal aorta wall was modeled as a homogenous, anisotropic, incompressible and hyperelastic continuum characterized by the strain energy density function W_A proposed by Gasser et al. (2006). It is expressed in (5).

$$W_A = \frac{\mu}{2}(I_1 - 3) + \sum_{i=4,6}\frac{k_1}{2k_2}\left(e^{k_2(K_i-1)^2} - 1\right) \tag{5}$$

$$K_i = \kappa I_1 + (1 - 3\kappa)I_i \qquad i = 4, 6 \tag{6}$$

The elastic potential (5) consists of an isotropic part, it is a neo-Hookean term depending on the first invariant of $\mathbf{C}$, and an anisotropic exponential part that depends on generalized structural deformation invariants denoted K_4 and K_6. The isotropic part is related to the elastic energy stored in the non-collagenous part of the arterial wall, whereas the anisotropic part is linked to the energy stored in bundles of collagen fibers. Since these fibers have a stochastic wavy pattern, their recruitment into the load-bearing process results in the strain-stiffening response, which is well described by an exponential function (Holzapfel et al. 2000). The model is based on the assumption that bundles of collagen fibers are arranged in the arterial wall with two dominant helices wound around the longitudinal axis at angles of $\pm(90^\circ - \beta)$. These helices can be in cylindrical coordinates (R, Θ, Z) characterized with unit vectors $\boldsymbol{M}_1 = (0, cos(\beta), sin(\beta))^T$, $\boldsymbol{M}_2 = (0, cos(-\beta), sin(-\beta))^T$. These preferred directions give rise to deformation invariants I_4 and I_6 according to (7).

$$I_4 = \boldsymbol{M}_1 \cdot (\mathbf{C}\boldsymbol{M}_1) = \boldsymbol{M}_2 \cdot (\mathbf{C}\boldsymbol{M}_2) = I_6 \tag{7}$$

In fact, however, the collagen fibers are not perfectly aligned with the directions $\boldsymbol{M}_1$ and $\boldsymbol{M}_2$. Rather, they exhibit some dispersion around the predominant directions. The used strain energy function takes this into account by using generalized structural invariants K_4 and K_6 that also include a contribution from invariant I_1. Nevertheless, it is worth noting that, although the model (5) enables structural interpretation, in fact it is a phenomenological model, and its parameters should not be confused with the exact internal architecture of the arterial wall.

2.4. Simulation of the inflation-extension behavior of the abdominal aorta with PVAT

2.4.1. Geometry and kinematics

The abdominal aorta was modeled as a homogenous thick-walled tube with the reference geometry corresponding to an open cylinder to take into account circumferential residual strains (Horný et al. 2014a, 2014b). Hence in the first step, the reference stress-free opened cylinder is closed to form a hollow

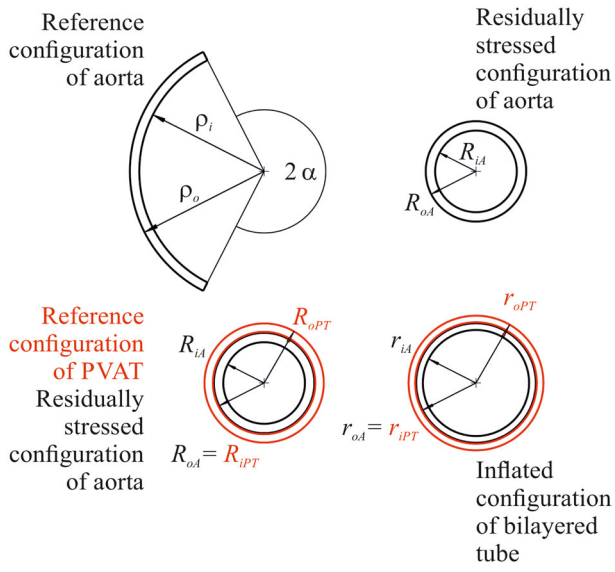

Figure 2. Reference and deformed configurations.

cylinder. The kinematics in polar cylindrical coordinates is expressed in Equations (8). (ρ, ϑ, ζ) are coordinates defined in the stress-free configuration, whereas (R, Θ, Z) are defined in the residually stressed but unpressurized state. In Equations (8b) and (8c), α is the opening angle, and δ is the axial stretch accompanying closing into a cylindrical geometry.

$$R = R(\rho) \qquad \Theta = 2\pi/(2\pi - 2\alpha)\vartheta \qquad Z = \delta\zeta \tag{8}$$

Subsequently, the aorta is elongated by axial force F_{red} to reach its in situ length, and inflation by internal pressure P follows. During pressurization, the aorta can further elongate or shorten, and that is governed by equilibrium equations. In (9), the deformed configuration is expressed in the polar cylindrical coordinates (r, θ, z).

$$r = r(R) \qquad \theta = \Theta \qquad z = \lambda Z \tag{9}$$

The total deformation gradient of the aorta $\mathbf{F}_A$ is then given as $\mathbf{F}_A = \mathbf{F}_{A2}\mathbf{F}_{A1}$, where $\mathbf{F}_{A1}$ is linked to the residual deformation and $\mathbf{F}_{A2}$ expresses subsequent inflation and extension. The matrices of the gradients are given in (10) and (11).

$$\mathbf{F}_A = \mathbf{F}_2\mathbf{F}_1 = \begin{pmatrix} \lambda_{r\rho} & 0 & 0 \\ 0 & \lambda_{\theta\vartheta} & 0 \\ 0 & 0 & \lambda_{z\zeta} \end{pmatrix} = \begin{pmatrix} \partial r/\partial\rho & 0 & 0 \\ 0 & \pi r/[\rho(\pi-\alpha)] & 0 \\ 0 & 0 & \lambda\delta \end{pmatrix} \tag{10}$$

$$\mathbf{F}_{A1} = \begin{pmatrix} \lambda_{R\rho} & 0 & 0 \\ 0 & \lambda_{\Theta\vartheta} & 0 \\ 0 & 0 & \lambda_{Z\zeta} \end{pmatrix} = \begin{pmatrix} \partial R/\partial\rho & 0 & 0 \\ 0 & \pi R/[\rho(\pi-\alpha)] & 0 \\ 0 & 0 & \delta \end{pmatrix} \tag{11}$$

$$\mathbf{F}_{A2} = \begin{pmatrix} \lambda_{rR} & 0 & 0 \\ 0 & \lambda_{\theta\Theta} & 0 \\ 0 & 0 & \lambda_{zZ} \end{pmatrix} = \begin{pmatrix} \partial r/\partial R & 0 & 0 \\ 0 & r/R & 0 \\ 0 & 0 & \lambda \end{pmatrix} \tag{12}$$

To account for the effect of perivascular tissue on the mechanics of the aorta, it is assumed that during its inflation and extension the aorta is surrounded by an external cylindrical layer composed of PVAT. $R_{oA} = R_{iPT}$ and $r_{oA} = r_{iPT}$ hold during the deformation. Here R_{iPT} and r_{iPT} denote the reference and deformed inner radius of the PVAT cylinder, Figure 2. It is assumed that the PVAT cylinder retains its cylindrical shape in the deformation, thus its deformation gradient has a form similar to $\mathbf{F}_{A2}$.

2.4.2. Equilibrium equations

Equilibrium equations for the bi-layered tube can be written in the forms (13-14). Here W^a denotes W with radial stretch being substituted from the incompressibility condition. W_A represents the strain energy stored in the aorta (5), and W_{PT} denotes the energy stored in PVAT (2).

$$P = \int_{r_{iA}}^{r_{oA}} \lambda_{\theta\vartheta}\frac{\partial \hat{W}_A}{\partial\lambda_{\theta\vartheta}}\frac{dr}{r} + \int_{r_{iPT}}^{r_{oPT}} \lambda_{\Theta\Theta}\frac{\partial \hat{W}_{PT}}{\partial\lambda_{\Theta\Theta}}\frac{dr}{r} \tag{13}$$

$$F_{red} = \pi\int_{r_{iA}}^{r_{oA}}\left(2\lambda_{z\zeta}\frac{\partial \hat{W}_A}{\partial\lambda_{z\zeta}} - \lambda_{\theta\vartheta}\frac{\partial \hat{W}_A}{\partial\lambda_{\theta\vartheta}}\right)rdr + \pi\int_{r_{iPT}}^{r_{oPT}}\left(2\lambda_{zZ}\frac{\partial \hat{W}_{PT}}{\partial\lambda_{zZ}} - \lambda_{\Theta\Theta}\frac{\partial \hat{W}_{PT}}{\partial\lambda_{\Theta\Theta}}\right)rdr \tag{14}$$

Equations (13) and (14) assume that the boundary conditions $\sigma_{rr}(r_{iA}) = -P \wedge \sigma_{rr}(r_{oPT}) = 0$ hold. The tube is considered to be closed, and F_{red} is an additional axial force which ensures the initial axial stretch ($\lambda_{z\zeta}^{ini}$) and which the aorta sustains independently of internal pressure P (Horný et al. 2013, 2014b, 2017).

2.5. Stress distribution through the wall

To evaluate stress distribution through the wall, Equations (15a), (15b), and (15c) have been adopted. Stresses acting in PVAT are obtained when substitution from (2) is performed, and $\lambda_{\theta\Theta}$, λ_{zZ}, and integration to r_{oPT} is considered.

$$\sigma_{rr}(r) = -\int_{r}^{r_{oA}} \lambda_{\theta\vartheta}\frac{\partial \hat{W}_A}{\partial \lambda_{\theta\vartheta}}\frac{dx}{x} - \int_{r_{iPT}}^{r_{oPT}} \lambda_{\theta\Theta}\frac{\partial \hat{W}_{PT}}{\partial \lambda_{\theta\Theta}}\frac{dr}{r}$$

$$\sigma_{\theta\theta}(r) = \lambda_{\theta\vartheta}\frac{\partial \hat{W}_A}{\partial \lambda_{\theta\vartheta}} + \sigma_{rr}$$

$$\sigma_{zz}(r) = \lambda_{z\zeta}\frac{\partial \hat{W}_A}{\partial \lambda_{z\zeta}} + \sigma_{rr} \tag{15}$$

2.6. Thickness of PVAT, loading conditions and material parameters

2.6.1. PVAT thickness

With regard to the amount of fat tissue, anatomical variations in the human population are rather large. To take this fact into account, three representative thicknesses of the PVAT layer were considered in our simulations. These cases were chosen with reference to the thickness of the aorta such that: (I) represents a very thin fat layer with 0.2 mm $= H_{PT} \ll R_{oA} - R_{iA}$, (II) $H_{PT} = R_{oA} - R_{iA}$ is the middle case, and (III) $R_{oA} - R_{iA} \ll H_{PT} = 40$ mm represents a situation in which the movement of aorta is significantly restricted by surrounding tissue.

2.6.2. Loading

External loading during the inflation-extension response of the aorta is represented by internal pressure P and the initial axial stretch $\lambda_{z\zeta}^{ini}$ that the aorta sustains independently of pressure. To account for prestretch, F_{red} necessary to elongate the aorta to $\lambda_{z\zeta}^{ini}$ was computed at $P = 0$. In the subsequent pressurization from 0 up to 16 kPa, F_{red} was held constant, which ensured that $\lambda_{z\zeta}$ would vary during inflation. Values where $\lambda_{z\zeta}^{ini} = 1$, 1.1, and 1.2 were considered in our study.

2.6.3. Material parameters for the aorta and PVAT

The material parameters for the abdominal aorta were adopted from Horný et al. (2014a). One representative sample of a 38-year-old male donor was considered (denoted M38). The specific values of the material parameters are provided in Table 1. In contrast to aortic tissue, the PVAT parameters are based on our experiments. In the inflation-extension simulation, average perivascular tissue behavior was considered. Since the constitutive equation for PVAT is nonlinear, the material parameters used in the study were fitted to all the data to obtain a mean model. Such an approach takes into account the effects of all observed responses and naturally produces a model which can be considered an average model.

Table 1. Constitutive parameters and geometry of the human abdominal aorta. Adopted form Horný et al. (2014a), sample denoted as M38.

μ [kPa]	k_1 [kPa]	k_2 [-]	κ [-]	β [°]	ρ_i [mm]	ρ_o [mm]	α [°]	R_{iA} [mm]	R_{oA} [-mm]
15.9	78.49	4.99	0.19	41.41	16.2	17.24	117	5.3	6.52

Table 2. PVAT samples summary and material parameters (a – the most compliant case, b – average model, c – the stiffest case).

Donor	Sex {M,}	Age [years]	n [–]
1	M	71	3
2	M	41	3
3	M	67	2
4	M	71	1
5	F	53	1
6	M	29	3
7	M	69	2
	c_1 [kPa]	c_2 [kPa]	
(a)	0.1	89.7	
(b)	0.723	418	
(c)	5.46	1439	

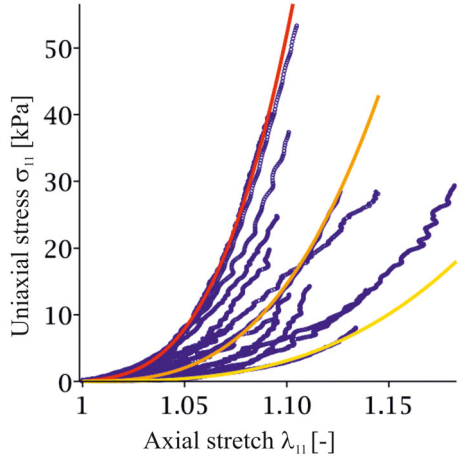

Figure 3. Uniaxial tensile tests of PVAT and model curves.

3. Results and discussion

3.1. Constitutive behavior of adipose tissue

Fifteen successful uniaxial tensile tests were conducted with samples of PVAT obtained from seven donors. Table 2 summarizes the age, sex, and number of samples obtained from each donor. The samples exhibited a nonlinear response at large strains, Figure 3. The

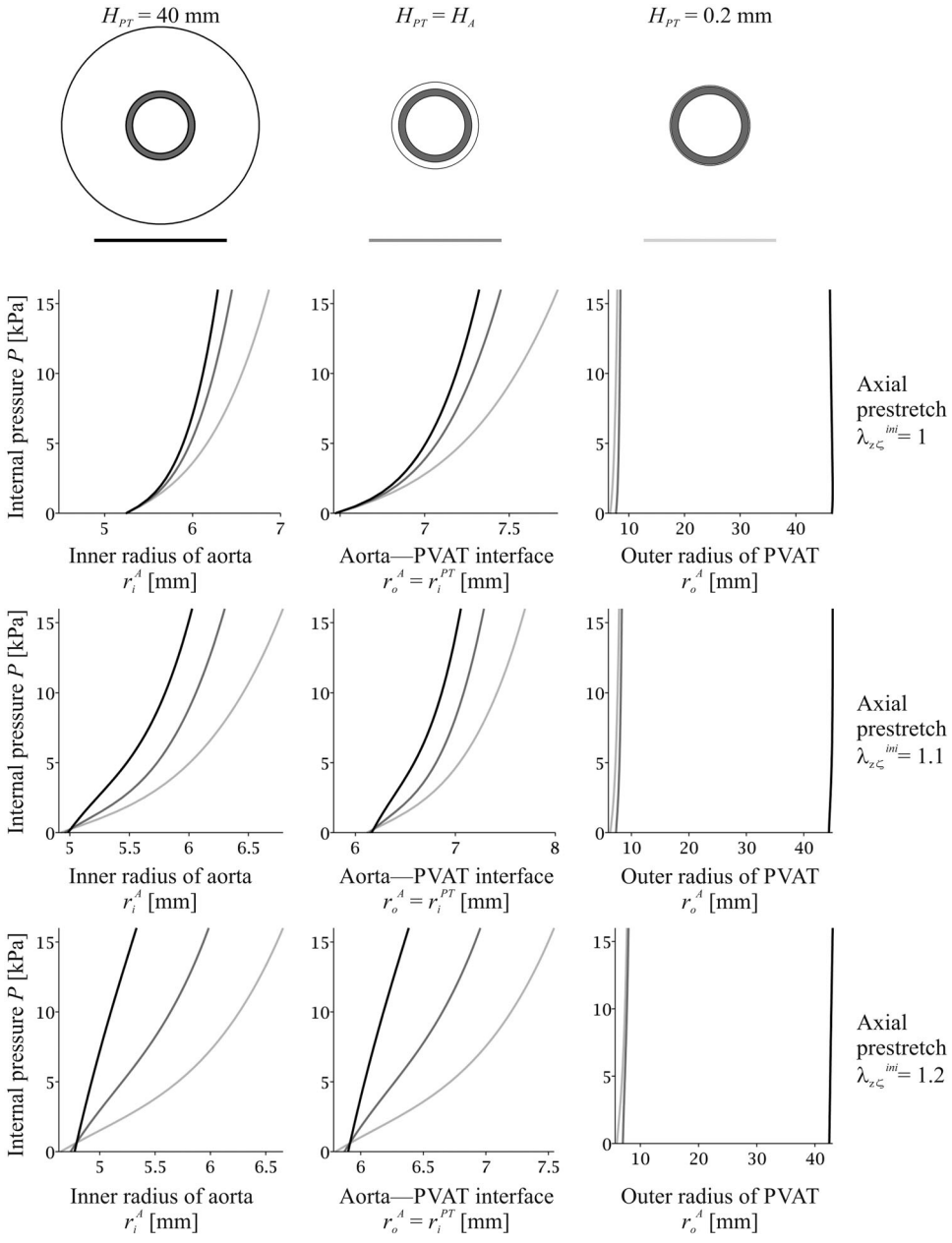

Figure 4. Inflation response of abdominal aorta M38 surrounded by PVAT with H_{PT} = 0.2, 1.22, and 40 mm.

model curves were computed by means of least square optimization for: (a) the most compliant case, (b) with all measured data pooled together which resulted in the set of material parameters that represents the average mechanical behavior, and finally (c) the stiffest case. The estimated material parameters appear in Table 2.

The uniaxial tensile tests confirmed that the elastic response of PVAT, similar to subcutaneous fatty tissue, is highly nonlinear (Sommer et al. 2013; Calvo-Gallego et al. 2018). Unfortunately, in contrast to Sommer et al. (2013), we cannot conclude that the observed behavior suggests anisotropic material properties, because we were not able to ensure the constant orientation of the samples during their separation. The highly compliant response of the tissue complicated manual preparation.

Omidi et al. (2014) studied the mechanical behavior of adipose tissue in the subcutaneous abdominal region by means of an indentation test. They employed the Yeoh hyperelastic model (third order polynomial in I_1) to express the constitutive properties of the tissue. They arrived at values of the material parameters that seem to be somewhat lower than those found in our study. c_1 = 0.16 kPa, c_2 = 0.018 kPa, and $c_3 = 1.1 \cdot 10^{-7}$ kPa are typical values estimated by Omidi et al. (2014). This discrepancy may be partially attributed to a different experimental

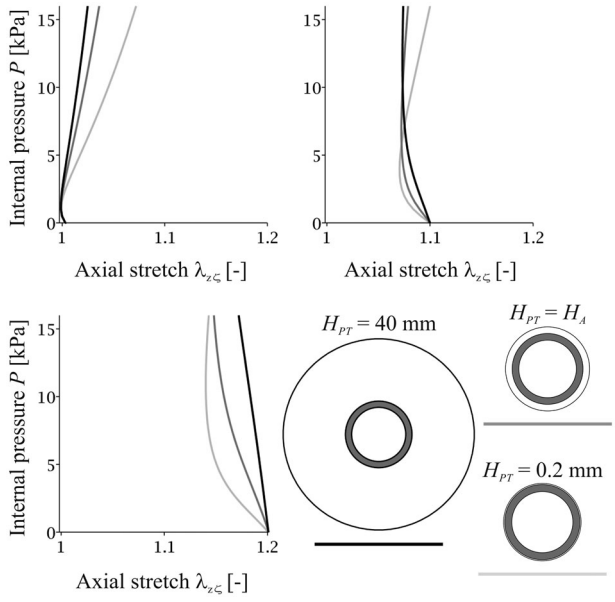

Figure 5. Extension response of abdominal aorta M38 surrounded by PVAT with H_{PT} = 0.2, 1.22, and 40 mm.

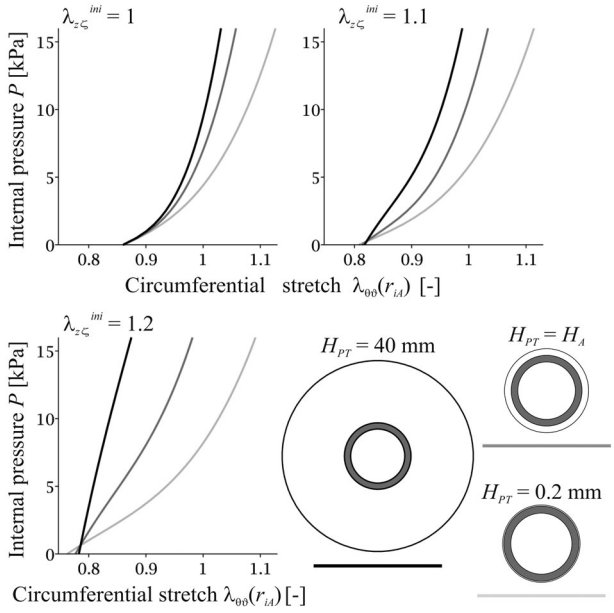

Figure 6. Dependence of circumferential stretch at the inner radius of the aorta during inflation of M38 on axial prestretch.

technique used in Omidi et al. (2014), but the most important difference seems to be the fact that Omidi et al. (2014) decellularized the tissue before testing, which can significantly change the mechanical properties of tissues (Bielli et al. 2018; Liao et al. 2008).

Although adipose tissue is very compliant and small values of an acting force can deform such an object to a state which requires employing the finite strain theory, small strain approximations are sometimes used in the literature. In this approach, the framework of linear elasticity is appropriate, and one can find studies reporting values for the Young elastic modulus for adipose tissue. Restricting our attention to the small strain theory, we can substitute the nonlinear model (2) with the slope of the tangent computed to a stress–strain curve at the beginning of the deformation. This slope is referred to as the initial elastic modulus. A consideration of the material parameters presented in Table 2 leads to 0.6 kPa, for the most compliant material response, to 4.3 kPa for an average response, and to 32.7 kPa for the stiffest case. Omidi et al. (2014) reported 3.4 kPa for the Young modulus obtained for abdominal subcutaneous tissue. Comley and Fleck (2010 2012), Nightingale et al. (2003), and Miller-Young et al. (2002) reported a Young modulus in the range of 1 – 14 kPa depending on the source of the tissue and the applied strain rate. Geerligs et al. (2008) reported the shear elastic modulus of subcutaneous tissue to be 7.5 kPa, which implies an elastic modulus of about 22 kPa. Thus, we conclude that our data suggest somewhat stiffer behavior for perivascular adipose tissue than is known for subcutaneous tissue; however, under small strains they do not differ significantly.

3.2. Inflation-extension response of abdominal aorta surrounded with adipose tissue

The effect of perivascular adipose tissue on the mechanics of the abdominal aorta was simulated by means of an analytical model based on the bi-layered thick-walled tube problem formulated within a framework of nonlinear elasticity and numerically solved in Maple. Figures 4 and 5 show the resulting inflation and extension behavior in terms of deformed radius and axial stretch obtained for the 38-year-old male individual (M38). To highlight the effect of PVAT and axial prestretch on the circumferential response of the aorta, Figure 6 depicts the dependence between circumferential stretch (computed at r_{iA}) and the inflating pressure. Figures 7 (aorta) and 8 (PVAT) show the stress distribution through the thickness of the wall computed at loading pressure $P = 16$ kPa for tubes with different H_{PT} and $\lambda_{z\zeta}^{ini}$.

With regard to inflation behavior, the figures document that PVAT restricts the radial motion of an artery. It is exhibited in each studied position (r_{iA}, $r_{oA} = r_{iPT}$, and r_{oPT}; see Figure 4). Where r_{oPT} for H_{PT} = 40 mm, the movement is almost negligible in comparison with the thickness of the fatty tissue. Thus, one could hypothetically conclude that the presence

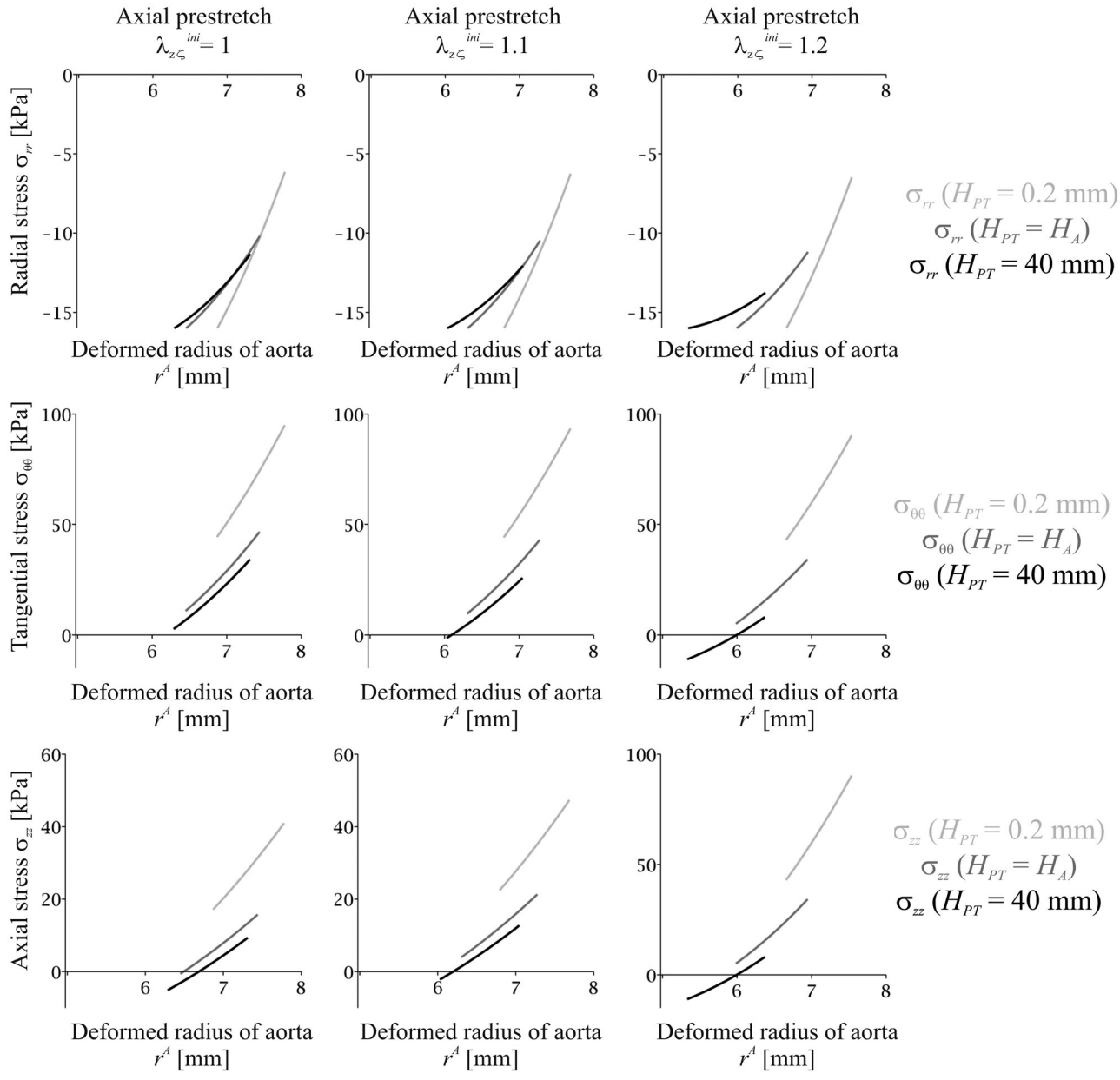

Figure 7. Distribution of in-wall stresses in aorta M38 pressurized to 16 kPa and surrounded by PVAT with H_{PT} = 0.2, 1.22, and 40 mm.

Table 3. Specific values of distensibility, (r_{iA}(16 kPa) – r_{iA}(10 kPa))/r_{iA}(10 kPa), obtained from the curves in Figure 6.

M38	H_{PT} = 0.2 mm	$H_{PT} = H_A$	H_{PT} = 40 mm
$\lambda_{z\zeta}^{ini} = 1$	0.0469	0.0333	0.0279
$\lambda_{z\zeta}^{ini} = 1.1$	0.0521	0.0340	0.0390
$\lambda_{z\zeta}^{ini} = 1.2$	0.0631	0.0612	0.0454

of the fatty surrounding is mechanically disadvantageous for the human body, because it prevents an artery from functioning as an elastic capacitor in the Windkessel effect. Later, we will see that this is just one side of the coin.

In contrast to PVAT, axial prestretch has, in the range of physiological pressure, the absolutely opposite effect. Figure 4 documents that the P – r responses are more compliant when longitudinal pretension is applied. Perhaps it is most clearly depicted in Figure 6, where circumferential stretch at the inner radius of the aorta is presented. In accordance with our previous study, Horný et al. (2014b), it can be said that the axial prestrain of the tube leads to higher circumferential distensibility in the inflation carried out at physiological pressures. Since the distensibility may not be easily recognized from the figure, Table 3 includes the specific results obtained for H_{PT} and $\lambda_{z\zeta}^{ini}$. The distensibility is quantified as (r_{iA}(16 kPa) – r_{iA}(10 kPa))/r_{iA}(10 kPa). From Table 3, we can conclude that, although increasing H_{PT} leads to

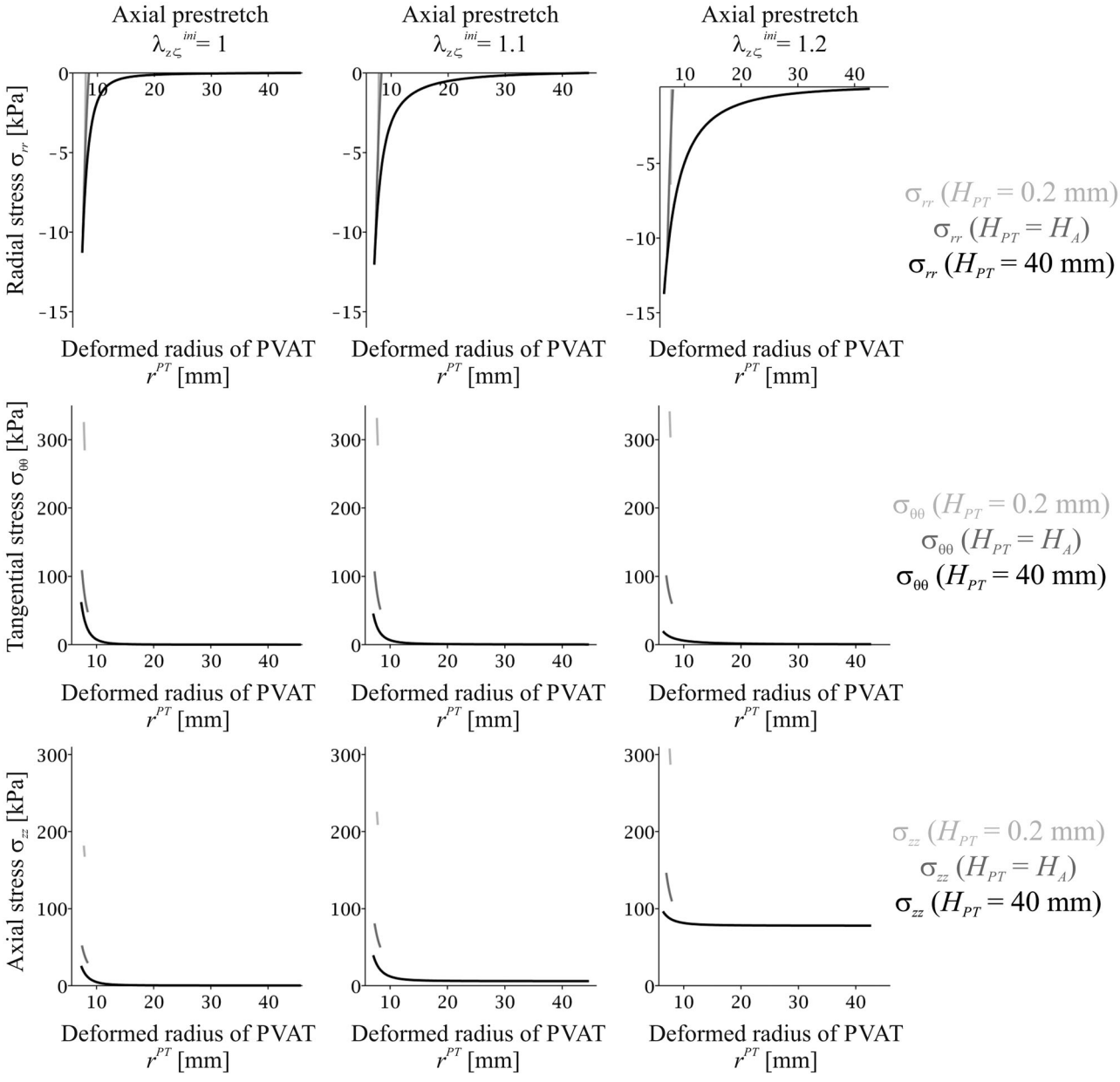

Figure 8. Distribution of in-wall stresses in PVAT at $P = 16$ kPa. PVAT tube thickness was H_{PT} = 0.2, 1.22, and 40 mm.

decreasing distensibility, axial preloading balances this influence.

The axial response is depicted in Figure 5. We again observe that including perivascular tissue into the model has, similar to circumferential behavior, an immobilization effect. The dark curves corresponding to H_{PT} = 40 mm exhibit a lower stretch variation, $\lambda_{z\zeta}(P_2)$ – $\lambda_{z\zeta}$ (P_1) for $P_1 < P_2$, than the light curves obtained for the thinner PVAT layers. At typical physiological pressures, P_2 = 16 kPa and P_1 = 10 kPa, it is also visible for $\lambda_{z\zeta}^{ini}$ = 1.1. In this case, the curve corresponding to H_{PT} = 40 mm is almost perpendicular to the horizontal axis of the graph, which suggests that the prestretched tube does not move axially during the pressure pulse. It has been hypothesized in the literature that minimization of the axial movement during the pressure pulse transmission is advantageous for arteries (Schulze-Bauer et al. 2003). Our results show that PVAT contributes to the minimization of axial movement of the aorta.

On the other hand, comparing the panels created for $\lambda_{z\zeta}^{ini}$ = 1.2 with panels for $\lambda_{z\zeta}^{ini}$ = 1.1 indicates that this behavior is not monotonic. It does not hold true in the sense that the higher the prestretch the lower the axial movement would generally be. Where $\lambda_{z\zeta}^{ini}$ = 1.2, the lowest variation of axial deformation

is obtained for $H_{PT} = 0.2$ mm. However, human arteries are not prestrained without limits. For the abdominal aorta, typical values can be found in Horný et al. (2014b, 2017). These studies suggest $\lambda_{z\zeta}^{ini} = 1.179$ for M38 is to be expected. The value comes from the studied interval $\lambda_{z\zeta}^{ini} = 1 - 1.2$. Computations show that somewhere inside this interval the longitudinal response changes from pressure-induced elongation to pressure-induced shortening. Our results suggest that the expected values of prestretch, presented in Horný et al. (2014b), fall close to a hypothetical optimal point not only in the case of bare aortas but also when the existence of PVAT and its mechanical role are considered.

In accordance with a solution known from the classical theory of elasticity for the bi-layered thick-walled tube, the computed distribution of radial stress confirms that PVAT bears some portion of the pressure load. Transmural pressure loading PVAT, $-\Delta P_{PT} = \sigma_{rr}(r_{iPT}) - \sigma_{rr}(r_{oPT}) = \sigma_{rr}(r_{iPT})$, increases when the thickness of PVAT increases. Reciprocally, the thicker the PVAT layer is, the lower is the loading of the aorta, $-\Delta P_A = \sigma_{rr}(r_{iA}) - \sigma_{rr}(r_{oA}) = -P + \Delta P_{PT}$. As a consequence of the decreasing loading of the aorta, the increasing thickness of PVAT causes a decrease in circumferential and axial stresses. This is another example showing that the existence of PVAT is advantageous from a mechanical point of view. It bears some portion of the loading and thus decreases the load acting on the aorta itself.

The role of axial prestretch is very interesting. The middle row in Figure 7 shows that increasing axial pretension leads to a decrease in circumferential stress in the aorta. Where $\lambda_{z\zeta}^{ini} = 1.2$ and $H_{PT} = 40$ mm, negative values for $\sigma_{\theta\theta}$ at r_{iA} are even reached. Interestingly, in the PVAT layer, an increase in circumferential stress at r_{iPT} is observed for $H_{PT} = 0.2$ (Figure 8). However, the maximum value of circumferential stress decreases with increasing $\lambda_{z\zeta}^{ini}$ for $H_{PT} = H_A$ and $H_{PT} = 40$ mm. This documents that the effect of axial pretension is not monotonic with respect to the simultaneous effect of the thickness.

4. Conclusion

Constitutive parameters of perivascular adipose tissue were found in our study. A hyperelastic constitutive description was employed in the form of the polynomial strain energy density. The obtained material parameters were subsequently used in the analytical solution of the bi-layer thick-walled tube problem simulating the mechanical effect of PVAT on the abdominal aorta. Simultaneous with examining the effect of PVAT, the effect of axial prestretch was also studied. It was found that the presence of PVAT reduces distensibility. Axial prestretch applied to the aorta embedded in PVAT had an opposite effect. Axially prestrained aortas exhibited higher distensiblity than non-prestrained aortas. It was also shown that the perivascular envelope bears some portion of the pressure loading and thus reduces the mechanical stresses inside the wall of the aorta. A similar effect was found for axial prestretch. The results suggest that perivascular adipose tissue is mechanically advantageous, due to it reducing wall stresses, and that decreased arterial distensibilty is compensated for by axial prestretch in the aorta.

Disclosure statement

No potential conflict of interest was reported by the authors.

Funding

This study has been financially supported by the Czech Science Foundation in the grant project no. GA18-26041S "Effect of axial prestretch on mechanical response of nonlinearly elastic and viscoelastic tubes".

References

Bielli A, Bernardini R, Varvaras D, Rossi P, Di Blasi G, Petrella G, Buonomo OC, Mattei M, Orlandi A. 2018. Characterization of a new decellularized bovine pericardial biological mesh: structural and mechanical properties. J Mechan Behav Biomed Mater. 78:420–426.

Brown NK, Zhou Z, Zhang J, Zeng R, Wu J, Eitzman DT, Chen YE, Chang L. 2014. Perivascular adipose tissue in vascular function and disease: a review of current research and animal models. Arterioscler Thromb Vasc Biol. 34(8):1621–1630.

Calvo-Gallego JL, Domínguez J, Gómez Cía T, Gómez Ciriza G, Martínez-Reina J. 2018. Comparison of different constitutive models to characterize the viscoelastic properties of human abdominal adipose tissue. A pilot study. J Mechan Behav Biomed Mater. 80:293–302.

Comley K, Fleck N. 2012. The compressive response of porcine adipose tissue from low to high strain rate. Int J Impact Eng. 46:1–10.

Comley K, Fleck NA. 2010. A micromechanical model for the young's modulus of adipose tissue. Int J Solids Struct. 47(21):2982–2990.

Gasser TC, Ogden RW, Holzapfel GA. 2006. Hyperelastic modelling of arterial layers with distributed collagen fibre orientations. J R Soc Interface. 3(6):15–35.

Geerligs M, Peters GWM, Ackermans PAJ, Oomens CWJ, Baaijens F. 2008. Linear viscoelastic behavior of subcutaneous adipose tissue. Biorheology. 45(6):677–688.

Hodis S, Zamir M. 2011. Mechanical events within the arterial wall under the forces of pulsatile flow: a review. J Mechan Behav Biomed Mater. 4(8):1595–1602.

Holzapfel GA, Gasser TC, Ogden RW. 2000. A new constitutive framework for arterial wall mechanics and a comparative study of material models. J Elast. 61(1-3):1–48.

Horný L, Adámek T, Kulvajtová M. 2017. A comparison of age-related changes in axial prestretch in human carotid arteries and in human abdominal aorta. Biomech Model Mechanobiol. 16(1):375–383.

Horny L, Adamek T, Zitny R. 2013. Age-related changes in longitudinal prestress in human abdominal aorta. Arch Appl Mech. 83(6):875–888.

Horný L, Netušil M, Daniel M. 2014a. Limiting extensibility constitutive model with distributed fibre orientations and ageing of abdominal aorta. J Mechan Behav Biomed Mater. 38:39–51.

Horný L, Netušil M, Voňavková T. 2014b. Axial prestretch and circumferential distensibility in biomechanics of abdominal aorta. Biomech Model Mechanobiol. 13(4): 783–799.

Humphrey JD, Na S. 2002. Elastodynamics and arterial wall stress. Ann Biomed Eng. 30(4):509–523.

Liao J, Joyce EM, Sacks MS. 2008. Effects of decellularization on the mechanical and structural properties of the porcine aortic valve leaflet. Biomaterials. 29(8): 1065–1074.

Liu Y, Dang C, Garcia M, Gregersen H, Kassab GS. 2007. Surrounding tissues affect the passive mechanics of the vessel wall: theory and experiment. Am J Physiol - Heart Circ Physiol. 293(6):H3290–H3300.

Masson I, Beaussier H, Boutouyrie P, Laurent S, Humphrey JD, Zidi M. 2011. Carotid artery mechanical properties and stresses quantified using in vivo data from normotensive and hypertensive humans. Biomech Model Mechanobiol. 10(6):867–882.

Miller-Young JE, Duncan NA, Baroud G. 2002. Material properties of the human calcaneal fat pad in compression: experiment and theory. J Biomech. 35(12): 1523–1531.

Moireau P, Xiao N, Astorino M, Figueroa CA, Chapelle D, Taylor CA, Gerbeau J. 2012. External tissue support and fluid-structure simulation in blood flows. Biomech Model Mechanobiol. 11(1–2):1–18.

Nightingale K, McAleavey S, Trahey G. 2003. Shear-wave generation using acoustic radiation force: in vivo and ex vivo results. Ultrasound Med Biol. 29(12):1715–1723.

Omidi E, Fuetterer L, Reza Mousavi S, Armstrong RC, Flynn LE, Samani A. 2014. Characterization and assessment of hyperelastic and elastic properties of decellularized human adipose tissues. J Biomech. 47(15): 3657–3663.

Schulze-Bauer C A. J, MöRth C, Holzapfel G A. 2003. Passive biaxial mechanical response of aged human iliac arteries. J Biomech Eng. 125(3):395–406.

Sommer G, Eder M, Kovacs L, Pathak H, Bonitz L, Mueller C, Regitnig P, Holzapfel GA. 2013. Multiaxial mechanical properties and constitutive modeling of human adipose tissue: a basis for preoperative simulations in plastic and reconstructive surgery. Acta Biomater. 9(11):9036–9048.

Zaborska KE, Wareing M, Austin C. 2017. Comparisons between perivascular adipose tissue and the endothelium in their modulation of vascular tone. B J Pharmacol. 174(20):3388–3397.